Renewable Integration Options for Remote New Zealand Communities

A thesis

submitted in fulfilment

of the requirements for the degree

of

Master of Engineering in Chemical and Biological Engineering

at

The University of Waikato

by

NAVEEN KUMAR JAYASANKAR

THE UNIVERSITY OF
WAIKATO
Te Whare Wānanga o Waikato

2025

Supervisor: Prof. Michael Walmsley

Abstract

About 35% of New Zealand's population lives in rural and remote areas like Whitianga and its nearby settlements. These areas are facing growing electricity demand due to rising population, business activity, and the shift to cleaner transport such as EV and FCEV. This trend is expected to put additional pressure on existing electricity infrastructure and networks, many of which were not built to handle such loads. A potential solution is to utilize local renewable energy sources, such as solar, wind, and green hydrogen, to reduce reliance on the national grid and delay costly infrastructure upgrades.

The first part of the thesis investigates the dynamic behaviour of a PEM electrolyser as a likely component in future integrated renewable energy systems. A Python-based simulation compares the hydrogen production output of dynamic and static models of a PEM under variable solar PV inputs. For the PEM capacity selected, there was a modest difference in cumulative hydrogen output from the dynamic model compared to the static model using one-minute input data over a whole day. Potentially, the dynamic model provides a more accurate way to size electrolyser and associated units like compressor and hydrogen storage vessels with the fluctuating electrical input conditions.

The second part evaluates the use of rooftop solar PV, wind, and hybrid solar-wind systems integrated with green hydrogen into a single residential house to achieve various levels of self-sufficiency over a full year. The study models energy balance, hydrogen storage, and levelized cost of energy (LCOE) for a range of system sizes, showing that 100% self-sufficiency is achievable in all three options, but only at extremely high LCOE levels between 0.52 and 0.78 NZD/kWh. Among the options, the hybrid system of solar and wind performs best, achieving complete self-sufficiency (100%) at the lowest cost of 0.52 NZD/kWh while balancing energy generation and storage needs with demand.

The third part presents a case study of the Whitianga township and region, exploring the integration of solar PV, Vehicle-to-grid (V2G), and green hydrogen to meet future energy demand. A techno-economic assessment examines residential, commercial, and transport energy needs from 2024 to 2050 and evaluates how a 32 MW_p solar PV energy system can supply local demand while reducing reliance on the national grid and the need for local transformer upgrades. Two approaches were investigated: a centralised solar farm approach plus local hydrogen production & EV charging demand, and a decentralised residential rooftop solar approach supported by V2G electricity storage. The results indicate that the centralised

approach has the lowest LCOE of 0.107 NZD/kWh, while the local grid upgrade remains unavoidable, even with higher solar penetration to the local grid. But in terms of payback period, the decentralised approach has a significant advantage, even with the higher investment cost, especially when V2G is incorporated into the energy management system. The initial investment amount can be recovered in 12.01 years with 20kWh of V2G battery storage.

Acknowledgements

First and foremost, I would like to express my deepest gratitude to my supervisor, Prof. Michael Walmsley, for his unwavering support throughout my research journey. His insights and guidance helped me develop as a researcher and critical thinker over this period.

I want to extend my appreciation to Shiva, Mathavan, Shridhar and fellow researchers at the Ahuora Lab for their support throughout my journey and for providing me with the assistance that made this research possible.

I would like to thank my parents for providing me with their unwavering financial support and motivation to pursue my master's degree in New Zealand. Without them, the journey would be impossible.

Lastly, a special thanks to the University of Waikato for providing me with the computing resources and research assistance through my journey.

Table of Contents

List of Figures

List of Tables

Nomenclatures

Abbreviations

AC	Alternating Current
BOP	Balance of Plant
CAPEX	Capital expenditure
DC	Direct Current
EMS	Energy Management System
EV	Electric Vehicle
FC	Fuel Cell
FCEV	Fuel Cell Electric vehicle
GXP	Grid Exit Point
HHV	Higher Heating Value
LCOE	Levelized Cost of Electricity
LCV	Light Commercial vehicle
LPV	Light Passenger Vehicle
MEA	Membrane Electrode Assembly
MVA	Mega Volt Ampere
NPV	Net Present Value
NZ	New Zealand
NZD	New Zealand Dollars
OPEX	Operational Expenditure
P2G2P	Power to Gas to Power
PEM	Proton Exchange Membrane
V2G	Vehicle to Grid
VKT	Vehicle Kilometre Travelled

Subscripts and symbols

$C_{battery}$	Cost of electricity used from battery
C_{export}	Cost of electricity exported to grid
C_{grid}	Cost of electricity used from grid
C_{solar}	Cost of electricity used from solar
C_t	Total cost of the system
$E_{H_2produced}$	Amount of hydrogen stored after supplying the demand
e^-	Electron
E_0	Reversible cell voltage
$E_{battery}$	Electricity used from battery
E_{cell}	actual cell voltage
E_{cell}	Actual cell voltage
E_{EL}	PEM electrolyser electricity consumption
E_{export}	Electricity exported to grid
E_{grid}	Electricity used from grid
E_{PRO}	Electricity produced from renewables
E_{solar}	Electricity used from solar
E_{SUR}	Surplus electricity produced from the renewables
E_t	Electricity produced over its lifetime
E_{tn}	thermoneutral voltage
E_{tn}	Thermoneutral voltage
E_{total}	Total electricity used
H^+	proton
m_{H_2}	Mass of the hydrogen
N_d	Electro-osmotic drag co-efficient
N_d	Osmotic drag
$P_{H_2,ca}$	Pressure of hydrogen at cathode
P_{H_2O}	Partial pressure of water
$P_{O_2,an}$	Pressure of oxygen at anode
P_{FC}	Power produced from the fuel cell
P_{LOAD}	Residential electricity demand
P_{PV}	Power produced from solar PV inverter

P_{WIND}	Power produced from the wind turbine inverter
V_{act}	Activation overpotential
V_{an}	Volume of anode
V_{ca}	Volume of cathode
V_{cell}	Total voltage of the cell
V_{con}	Concentration overpotential
V_{ohm}	Ohmic overpotential
V_{th}	Theoretical cell voltage
η_{EL}	PEM electrolyser efficiency
$\eta_{FC, (DC/AC)}$	Efficiency of the inverter
$\eta_{voltage}$	Voltage efficiency
λ_m	Water content of the membrane
σ_{me}	Membrane conductivity
E_{CON}	Electricity consumed from the renewables
E_{DEF}	Electricity supplied from the fuel cell
F	Faraday constant
H_2	Hydrogen
H_2O	Water
I(t)	Change of current over time
ln	logarithmic
log	logarithmic
n	Number of cells
n	No. of. years
O_2	Oxygen
R	Universal gas constant
r	Discount factor
T	Temperature
t	time
ΔG^0	Gibbs free energy change
ΔH^0	Enthalpy change
ΔS^0	Entropy change
τ	Time constant

Units

A	ampere
°C	Celsius
cm^2	Centimetre square
C	coulomb
m^3	Cubic meter
GWh	Giga Watt hour
J	joule
K	Kelvin
kWh	Kilo Watt hour
kW_p	Kilo Watt Power
kg	kilogram
kg/min	Kilogram per minute
kV	Kilovolts
MWh	Mega Watt hour
MW_p	Mega Watt Power
mol	moles
s	seconds
V	volt

1 Introduction

1.1 Context of the study

Around 35% of New Zealand's population lives in rural and remote communities, such as small settlement towns like Whitianga and their surrounding areas [1]. These areas are experiencing a steady increase in electricity demand. This rise in electricity demand is primarily due to population growth, the expansion of local businesses, and the shift towards cleaner forms of energy, particularly in the transportation sector. Technologies like Electric Vehicles (EV) and Fuel Cell Electric Vehicles (FCEV) are becoming more common, which adds new pressure on existing electricity networks. However, many of these grid systems were not originally designed to handle such growing and variable loads. Without alternate evaluation and planning, much of the electrical infrastructure will require costly upgrades to meet future energy demand [2].

To address these challenges, one promising solution is to utilize local renewable energy sources, such as solar and wind energy, combined with local hydrogen production and use. Solar power can be generated through either rooftop panels on individual houses or commercial buildings, or larger community-scale solar farms. Hydrogen production can be through a small-scale household electrolyser, or a large-scale electrolyser at centralised hydrogen refuelling stations. Since the electricity is produced close to where it is consumed, this approach can reduce the need to import electricity from the national grid. It can also delay or reduce the cost of upgrading transmission infrastructure in the future.

The potential use of green hydrogen for some transport applications and for a seasonal long-term energy storage solution is also investigated in this thesis. Green hydrogen is produced by splitting water into hydrogen and oxygen using electricity from renewable sources through a process called electrolysis. The hydrogen can then be stored and later used to produce electricity again through fuel cells or to support residential and transport needs. This approach could be especially useful in remote locations, where solar or wind energy is not always available throughout the day or year. Small-scale hydrogen systems, such as those provided by companies like Hiringa Energy [3] may offer a practical solution.

The research is divided into three key parts. First, the dynamic behaviour of a Proton Exchange Membrane (PEM) electrolyser when powered by variable solar PV electricity is modelled and examined. The work specifically quantifies the impact of power supply changes on the rate of

daily hydrogen production. In the second body of work, the potential for achieving energy self-sufficiency in a single residential NZ house using various levels of rooftop solar and/or wind energy capacity, and/or green hydrogen production and storage capacity is examined. The third body of work focuses on the Whitianga region (Figure 1-1), where energy demand is increasing and the local network substation's transformer capacity is nearing its full limit (17 MVA).

Figure 1-1: The network map of Whitianga and its surrounding regions [2].

The Whitianga case study examines the extent to which solar PV electricity, either through a centralised 32 MW_p solar farm or on residential roof-tops of a similar capacity, plus centralised green hydrogen production, can meet the future energy needs of Whitianga out to 2050. The extent to which localised electricity reduces the need for extra national grid supply and local network upgrades will also be reported, and how it contributes to a more resilient and sustainable community energy system is discussed.

1.2 Scope of the study

The primary objective of this work is to investigate how renewable energy sources, such as solar and wind, and energy carriers like green hydrogen, can enhance rural community energy independence and reduce the need for substantial investments in grid upgrades.

This study does not provide a detailed demand analysis of the electrical system, including transmission losses, grid capacity, voltage, and upgrade control. Instead, it examines the hourly balance between electricity supply and demand based on estimated energy use in residential homes, commercial buildings, and the transportation sector.

The electricity demand for residential, commercial, and transport services in remote communities, like Whitianga, has been estimated using data on population, building numbers, and vehicle fleet statistics [4-6]. According to a report by the Waikato Council [7], there are no major industries in the Whitianga region. Therefore, industrial electricity demand has not been included in the community demand estimation.

The focus is on how renewable energy and green hydrogen systems can be utilized locally, either at the household or community level, to meet overall energy needs. Where possible, this approach can also store excess energy via V2G or hydrogen to support the local electricity grid network in delivering electricity to remote communities affordably.

1.3 Research questions

The study addresses the challenges and opportunities of integrating renewable energy and green hydrogen technologies into residential applications and community energy systems in New Zealand. Based on the scope and context of the study outlined, this research aims to answer the following questions.

1. Does variable electricity from solar PV significantly affect the rate of hydrogen (H_2) production from a PEM electrolyser?
2. What is the LCOE for a single New Zealand house to become electricity independent from the grid through integrating renewable energy and green hydrogen?
3. Do centralized solar farms provide cheaper electricity for an isolated community compared to the equivalent capacity provided through rooftop solar systems integrated with private electric vehicles for battery storage?

1.4 Thesis structure

Chapter 1 outlines the context of the study in NZ and the issues faced by remote communities as they decarbonise and upgrade their networks to meet future demand.

Chapter 2 discusses the background studies relevant to the research work conducted in the past and identifies the research gap to address the issue by proposing a new solution.

Chapter 3 analyses the dynamics of the PEM electrolyser, powered by intermittent renewable sources.

Chapter 4 addresses integrating renewables and green hydrogen into the residential application to achieve complete self-sufficiency and assesses the system's LCOE.

Chapter 5 investigates the integration of renewable energy into a remote community. The case study conducted was the Whitianga township and region of NZ. The aim was to offset future electricity demand through local renewable energy production, thus minimizing the local grid network extensions that might be needed in the future. Two scenarios of integration have been considered to assess their techno-economic feasibility and the best cost option.

Chapter 6 concludes the major areas investigated in the above chapters.

2 Literature Review

This chapter provides an overview of the concepts discussed in the thesis by examining the relevant literature and identifying the trends and gaps that have been addressed in prior work.

2.1 Introduction

As countries move toward cleaner energy systems, green hydrogen produced through water electrolysis powered by renewable energy is emerging as a key solution. Among different electrolysis methods, Proton Exchange Membrane (PEM) electrolysers are especially suited for use with variable energy sources such as solar and wind. This is due to their fast response time and compact design. However, renewable sources are not constant throughout the day, making it difficult to ensure stable hydrogen output. To address this, dynamic modelling has been developed to simulate how PEM electrolysers behave under fluctuating power conditions. These models account for real-time system changes, such as voltage losses and water transport, providing a more accurate understanding than static models [8].

In residential applications, integrating solar PV and wind energy can reduce dependence on the electricity grid. However, challenges remain due to the intermittent nature of renewables and the high cost of battery storage systems [9]. Batteries degrade over time and are not always sized to store enough energy for long-term or seasonal needs. Green hydrogen presents a potential solution by acting as both an energy carrier and a long-term storage option. Several studies from countries like Australia, Canada, and Slovenia have explored how hydrogen systems can improve residential energy self-sufficiency, but the high investment costs remain a barrier [10].

At the community level, local renewable energy generation through solar PV, either as rooftop systems or solar farms, can help rural areas reduce grid reliance and make them more energy self-sufficient. Community energy modelling allows for the design and optimisation of such systems. However, despite various case studies, there is still limited research comparing centralised versus decentralised approaches in terms of cost and feasibility [11].

This literature review addresses these knowledge gaps and evaluates the application of renewable-hydrogen systems in both residential and community settings, particularly in the context of rural New Zealand. The overview of the literature work is illustrated in Figure 2-1.

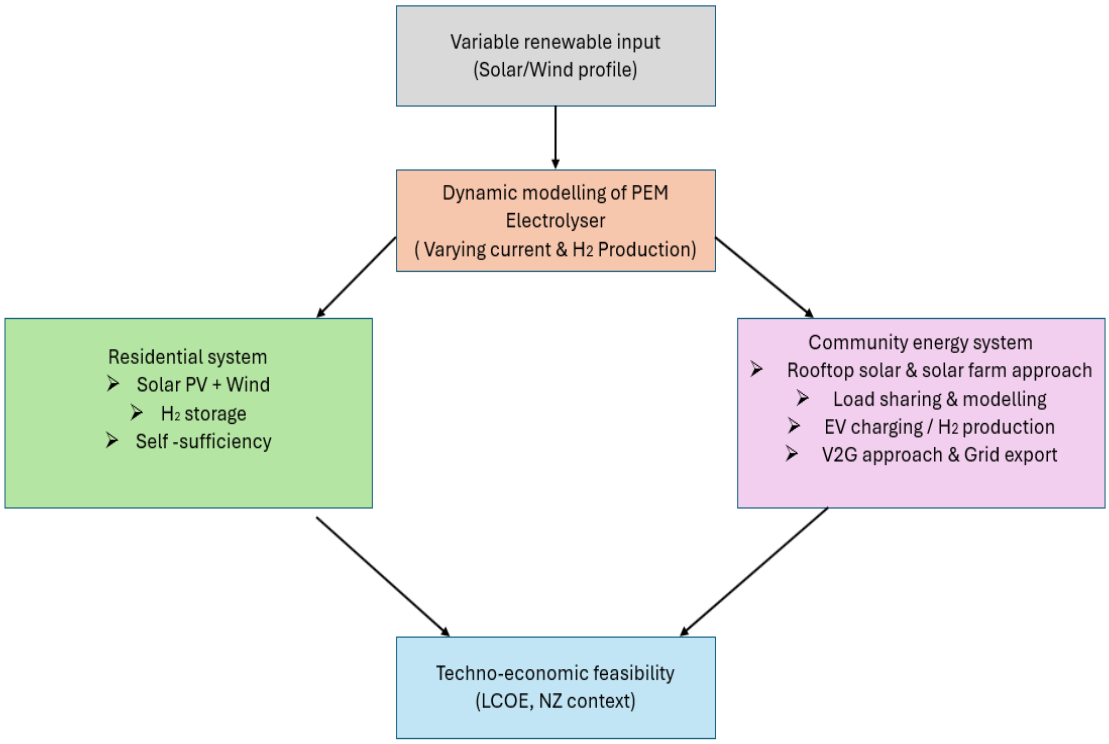

Figure 2-1: The overview of the literature review.

2.2 Dynamics of PEM electrolyser

Green hydrogen produced through water electrolysis using renewable electricity is widely regarded as a key solution for clean energy systems. This is because the process does not make direct carbon emissions. Over the past 15 years, the cost of renewable energy technologies, especially solar and wind, has dropped significantly due to improvements in design and larger-scale use. Since electricity makes up around 40–70% of the total cost of green hydrogen production [8], any reduction in electricity prices at the time of use can significantly lower the overall hydrogen cost. Additionally, new materials and better electrolyser designs are being developed to reduce system costs. If both electricity and electrolyser costs continue to fall, or periods of excess solar at very low market value become more common, this could lead to wider global adoption of green hydrogen technologies [12].

Among the available electrolysis technologies, Proton Exchange Membrane (PEM) electrolysers and Alkaline Electrolysers are the most developed. PEM electrolysers are particularly suitable for use with fluctuating power sources, such as solar and wind. This is because they respond quickly to input changes, are compact, and are more efficient under variable conditions [13]. However, the variability in solar or wind energy potentially creates

challenges for hydrogen production, which ideally needs stable power. To investigate this, researchers have developed dynamic models that can simulate the behaviour of PEM electrolysers as the power supply changes over time [14].

Static models assume that the hydrogen output instantly follows the input power without delay. In contrast, dynamic models consider how real systems respond over time, including delays due to gas buildup, pressure changes, and internal limitations [15]. For example, when solar power increases rapidly in the morning, there may be a short delay before the hydrogen output rises, due to system inertia. Awasthi et al. [16] emphasize that these short-term effects are crucial for understanding actual performance and preventing errors in system design.

Dynamic models also help us understand how voltage efficiency changes as input current changes. As current increases, the system experiences more internal resistance and heat, which lowers efficiency [17]. According to Liso et al. [18], this drop in efficiency becomes clear when the cell voltage goes above 1.48 V, which is the thermo-neutral point, the point where all energy needed for water splitting is provided as electrical energy. These losses are modelled using electrochemical principles, such as the Nernst equation and empirical relations, to estimate overpotentials resulting from activation and ohmic resistance.

Another important thing in dynamic models is osmotic drag, where water molecules are pulled through the membrane along with hydrogen ions. This affects the membrane's hydration level and influences its long-term performance. Researchers suggest incorporating these water transport effects into their models, thereby improving the accuracy of simulations under real operating conditions [19, 20].

Abin et al. [21], suggested using dynamic modelling to design hybrid energy systems that incorporate both solar power and hydrogen production. These models are beneficial for off-grid or remote communities where the power supply is not always reliable.

In summary, dynamic modelling of PEM electrolysers provides a better understanding of how hydrogen systems behave under variable renewable energy sources. It captures system delays, voltage losses, and efficiency changes that static models ignore. The fundamental equations required for creating a dynamic PEM model have not been covered in this chapter but are covered in Chapter 3 as part of the modelling approach.

2.3 Single residential application

Most of the countries, such as India, Australia, and Chile, are focusing on implementing renewables such as solar and wind into residential applications to reduce grid dependency and have a positive impact on the environment [22-24]. However, there have been a lot of challenges faced by renewables due to their intermittent nature. The intermittency is due to the nature of the weather and seasonal fluctuation [25]. A residential renewable energy system of solar PV panels and/or wind turbines, sized to meet annual demand, can meet between 30% and 70% of the single residential demand. The remaining renewable electricity is often not able to be used by the resident due to a lack of storage, and the excess electricity has to be exported immediately to the grid at discounted prices [26].

While studies agree on rising residential demand, few address the scalability of storage solutions for off-grid options to achieve self-sufficiency using battery or hydrogen technologies. Battery technology poses a lot of challenges due to high initial investment cost, degradation over the life cycle, and a lack of sizing at a reasonable price for seasonal storage [27].

In Australia, battery storage issues have been addressed by integrating solar PV-battery systems with the grid. The system sells the excess electricity produced during peak generation to the local grid at low prices, but only after charging the home battery for later use when prices are high. However, this system requires a proper control system to discharge and charge the batteries. PV/battery/grid is a nascent technology and requires a massive upfront cost to install, but still, the system cannot achieve complete self-sufficiency, especially during winter [10].

To address the seasonal energy storage challenges, integrating renewables with green hydrogen is a crucial solution for achieving self-sufficiency in residential settings [24]. Green hydrogen stands out as a viable solution as a clean fuel, with the ability to store energy for extended periods and act as a backup generator via a fuel cell when renewable energy generation is limited. The cost of a green hydrogen integrated system, which consists of an electrolyser, compressor, and a fuel cell, varies by location, depending on factors such as the availability of raw materials, labour, and the site's geography [28]. A comprehensive study has been conducted in the UK to investigate public involvement in integrating 100% clean energy, including green hydrogen and renewable electricity, into residential electricity demand. Seventy percent of the participants voted in favour of cleaner energy in the survey, indicating their willingness to adapt [29].

The standalone system has been designed for residential applications, utilizing a combination of electrolysis, fuel cell, battery, solar PV, and wind turbine, for a proposed system in South Africa and Nigeria [9]. The system harnesses the excess electricity to produce green hydrogen and achieves 100% self-sufficiency. However, the Levelized Cost of Energy (LCOE) remains relatively expensive, at 0.754 USD/kWh and 0.701 USD/kWh. Farukh et al. [30] conducted several trials and assessed the integration of solar panels and a Fuel cell in a tall building in Oshawa using HOMER Pro software. The integrated system achieves energy and exergy efficiencies of 26% and 26.8%, respectively, with an optimized LCOE for the proposed system of 0.86 CAD/ kWh.

Jane et al. [10] have developed a surrogate model for integrating the hybrid solar-green hydrogen system into residential applications in Slovenia. During winter, electricity needs to be supplied from the grid, and the system achieves only 62.13% self-sufficiency. To achieve 100% self-sufficiency, larger PV panels and an excess hydrogen storage tank are needed, acknowledging the high initial investment cost of the system. Barcelo et al. [31] have proposed an optimised system using solar PV and H_2 production system for residential applications in Ecuador. The LCOE of the system is four times higher than the current electricity cost in Ecuador.

According to the above literature, integrating renewable energy and green hydrogen into residential settings is unlikely to be economically viable soon. However, there is still a lack of research that has been conducted in this area in the NZ context, which compares the LCOE of this approach with the grid electricity price as a benchmark. The following section will explore how communities can harness and produce renewable energy by themselves.

2.4 Energy community modelling approach

The global shift toward sustainable energy has increased interest in both centralized and decentralized renewable energy systems. These systems support the development of community-based energy projects, where residents, businesses, and public organizations can produce and use their own renewable electricity. This approach helps improve energy independence, reduce emissions, promote social equality, and create local jobs [11]. Community energy modelling plays an important role in planning and optimizing these systems. By simulating different system designs, demand patterns, and integration methods, modelling supports informed decisions on infrastructure development and policy [32].

Among renewable energy technologies, solar photovoltaic (PV) systems are particularly well-suited for community-scale applications. Their compact design, low cost, and ease of installation make them ideal for rural or remote areas that lack reliable access to traditional grid infrastructure. Research shows that rooftop and small-scale solar farms can reduce peak electricity demand, lower transmission losses, and delay the need for costly grid upgrades when implemented locally [33].

Case studies from countries like Australia and Germany demonstrate the successful integration of solar energy at the community level. These successes are linked to effective demand-side management and supportive policies such as feed-in tariffs from the government [34]. For example, a case study on a remote Croatian island with a population of about 15,000 showed that while a solar farm helped reduce the use of conventional energy, the midday electricity surplus caused difficulties in exporting power to the local grid [35].

To solve such challenges, hybrid energy systems have been developed to produce and store excess renewable electricity. One solution combined a gravity-based energy storage system with solar and wind power in a remote community. In this setup, surplus electricity lifts weights to store energy, which can be later released to generate power. While this reduced the community's annual grid electricity use by 20%, the cost remained high, with a levelized cost of electricity (LCOE) of ranges from 0.15- 0.40 USD/ kWh due to the expensive energy storage infrastructure [36].

Other approaches have aimed to use excess electricity more cost-effectively. In India, a project combined solar PV systems with limited grid use and electric vehicle (EV) charging stations. Here, midday solar surplus was used to charge EV rather than export electricity to the grid. This helped ease pressure on the grid and kept the LCOE low, around 0.10 USD/kWh [37].

The above global context study highlights the need for careful planning to manage excess renewable electricity. They also show the value of hybrid system designs in improving energy efficiency and lowering costs. Based on above insights, this study focuses on New Zealand's rural energy challenges. A case study has been conducted to compare centralized and decentralized community energy systems and assess their techno-economic feasibility. The goal is to identify the best strategy for using local renewable energy, managing surplus electricity, and strengthening energy resilience in remote areas.

3 Dynamic Modelling of PEM Electrolyser

3.1 Introduction

This chapter focuses on the dynamic modelling of a PEM electrolyser connected to a fluctuating solar PV power source. The main objective is to assess how time-varying electrical input affects hydrogen generation on an hourly basis. A first-order dynamic system captures hydrogen accumulation and removal, with the time constant as a key parameter. Results from the dynamic model are compared with a static model to highlight performance differences, especially during periods of rapid power fluctuation.

This study focuses on short-term system behaviour (in a day) rather than long-term degradation or experimental validation. It models only the electrochemical processes within the PEM stack and excludes Balance-of-Plant (BOP) components like pumps, separators, and cooling systems.

The following sections describe the development of the dynamic model and analyse the variable nature of solar PV electricity effects on H_2 production.

3.2 PEM electrolyser modelling approach

A dynamic model for a PEM electrolyser stack has been programmed in Python using the modelling approach developed by Yigit et al [17] and Sumit et al [38]. The model involves a significant number of equations, and for clarity, these are presented in this chapter along with the results of the Python model created (Appendix - 1, 2). The fundamentals of the electrolyser and the system assumptions are discussed in Sections 3.2.1 and 3.2.2. The overall modelling approach and stack-level modelling are described in more detail in Sections 3.2.3 and 3.2.4.

3.2.1 Electrolyser thermodynamics

Water is fed into the PEM electrolyser through the anode chamber (Figure 3-1). When a potential difference is applied across the cell, water molecules undergo electrochemical dissociation, splitting into oxygen gas and protons. The half-cell reactions occur at the catalyst-coated electrodes and are classified as redox reactions.

At the anode, water is oxidized to produce oxygen gas (O_2), protons (H^+), and electrons:

$$2H_2O \rightarrow 4H^+ + 4e^- + O_2 \quad (3.1)$$

At the cathode, the protons migrate through the proton exchange membrane and combine with electrons from the external DC power source to form hydrogen gas (H_2):

$$4H^+ + 4e^- \rightarrow 2H_2 \quad (3.2)$$

The overall water electrolysis reaction is represented as

$$H_2O \rightarrow H_2 + ½O_2 \quad (3.3)$$

These reactions occur on the surface of the catalyst embedded in the Membrane Electrode Assembly (MEA). The MEA includes a diffusion layer on both the anode and cathode sides, which ensures efficient current distribution and gas transport.

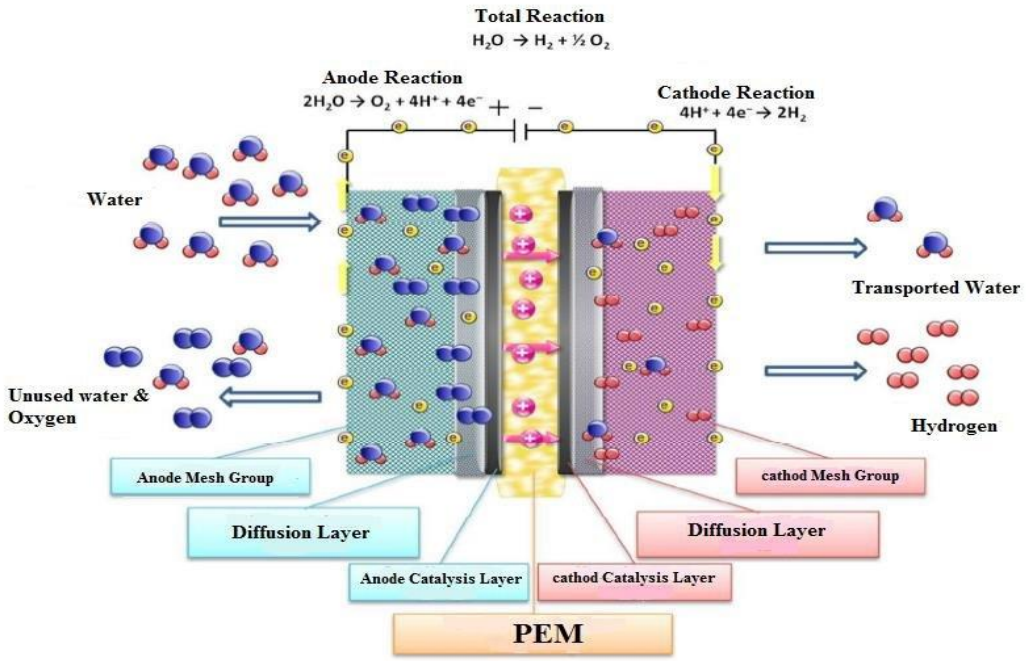

Figure 3-1: Schematic diagram of a single PEM electrolyser stack, showing the water feed, proton movement across the membrane, and the production of H_2 & O_2 gases [39].

Table 3-1: Thermodynamic properties of the water diffusion reaction in the PEM electrolyser.

Species	ΔH^0 (kJ/mol)	ΔG^0 (KJ/mol)	ΔS^0 (J/mol K)
H_2O (l)	-285.83	-237.129	69.91
H_2 (g)	0	0	130.684
O_2 (g)	0	0	205.138

The thermodynamic coefficient for Equation (3.3) at 25°C and 1 bar is presented in Table 3-1. Where, ΔH^0 is the enthalpy of the reaction, ΔG^0 is the Gibbs free energy of the reaction, and ΔS^0 is the entropy of the reaction. The reaction is endothermic, and electrical work is needed from an external source to make the reaction possible.

3.2.2 System description and assumptions

The system's core component is an electrochemical stack composed of multiple (PEM) cells connected in series. Each cell performs water electrolysis by splitting the H_2O molecule into H_2 and O_2 gases when the electric current (DC) is applied.

The electrical power input to the electrolyser varies throughout the day based on the solar irradiance profile, resulting in a time-dependent current input, I(t). This variability directly influences the cell voltage and the rate at which gases are produced.

The assumptions for modelling the PEM electrolyser stack for the current study are as follows:

- The cells constituting the stack are identical and connected in series. Thus, the stack with N cells can be modelled as an equivalent single cell that has the same dynamics as the stack.
- Uniform current and fluid flow are distributed among the cells
- The gas flow rate produced is calculated based on Faraday's law of electrolysis.
- The temperature of the stack (T) is assumed to be homogeneous and operated at 80°C.
- The water flow rate fed into the system is assumed to be constant and doesn't simulate fluid flow dynamics.
- The gas produced is assumed to have a similar property to an ideal gas, and Dalton's law calculates the partial pressure of these gases.

These assumptions simplify the model while capturing the electrochemical behaviour of the PEM stack.

3.2.3 Modelling overview

The schematic diagram of the PEM electrolyser stack and its physical variables and parameters are shown in Figure 3-2. The model simulates how water and electrical current are processed within the system to produce hydrogen and oxygen.

In the figure, the input parameters of the model are represented in the black line, which is the current density (A/cm²) and the flow rate of water ($N_{H_2O,an}$). The current density is the ratio of current (A) to active cell area (cm²). The blue line represents the anode-related flows, the membrane transport is represented in the green line, the grey line represents the output from the cathode chamber, and finally, the orange line represents the Thermal module (T), which is assumed to be constant.

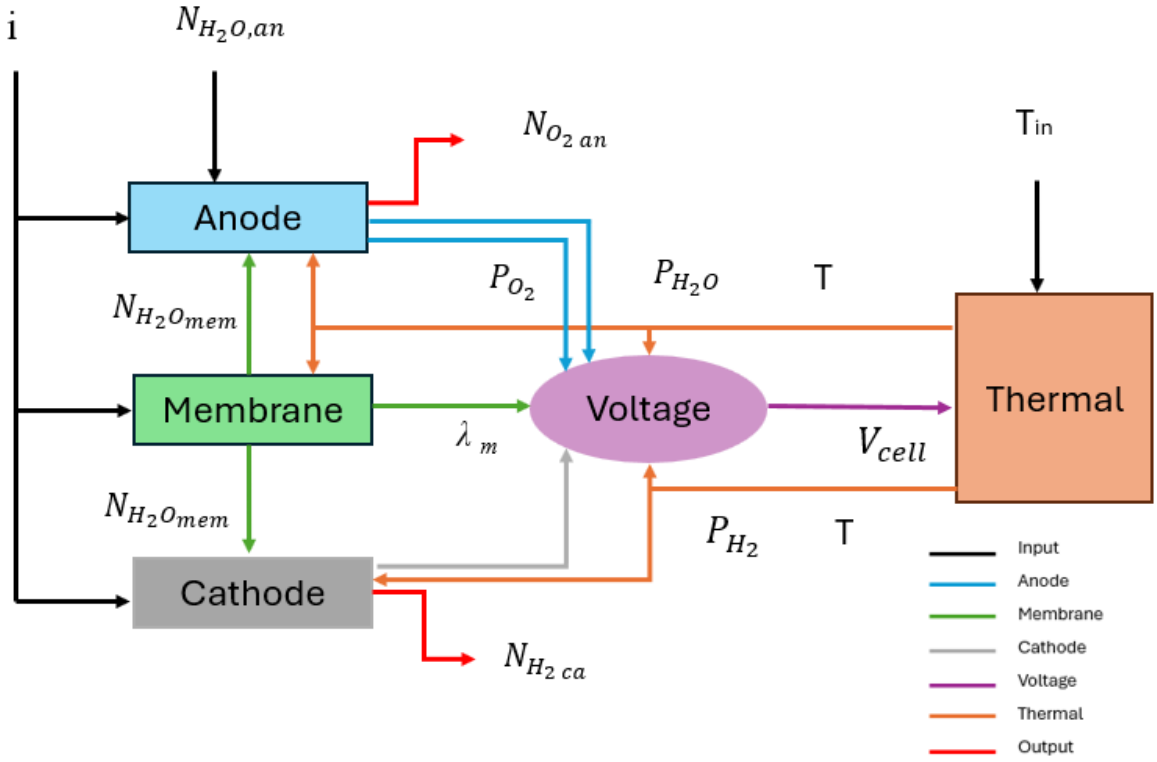

Figure 3-2: Overview of the developed PEM stack model in Python.

The internal parameters and variables of one module have been interrelated with the other module to get the output, which is shown as a red line $N_{O_2,an,gen}$ & $N_{H_2,ca,gen}$. With this integrated model approach, it is possible to predict the H_2 production and losses. The model was implemented using Python to simulate the dynamic behaviour of the electrolyser when subjected to a variable solar power input.

3.2.4 PEM stack modelling

The stack modelling has been divided into four modules: cathode module, anode module, membrane module, and voltage module, which are discussed in more detail in the following sections.

3.2.4.1 Anode module

First, the deionised water is fed into the anode module. When the potential difference (V) is applied, the oxygen evolution reaction and water splitting occur in the anode compartment. Based on the equations (3.2), the flux of moles of oxygen and water with respect to time in the anode can be written as follows.

$$\frac{dN_{H_2O_{an}}}{dt} = N_{H_2O_{an,in}} - N_{H_2O_{an,cons}} - N_{H_2O_{mem}} - N_{H_2O_{an,out}} \qquad (3.4)$$

$$\frac{dN_{O_{2,\text{an}}}}{dt} = N_{O_{2,\text{an,in}}} + N_{O_{2,\text{an,gen}}} - N_{O_{2,\text{an,out}}} \quad (3.5)$$

$N_{H_2O_{\text{an,in}}}$ is the flux of moles of water entering the anode compartment; $N_{H_2O_{\text{an,cons}}}$ is the flux of moles of water consumed in the anode; $N_{H_2O_{\text{mem}}}$ is the flux of moles of water consumed in the membrane and $N_{H_2O_{an,out}}$ is the flux of moles of water coming out from the anode.

The flux of moles of oxygen at the inlet ($N_{O_{2,\text{an, in}}}$) is assumed to be zero. The water has been supplied continuously to the anode compartment; meanwhile, a small amount of water has been dragged to the cathode compartment by H_2 ions through the membrane (Osmotic drag). The flux of moles of membrane ($N_{H_2O_{\text{mem}}}$) has been calculated and explained in detail in the membrane module (see section 3.2.4.3).

According to Faraday's law of electrolysis, the molar flux of consumed water ($N_{H_2O_{an,\ cons}}$) and generated oxygen ($N_{O_{2,\text{an, gen}}}$) is directly proportional to the flow of electric current. The $N_{O_{2,\text{an, out}}}$ is the flux of moles of oxygen removal from the anode is considered.

$$N_{H_2O_{\text{an,cons}}} = \frac{nI(t)}{2F} \quad (3.6)$$

$$N_{O_{2,\text{an,gen}}} = \frac{nI(t)}{4F} \quad (3.7)$$

$$N_{O_{2,\text{an,out}}} = \frac{O_2(t)}{\tau} \quad (3.8)$$

n is the number of the cells; *I(t)* is the applied current with respect to time; *F* is the Faraday constant; $O_2(t)$ is the moles of oxygen generated in the anode; and τ is the time constant.

The equations (3.7,3.8) have been substituted into equation (3.5) to get the dynamic output of the production.

Note that, for the static model $\frac{dN_{O_{2,\text{an,gen}}}}{dt}$, $N_{O_{2,\text{an, out}}}$, $N_{O_{2,\text{an,in}}}$ are assumed to be zero in equation (3.5), and only the $N_{O_{2,\text{an, gen}}}$ is calculated to calculate the O_2 production.

By solving the above equations, the pressure of oxygen at the anode ($P_{O_{2,an}}$) can be derived via the ideal gas equation as follows.

$$P_{O_{2,an}} = \frac{N_{O_2an,gen} \cdot R \cdot T}{V_{an}}$$

$N_{O_2an,gen}$ is the number of moles of oxygen at the anode respectively; T represents the electrolyser's operating temperature; R is the universal gas constant; and V_{an} denotes the anode volume (electrode).

The partial pressure of water is calculated from the Antoine equation[18].

$$log_{10}(P_{H_2O}) = 8.07131 \frac{1730.63}{233.426+T}$$

The total pressure at the anode (P_{an}) is the sum of the partial pressure of the water and oxygen, described as:

$$P_{an} = P_{H_2O} + P_{O_2an}$$

The mole fraction of water (X_{H_2O}) and mole fraction of oxygen (X_{O_2}) at the anode can be calculated as

$$X_{H_2O} = \frac{P_{H_2O}}{P_{an}}$$

$$X_{O_2} = \frac{P_{O_2an}}{P_{an}}$$

3.2.4.2 Cathode module

In the cathode module, hydrogen is produced when protons pass through the membrane and combine with electrons at the cathode. A similar modelling method is used here as in the anode module, but hydrogen forms as the product instead of oxygen. Thus, the molar flux of water and hydrogen with respect to time at the cathode can be represented as

$$\frac{dN_{H_2O\ ca}}{dt} = N_{H_2O\ ca,in} + N_{H_2O\ mem} + N_{H_2O\ ca,out} \quad (3.9)$$

$$\frac{dN_{H_2ca}}{dt} = N_{H_2\ ca,in} + N_{H_2\ ca,gen} - N_{H_2ca,out} \quad (3.10)$$

In this model, the inlet flux of moles of hydrogen ($N_{H_2O\ ca,\ in}$) and water ($N_{H_2\ ca,in}$) entering the cathode module is considered as zero. Where $N_{H_2ca,out}$ denotes the flux of moles of water removed at the cathode. The flux of moles of hydrogen generated ($N_{H_2\ ca,gen}$) can be calculated from Faraday's first law of electrolysis,

$$N_{H_2\ ca,gen} = \frac{n\ .I(t)}{2F} \quad (3.11)$$

$$N_{H_2ca,out} = \frac{H_2(t)}{\tau} \quad (3.12)$$

I(t) is the current with respect to time, *H_2 (t)* is the moles of hydrogen produced at the cathode, and F is Faraday's constant.

The equations (3.11,3.12) have been substituted into equation (3.10) to get the dynamic output of the hydrogen production.

Note that, for the static model $\frac{dN_{H_2ca}}{dt}$, $N_{H_2ca,out}$ & $N_{H_2\ ca,in}$ are assumed to be zero in equation (3.10), and only the $N_{H_2\ ca,gen}$ is calculated for the H_2 production.

The partial pressure of hydrogen ($P_{H_2,ca}$) can be obtained from the ideal gas law,

$$P_{H_2,ca} = \frac{N_{H_2,ca,gen} \cdot R \cdot T}{v_{ca}}$$

N_{H_2O} and N_{H_2} are the number of moles of water and hydrogen at the cathode, subsequently v_{ca} is the volume of the cathode.

The total pressure at the cathode (P_{ca}) is the sum of the partial pressure of water and hydrogen, described as:

$$P_{ca} = P_{H_2O} + P_{H_2}$$

The mole fraction of each species in the cathode can be calculated as,

$$X_{H_2O} = \frac{P_{H_2O}}{P_{ca}}$$

$$X_{H_2} = \frac{P_{O_2ca}}{P_{ca}}$$

3.2.4.3 Membrane Module

During the electrolysis process, a small portion of water undergoes the oxygen evolution reaction, leading to the generation of protons and oxygen. However, a substantial amount of water is passed through the membrane to keep it hydrated and enable long-term operation. The primary factors that drive the water transport mechanism across the membrane are osmotic drag ($N_{H_2O,od}$), diffusion-driven transport ($N_{H_2o,dif}$), and the hydraulic pressure effect ($N_{H_2O,hp}$). The first two mechanisms will transport water from anode to cathode; the hydraulic pressure mechanism works in the opposite direction of water transport. This mechanism may

change according to the manufacturer's specifications. As a result, the molar flow rate of water through the membrane can be derived as

$$N_{H_2O,mem} = N_{H_2O,od} + N_{H_2o,dif} + N_{H_2O,hp} \quad (3.13)$$

Among the three transport options, osmotic drag is the predominant one, while the other two contribute a minimal amount so that they can be neglected.

As the proton crosses the proton-conducting membrane, it drags water molecules with it, a process known as osmotic drag. This process is quantified by using the dimensionless electro-osmotic coefficient, denoted as N_d. This represents the water molecule traveling per proton from anode to cathode (mol [H_2O]/mol [H^+]). For every molecule of proton, four molecules of water have been dragged through the membrane [16]. The molar flux of water through the membrane due to osmotic drag can be calculated as

$$N_{H_2O,od} = \frac{N_d.\ I(t)}{F} \quad (3.14)$$

Several methods have been used to calculate the osmotic drag coefficient, including fitting parameters, using constant values, and substituting values into quadratic equations. However, no standard value has been used in the literature. In this work, the empirical equation is used as a function of temperature, expressed in Kelvin(K), and is given as

$$N_d = -2.89556 + 0.016T(K)$$

In summary, deriving equation (3.13) and substituting the values yields equation (3.14). The flux of moles of water molecules passed through the membrane ($N_{H_2O,mem}$) is expressed as

$$N_{\mathrm{H_2}O,mem} = \frac{N_d \cdot I}{F}$$

3.2.4.4 Voltage Module

Typically, PEM electrolyser operation is an energy-intensive process. Under standard ideal conditions, the voltage required to operate the PEM electrolyser is known as the reversible voltage, also referred to as the open-circuit voltage. Let's assume there is no heat loss during operation, and the voltage is known as the thermo-neutral voltage. However, in the real world, the voltage required will be higher than the thermo-neutral voltage, due to system inefficiency

and heat loss. These losses may be termed as overpotentials. The total voltage of the cell (V_{cell}) can be calculated as the sum of the reversible voltage and other overpotentials.

$$V_{cell} = V_{th} + V_{act} + V_{ohm} + V_{con} \quad (3.15)$$

V_{th} is the theoretical cell voltage, V_{act} is the activation overpotential, V_{ohm} is the ohmic overpotential, and V_{con} is the concentration overpotential. The overpotentials arise due to the accumulation of gases such as oxygen and hydrogen in the catalyst layer of the cathode and anode. For the current density less than 3 A/cm², the activation overpotentials and ohmic overpotentials are significantly higher than the concentration overpotentials. Therefore, concentration overpotential can be neglected.

Theoretical voltage can be calculated using the Nernst equations as follows.

$$V_{th} = E_0 + \frac{RT}{2F} ln\left(\frac{P_{H_2}\sqrt{P_{O_2}}}{P_{H_2O}}\right) \quad (3.16)$$

where E_0 is the reversible cell voltage under standard conditions, P_{H_2} is the partial pressure of H_2, P_{O_2} is the partial pressure of O_2 and P_{H_2O} is the partial pressure of water. The standard value for E_0 at different operating temperatures can be calculated from the following equations.

$$E_0 = 1.229 - 0.9 * 10^{-3} (T(K) - 298)$$

The activation overpotentials can be described as the voltage required to start the electrochemical reaction in the electrolysis process. In other words, the energy losses are due to charge transfer kinetics in the electrolysis process. Thus, the activation overpotential can be calculated using the Butler-Volmer equation, given as

$$V_{act} = V_{act,an} + V_{act,ca} \quad (3.17)$$

$$V_{act,an} = \frac{RT}{\alpha_{an}F} arcsinh\left(\frac{i}{2i_{0,an}}\right)$$

$$V_{act,ca} = \frac{RT}{\alpha_{ca}F} arcsinh\left(\frac{i}{2i_{0,ca}}\right)$$

Where, α Is the charge transfer coefficient taken as α_{ca} = 0.5 and α_{an} = 2, i is the current density and i_0 is the exchange current density, which is considered as $i_{0,an}$ = 1 * 10^{-7} and $i_{0,ca}$ = 1 * 10^3 in this study.

The ohmic overpotential can be divided into two categories: electronic and ionic resistance. The electronic doesn't account for the significant proportion; it can be neglected. The ionic overpotential is dependent on the membrane water content, temperature, and the operating current. It is calculated by

$$V_{ohm} = I\ R_{ohm} \tag{3.18}$$

$$R_{ohm} = \frac{t_{me}}{\sigma_{me}}$$

σ_{me} ,is the membrane conductivity can be obtained from the equation below

$$\sigma_{me} = (0.00514 \cdot \lambda_m - 0.00326) \cdot exp\left[1268\left(\frac{1}{303} - \frac{1}{T}\right)\right]$$

λ_m, is the water content of the membrane and can be calculated as

$$\lambda_m = 0.08533 \cdot T(K) - 6.77632$$

On the other hand, the electronic overpotential has been negotiated, due to low current density (less than 3A/cm^2), which accounts for the very minimal losses. But some literature uses a constant value for their model. Finally, the total cell voltage can be calculated by adding equations (3.16, 3.17, and 3.18).

3.2.5 Efficiency

The voltage efficiency (η_{voltage}), which reflects the electrochemical effectiveness of the cell, is given by the ratio of thermoneutral voltage (E_{tn}) to actual cell voltage (E_{cell}).

$$\eta_{voltage} = \frac{E_{tn}}{E_{cell}}$$

A higher actual cell voltage results in lower voltage efficiency due to increased overpotential losses. Therefore, understanding and minimising these losses is crucial for improving the overall performance and energy efficiency of the PEM electrolyser system.

3.3 Results and discussions

This section presents the results of the static and dynamic response of the PEM electrolyser Python model coupled with a variable power source to predict the hydrogen (H_2) production behaviour. The analysis is conducted over a 12-hour period representing a solar day, where the input power varied continuously from morning to evening. While the complete stack-level model was developed in the above section 3.2.4, this analysis utilises a reduced set of governing

equations sufficient for simulating the transient behaviour under variable input conditions. The Python coding for the model is presented in (Appendix – 1, 2).

3.3.1 System specifications.

The simulated system consists of a 20 kW solar PV panel connected to a 10 kW PEM electrolyser. The solar power profile used in the model were obtained from the open-source database [40] and represents a 12-hour period (6:00 AM to 6:00 PM), resulting in a total of 720 data points at 1 minute interval.

The specifications of the electrolyser are based on Nel Hydrogen's S-series PEM electrolyser model [41] and are summarised in Table 3-2. Some parameters are not available on the manufacturer's website, so the values from the literature have been used [18-20]. The thermodynamic parameters are listed in the Table 3-3.

Table 3-2: Specification of the PEM stack.

Parameter	Value	Unit
Number of cells (n)	25	Cells
Molecular weight of water (M_{H2O})	18.016	g/mol
Molecular weight of hydrogen (M_{H2})	2.016	g/mol
Molecular weight of oxygen (M_{O_2})	31.988	g/mol
Membrane thickness (t_{me})	0.0254	cm
Active cell area (A)	100	cm^2
Flow rate of water	48.61	mol/h
Thermo − neutral voltage (E_{tn})	1.48	V
Volume of cathode & anode (Van & Vca)	0.001	m^3

Table 3-3: Thermodynamic parameters used in the simulation.

Parameters	Value	Units
Universal gas constant (R)	8.314	J/(mol·K)
Thermo − neutral voltage (E_{tn})	1.48	V
Faraday constant (F)	96485	C/mol
Operating temperature (T)	353.18 (80)	K (°C)

The following section focuses on assessing the electrolyser's performance under variable power input by evaluating overpotentials and voltage efficiency before analysing the dynamic behaviour of H_2 production.

3.3.2 Polarisation curve

The polarisation curve is a key performance indicator for a PEM electrolyser, as it shows the relationship between cell voltage and current density. Figure 3-3 presents the polarisation behaviour at an operating pressure of 1 atm and temperature of 80°C. This curve is used to assess various internal voltage losses occurring at different operating conditions. The total cell voltage increases with current density, and the rise can be attributed to three main types of losses. Typically, the voltage loss occurs through three different regions, namely activation loss, ohmic loss, and concentration loss.

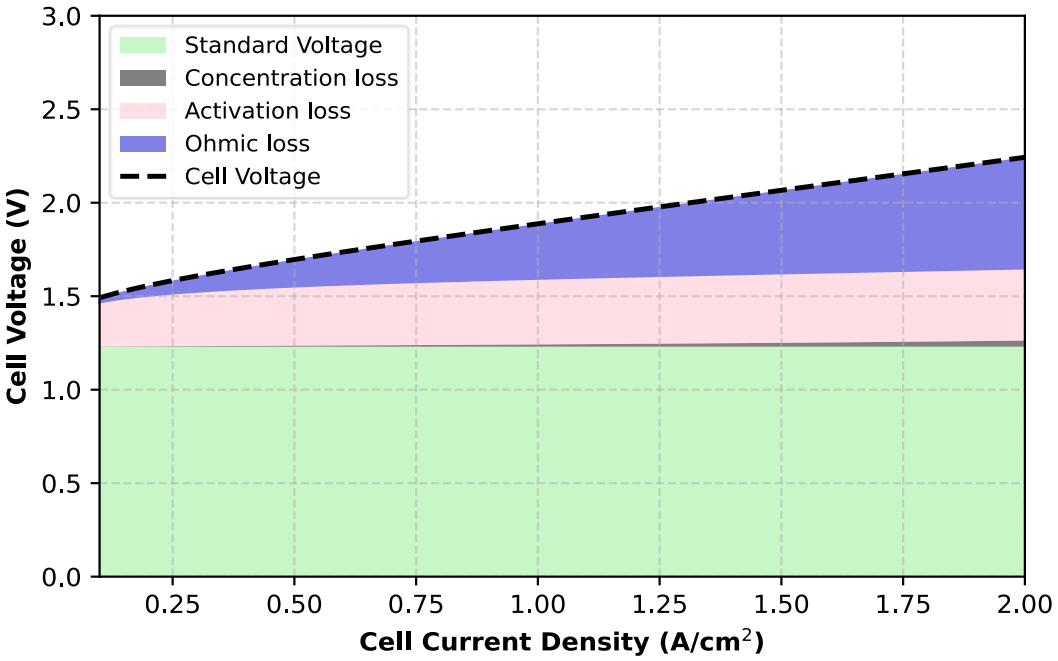

Figure 3-3: Current and voltage characteristics of the PEM electrolyser under at 80°C and 1 atm.

Activation losses dominate at low current densities due to sluggish electrochemical reaction kinetics at the electrodes. As the current density increases, ohmic losses become more prominent, rising linearly because of resistance to ion transport through the membrane and the electronic resistance within the cell components. At even higher current densities, concentration losses can occur when the supply of reactants becomes limited, leading to a sharp

rise in cell voltage. However, in the present study, concentration losses are observed to be minimal.

3.3.3 Voltage efficiency of the cell

Figure 3-4 illustrates the variation in voltage efficiency of the PEM electrolyser with respect to cell voltage. Voltage efficiency is defined as the ratio of the thermo-neutral voltage (V_{th}) to the actual operating voltage (V_{cell}) , and it serves as a key performance indicator for electrolysis systems.

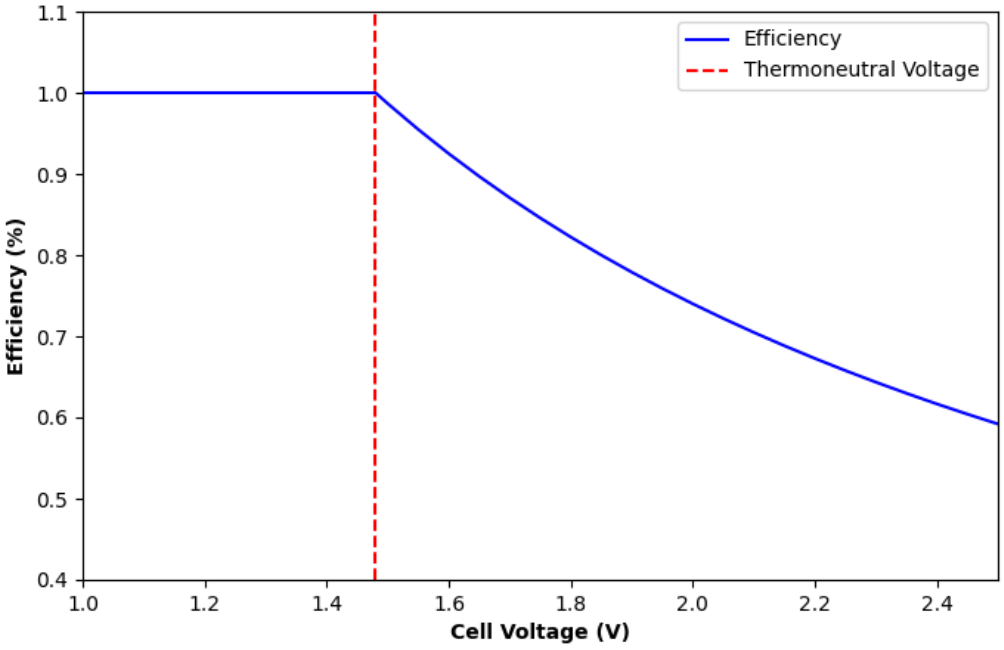

Figure 3-4: The voltage vs voltage efficiency of the electrolysis cell

As shown in the figure, the efficiency remains constant and close to 100 percent, when the cell voltage is below the thermo-neutral voltage, which is indicated by the red dashed vertical line at approximately 1.48 V. This implies that the electrolyser is operating with minimal overpotentials, and that the supplied electrical energy is effectively used for the water-splitting reaction.

At the thermoneutral point (1.48 V), the system is in a state where all the energy required for the reaction, both electrical and thermal, is provided electrically. Beyond this point, as the cell voltage increases, the efficiency begins to decline. This decrease in voltage efficiency is due to the rise in electrochemical losses, including activation and ohmic overpotentials. At higher

voltages, a larger portion of the input energy is dissipated as heat rather than being converted into chemical energy in the form of hydrogen.

Therefore, optimizing the operating voltage is critical for improving the overall energy performance of PEM electrolyser systems.

3.3.3. Power Inputs

The solar panel's installation capacity is 20 kW. It represents the power produced from solar energy in a daytime data set from 6:00 AM to 6:00 PM in the summer, taken at a 1-minute interval.

Figure 3-5 illustrates the variation in solar power generation for the 12-hour period. The power output gradually increases in the morning, peaks around midday, and then declines towards the evening. The black dotted line in the figure represents the maximum power that the 10 kW electrolyser can consume at full capacity.

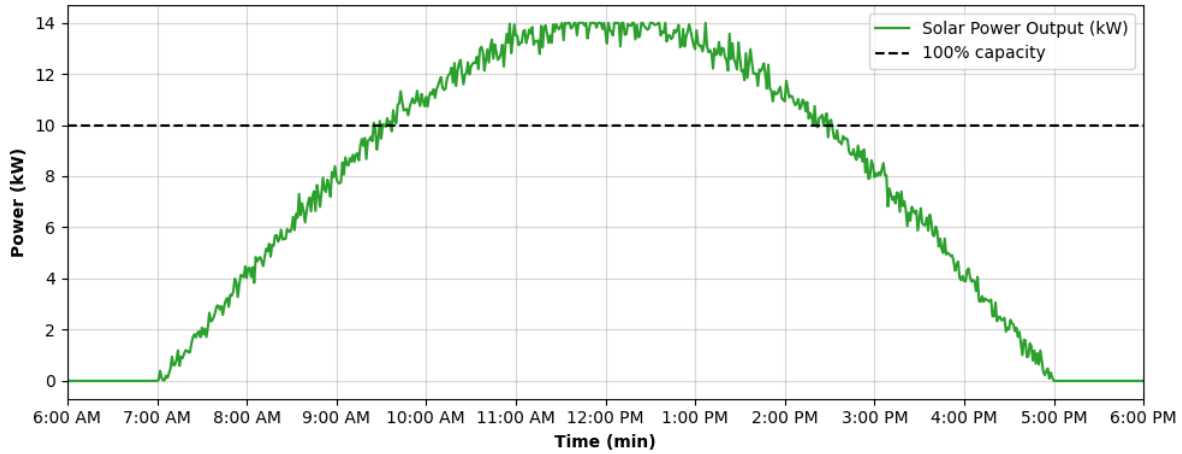

Figure 3-5: Solar power profile from 6:00 AM to 6:00 PM.

Figure 3-6 represents the input current and voltage of the PEM electrolyser model throughout the 12-hour period. The voltage exhibits a non-linear relationship in response to rising current, due to the combined effects of activation and ohmic losses. During the lower current period, the voltage remains relatively stable around 1.4 - 1.6 V. However, as the solar input increases and the current reaches its peak in midday, the voltage increases significantly, reaching up to 2.14 V per cell. This behaviour matches the expected trend from the polarisation curve, where activation and ohmic overpotentials cause the voltage to rise proportionately at higher current.

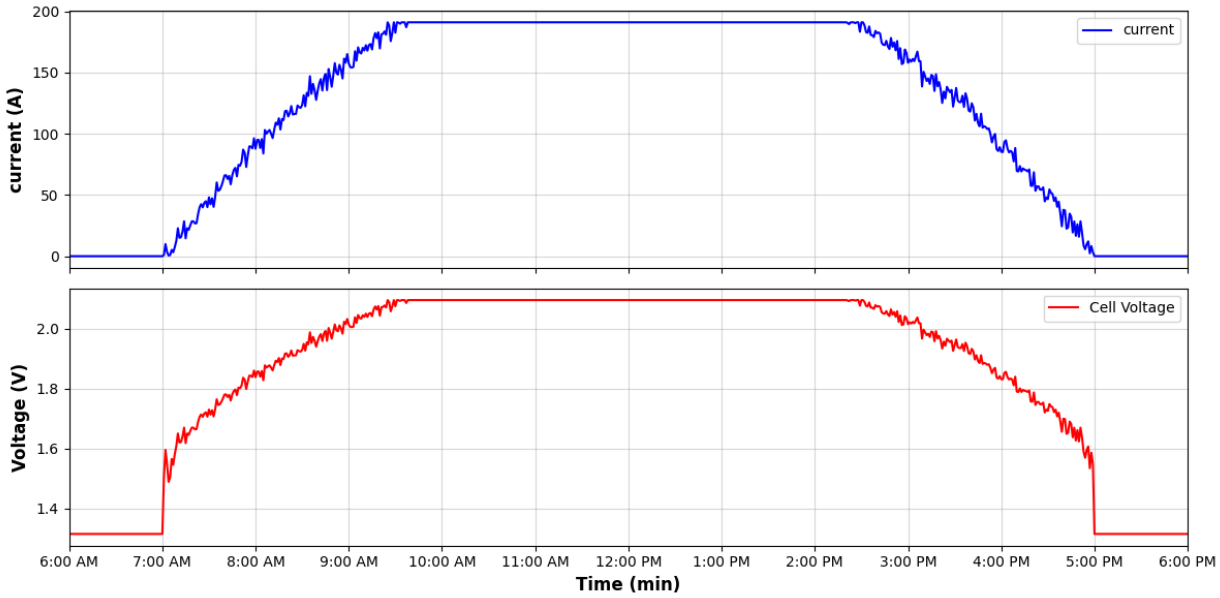

Figure 3-6: Input current and voltage response of the PEM electrolyser over a 12-hour period for the single cell in the stack.

3.3.4 Static and Dynamic H_2 Production Comparison

Figure 3-7 compares the hydrogen production rates predicted by the static and dynamic models over a 12-hour solar day, from 6:00 AM to 6:00 PM. The production rate is expressed in kilograms per minute (kg/min). In the static model, hydrogen production closely follows the input current. This is because the model assumes that all electrical energy is instantaneously and fully converted into hydrogen, without accounting for system delays or gas dynamics.

In contrast, the dynamic model uses a time constant (τ = 5 minutes), which causes a delayed response in hydrogen output. The time constant values do not significantly affect hydrogen production, but it minimises the lag during period of rapid fluctuation based on the time constant values; therefore, a time constant of 5 minutes was chosen for the model. This delay is most noticeable in the early morning (6:30 AM to 9:00 AM), when the input power increases rapidly. During this period, the dynamic model underestimates hydrogen production compared to the static model, as the system takes time to accumulate and release hydrogen.

Both models yield similar production rates during midday (9:00 AM to 3:00 PM), as the system reaches a steady state, there is no dynamic lag to enact on. In the late afternoon, as solar power decreases, the dynamic model again lags the static model due to delayed gas release. With larger time constants the lag between the two models increases but over a full day H_2 production will remain similar.

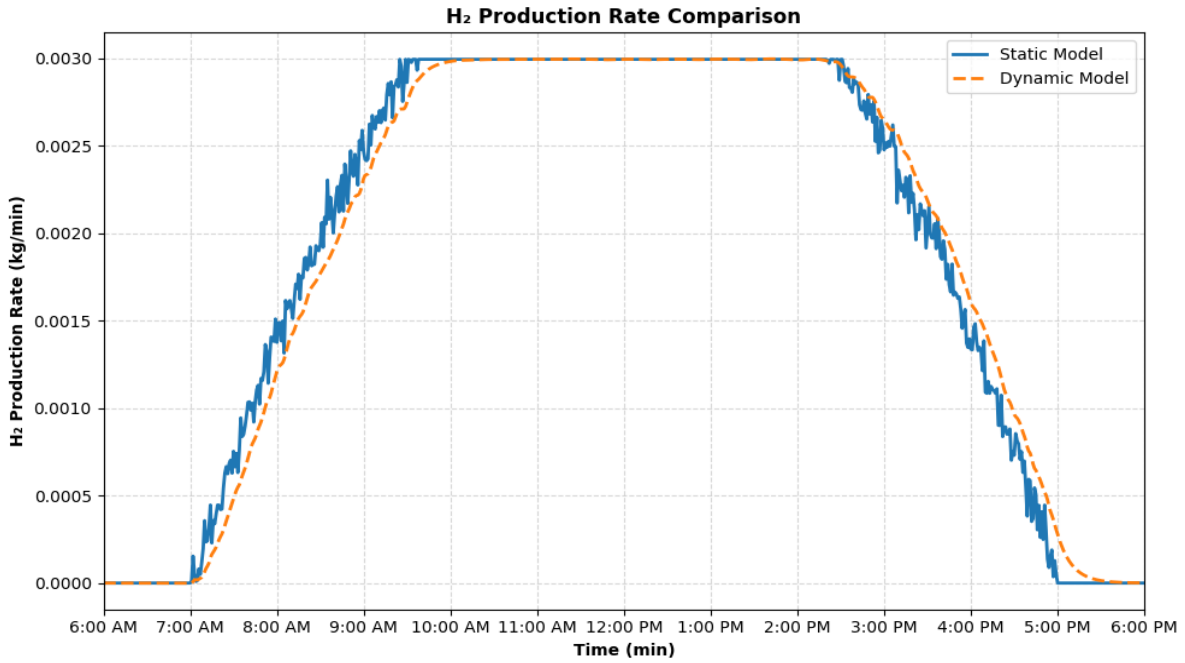

Figure 3-7: Comparison between the hydrogen production rates from the static and dynamic models during a 12-hour solar day, from 6:00 AM to 6:00 PM.

This comparison reveals an important limitation of the static model, which is that it tends to overestimate hydrogen availability initially during rapid power changes. In renewable-powered systems, such overestimation can lead to incorrect sizing of components like compressors, storage tanks, and purification dryers.

Although it is more complex, the dynamic model better represents how the real system behaves when the input changes. Therefore, it is more suitable for designing and controlling the system.

3.3.5 Cumulative H_2 production

Figure 3.8 presents the cumulative hydrogen production (kilograms) over the 12-hour simulation period for both the static and dynamic models, 1 minute time constant.

In the early part of the day, the static model shows a higher cumulative hydrogen output. This is because it assumes instantaneous conversion of electrical energy into hydrogen, without accounting for system loss or gas buildup time.

The dynamic model, on the other hand, exhibits a slower increase in cumulative hydrogen production during the initial hours. This is due to the time constant effect, which delays the release of produced hydrogen. As a result, a gap forms between the static and dynamic production curves.

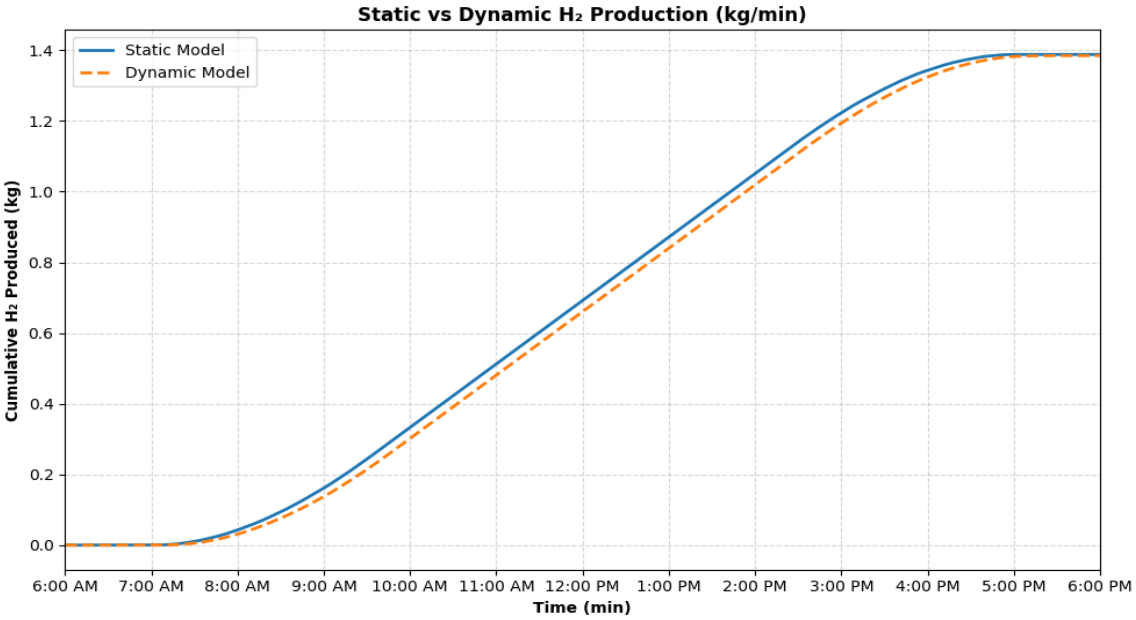

Figure 3-8: Cumulative H_2 production (Static and dynamic model) for a 12-hour period, 1 minute time constant in PEM.

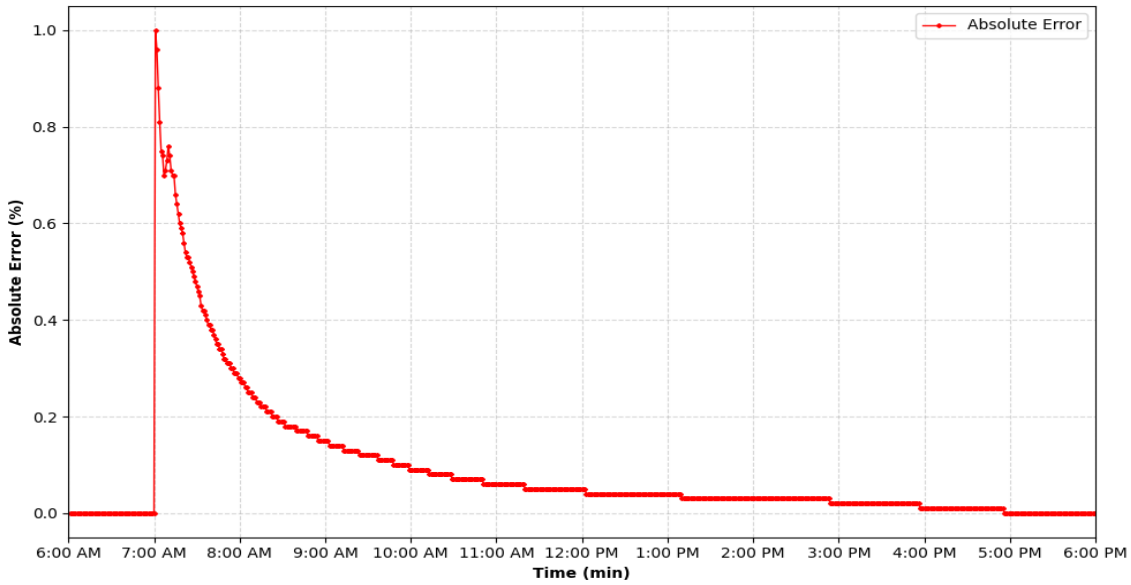

Figure 3-9: Percentage error between cumulative static and dynamic H_2 production.

As the simulation progresses and the input current stabilises around midday and near the end of the day, the difference between the two models is reduced. By the end of the 12 hours (6:00 PM), both models produce nearly the same total amount of hydrogen, with a difference of less than 0.05% as shown in Figure 3-9. The Absolute error is calculated based on the difference between cumulative of static and dynamic model hydrogen production values.

3.4 Conclusion

This chapter presented a comparative analysis of a static and dynamic model of a PEM electrolyser subjected to variable power input from a solar PV system. A Python-based simulation evaluated system performance over 12 hours, representing a typical solar day.

The results show that both models produce nearly the same amount of hydrogen by the end of the 12-hour simulation, with an absolute error of 0.05%. While the dynamic model exhibits slightly lower production at the start, especially during the period of rapid power fluctuation, due to the time constant effect, it reaches a steady state at 100% capacity with no dynamic lag.

For the following chapters, the steady-state simulation has been considered as a reasonable prediction of hydrogen production.

4 Integration of Renewables and Green Hydrogen into Residential Applications

4.1 Introduction

Renewables such as solar and wind, due to their intermittent nature, are not consistent enough to supply electricity every hour of the year to achieve self-sufficiency (without relying on the grid). Green hydrogen produced via electrolysis, powered by renewable electricity, offers a promising solution. Unlike batteries, green hydrogen can store a large amount of energy for extended periods without significant energy loss, making it ideal for offsetting seasonal fluctuations in renewable energy supply and residential demand. The combination of rooftop-installed renewables with PEM electrolyser and fuel cell for residential applications presents a promising solution in the NZ context.

The energy system requires green hydrogen to be produced from surplus renewable electricity, compressed, and stored, then used to generate power when renewable sources are not producing. This potentially creates a closed-loop, carbon-free system with no direct CO_2 emissions (scope 1 emissions) involved. This integration approach could potentially enable 100% self-sufficiency to be achieved for residential applications without relying on a local grid, while also addressing the intermittency and storage challenges associated with standalone systems.

This chapter examines the techno-economic feasibility of integrating rooftop-installed renewable energy sources with green hydrogen to achieve various levels of self-sufficiency at a single residential house. Three options for rooftop renewable energy supply integrated with green hydrogen have been studied: solar PV, wind turbines, and hybrid solar PV and wind systems. Key research questions include:

1. What is the size of an integrated renewable energy-hydrogen system required to meet the residential demand of one house at 50, 70, 90, and 100% levels of self-sufficiency?

2. What is the corresponding Levelized Cost of Energy (LCOE) for the three options at varying self-sufficiency levels, compared to the average yearly residential electricity price in Whitianga as a benchmark cost?

4.2 Methodology

This section provides a detailed discussion of the system specifications, simulation approach, and the energy balance equations used in this study.

4.2.1 System description

A simulation-based approach is used to model the system's energy balance analysis and assess its performance. The system is modelled using an Excel spreadsheet, considering real-time hourly solar and wind profiles, as well as residential demand data. The system comprises a rooftop solar array, a rooftop wind turbine, a Proton Exchange Membrane (PEM) electrolyser, a Proton Exchange Membrane (PEM) fuel cell, an inverter, a compressor, an Energy Management System (EMS), and a high-pressure hydrogen (H_2) storage tank. The efficiency of the system's components has been considered in calculating the supply and demand, as mentioned in Table 4-1. The sizing of the auxiliary equipment's has been decided based on the system and the level of self-sufficiency requirement. The data for solar and wind power generation has been taken from the Renewable Ninja [42]. The residential house demand has been taken from the actual smart metering of a typical house in NZ. [43].

Table 4-1: The systems auxiliary equipment and their efficiency.

Parameters	Value / Range	Source
Residential house demand	Hourly demand profile	[43]
PEM electrolyser efficiency	70%	[19]
PEM Fuel efficiency	50%	[19]
Compressor efficiency	90%	[19]
Inverter efficiency	97%	[44]
Solar / Wind profile	Hourly generation profile	[42]

The system data has been evaluated on an hourly basis over the year to calculate the imbalance in supply and demand. The Energy Management System (EMS) prioritises electricity generated by rooftop solar and wind, is utilised by the house, and then diverts the excess amount to the electrolyser to produce green hydrogen. The produced green hydrogen has been compressed to 350 Bar and stored in the high-pressure storage tank. The stored green hydrogen has been used to produce electricity from the PEM fuel cell. This method is known as the Power-to-Gas-to-Power (P2G2P) transition. The heat produced by a PEM fuel cell and electrolyser can be

recovered and utilized for space heating or preheating hot water. The PEM electrolyser and fuel cell heat recovery have not been considered in this work, but are areas for future work. The Schematic diagram of the integrated system in the residential house has been illustrated in Figure 4-1.

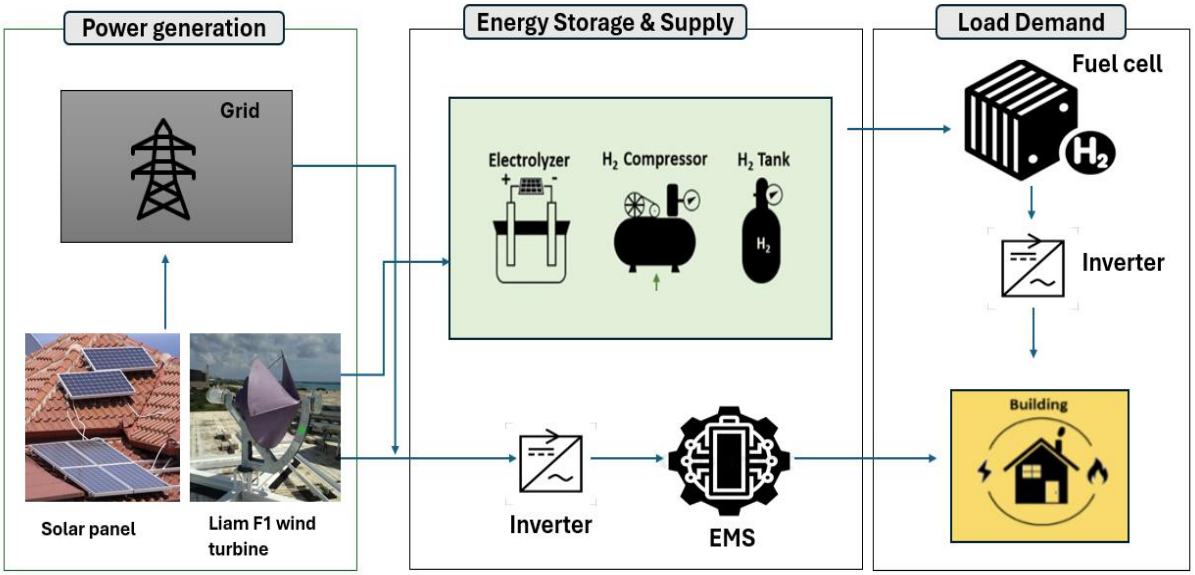

Figure 4-1: Schematic diagram of the integrated system in the residential house.

This system utilizes three options for renewable electricity production, namely, rooftop solar PV, rooftop wind, and rooftop hybrid solar PV-wind, integrated with a PEM FC and hydrogen storage as an additional power supply source for the residential house. The performance of the integrated renewable hydrogen system has been evaluated based on its self-sufficiency, hydrogen production rate, and levelized cost of energy (LCOE). Self-sufficiency denotes the percentage of total residential demand that was met using rooftop renewable generation and stored green hydrogen, without relying on the grid. The model tracks the daily and annual hydrogen production rates to assess how much hydrogen can be stored and how much is needed daily. The LCOE is calculated using the capital cost, operational cost, and expected system lifespan to determine the cost of energy (NZD/kWh).

4.2.2 Energy balance

The energy balance equation has been created for the model based on [45]. The power dispatched from the solar photovoltaic panel and the wind turbine system has been consumed by the residential house, and any excess power left has been fed to the PEM electrolyser to produce green hydrogen and to compress it over time (t). In contrast, when there is a deficit from solar generation, the power produced from FC has been utilized by the residential house

over time (t). The power balance equation for the system is presented in Equation (4.1). The LHS represents the power supply, and the RHS represents the electricity demand in Equation (4.1).

$$P_{FC}(t) \pm P_{PV}(t) \pm P_{WIND}(t) = P_{LOAD}(t) + P_{EL}(t) + P_{COM}(t) \qquad (4.1)$$

Where $P_{FC}(t)$ is the power produced from the fuel cell over the time, $P_{PV}(t)$ is the power produced from solar PV inverter over the time, $P_{WIND}(t)$ is the power produced from the wind turbine inverter over the time, $P_{COM}(t)$ is the power consumption by the compressor over the time, $P_{EL}(t)$ is the electrolyser power consumption over the time and $P_{LOAD}(t)$ is the residential electricity demand over the time. All the power supply and demand are in the AC, except for the electrolyser, where the current produced from the solar panel is used directly, without an inverter. All possible combinations of the power flow are accounted for in the above equation (4.1), and their efficiency has been assessed in detail in equations (4.2-4.4) below.

It is better to consider the efficiency of the fuel cell presented in Eq. (4.2), the electrolyser efficiency in Eq. (4.3), and the inverter efficiency presented in Eq. (4.4).

$$P_{AC}^{FC}(t) = \eta_{FC} \cdot \eta_{AC/DC} \cdot P_{DC}^{FC}(t) \qquad (4.2)$$

$$P_{DC}^{EL}(t) = \eta_{EL,\,AC/DC} \cdot P_{DC}^{EL}\ (t) \qquad (4.3)$$

$$P_{AC}^{PV}(t) \pm P_{AC}^{WIND}(t) = \eta_{PV \pm WIND,\,(AC/DC)} \cdot \left(P_{DC}^{PV}(t) \pm P_{DC}^{WIND}(t)\right) \qquad (4.4)$$

While η_{FC} is the efficiency of the fuel cell, $\eta_{(AC/DC)}$ is the efficiency of the inverter. $\eta_{EL,\,AC/DC}$ is the efficiency of the electrolyser, and $\eta_{PV \pm WIND\,(AC/DC)}$ is the efficiency of the solar PV and wind inverter.

4.2.3 Fuel cell production

The system operates in fuel cell mode when the sky is cloudy or dark at night, and when there is insufficient sunlight or wind. The green hydrogen stored in the high-pressure tank (350 bar) is passed through the PEM fuel cell to produce electricity by combining H_2 with O_2 in the air. The stoichiometric reaction of the PEM FC operation is presented in Eq. (4.5)

$$2H_2(g) + O_2(g) \longrightarrow 2H_2O(g) + electrical\,energy + heat \qquad (4.5)$$

To calculate the efficiency of the fuel cell, the higher heating value (HHV) of the H_2 is taken as the reference value. The hydrogen's energy value is E_{H2} = 142 MJ/kg or 39.44 kWh/kg.

The fuel cell efficiency is the ratio of electricity produced to the hydrogen energy introduced.

$$\eta = \frac{E_{FC}}{E_{H_2}} \tag{4.6}$$

Where E_{FC} is the energy produced by the fuel cell, and E_{H_2} is the introduced energy value of hydrogen. In this work, the PEM FC efficiency is assumed to be 50%.

By combining Equation (4.6) above, the energy deficit for the system can be calculated.

$$m_{H_2} = \frac{E_{DEF}}{E_{H_2} \cdot \eta_{FC,(DC/AC)}} \tag{4.7}$$

Where m_{H_2} is the mass of hydrogen in kg, E_{DEF} is the deficit amount of energy in kWh according to the results, $\eta_{FC,(DC/AC)}$ is the efficiency of the inverter and E_{H2} is the specific energy of 1kg of H_2 in kWh.

4.2.4 Hydrogen production

The surplus energy from the renewables has been used to produce hydrogen from an electrolyser. The surplus energy equation (4.8) is presented as

$$E_{EL} = E_{SUR} \tag{4.8}$$

E_{SUR} is the surplus electricity produced from the renewables, and E_{EL} is the electrolyser electricity consumption.

The amount of hydrogen production entirely depends on the efficiency of the electrolyser. The hydrogen produced has been calculated using equation (4.9).

$$m_{H_2} = \frac{E_{EL} \cdot \eta_{EL}}{E_{H_2}} \tag{4.9}$$

where E_{EL} is the energy input to the electrolyser, η_{EL} is the electrolyser's efficiency, and E_{H2} is the energy value of the hydrogen.

4.3 Results and discussion

This section presents the modelling results for a single residential house from the case study conducted in Whitianga, a rural town in the Coromandel region. The system has been assessed with three options: rooftop solar PV, rooftop wind turbines, and rooftop hybrid solar PV–wind turbine system, each integrated with green hydrogen, to achieve different levels of self-

sufficiency in a single residential application. The model was analysed over 12 months, with hourly data collected from renewable energy supply and residential demand.

For all three options, the analysis has been conducted using the energy balance Equations (4.1–4.9) to calculate the level of self-sufficiency, hydrogen (H_2) storage capacity, and the Levelized Cost of Electricity (LCOE). In this context, the deficit electricity (E_{DEF}) is the amount of electricity supplied by the fuel cell, calculated as the difference between renewable electricity production and residential electricity demand. E_{PRO} refers to the total electricity generated from renewable sources, while E_{CON} denotes the portion of that electricity directly used to meet residential demand. The ($E_{H_2 produced}$) represents the amount of hydrogen produced after meeting electricity demand from the fuel cell, where a positive value indicates surplus hydrogen production and a negative value indicates the hydrogen deficit in kilograms. The detailed results and comparisons of the three options are discussed in the following subsection.

4.3.1 Solar PV integrated system

This subsection assesses the integration of a rooftop solar photovoltaic (PV) system with green hydrogen to meet residential energy demands. Four different solar PV capacities were analysed: 5 kW, 8 kW, 10 kW, and 11 kW, each coupled with appropriately sized PEM electrolyser, PEM fuel cells, and hydrogen storage tanks. The appropriate size is chosen based on the maximum residential demand values in the model for the equipment. Table 4-2 presents the specifications of the four solar-integrated system scenarios, which achieve various levels of self-sufficiency. The results indicate that Scenario 4, which consists of an 11 kW solar PV system combined with a 9 kW PEM electrolyser, a 4 kW PEM fuel cell, and 68 kg of H_2 storage, can achieve complete (100%) self-sufficiency throughout the entire year.

Table 4-2: Specification of the solar integrated system achieving various levels of self-sufficiency.

Variables	Scenario 1	Scenario 2	Scenario 3	Scenario 4
Solar PV	5 kW	8 kW	10 kW	11 kW
PEM E	4 kW	6 kW	8 kW	9 kW
Pem FC	8 kW	7 kW	6 kW	4 kW
Storage	20 kg	32 kg	55 kg	68 kg
self-sufficiency	61%	80%	94%	100%

The 11 kW system (Scenario 4) was further analysed across four seasons in a day, on an hourly basis, and results are illustrated in Figure 4-2. During the summer, due to the long daylight hours, most of the electricity has been supplied by solar PV, and the excess has been utilised by the PEM electrolyser to produce green hydrogen for later use at night or for longer term storage to coverage low sunlight days or periods. In winter, only 6 hours of electricity are produced from the solar panels, due to shorter daylight hours, and for the rest of the time electricity has been supplied from the fuel cell via the stored hydrogen produced during times of high excess electricity, like in the summer.

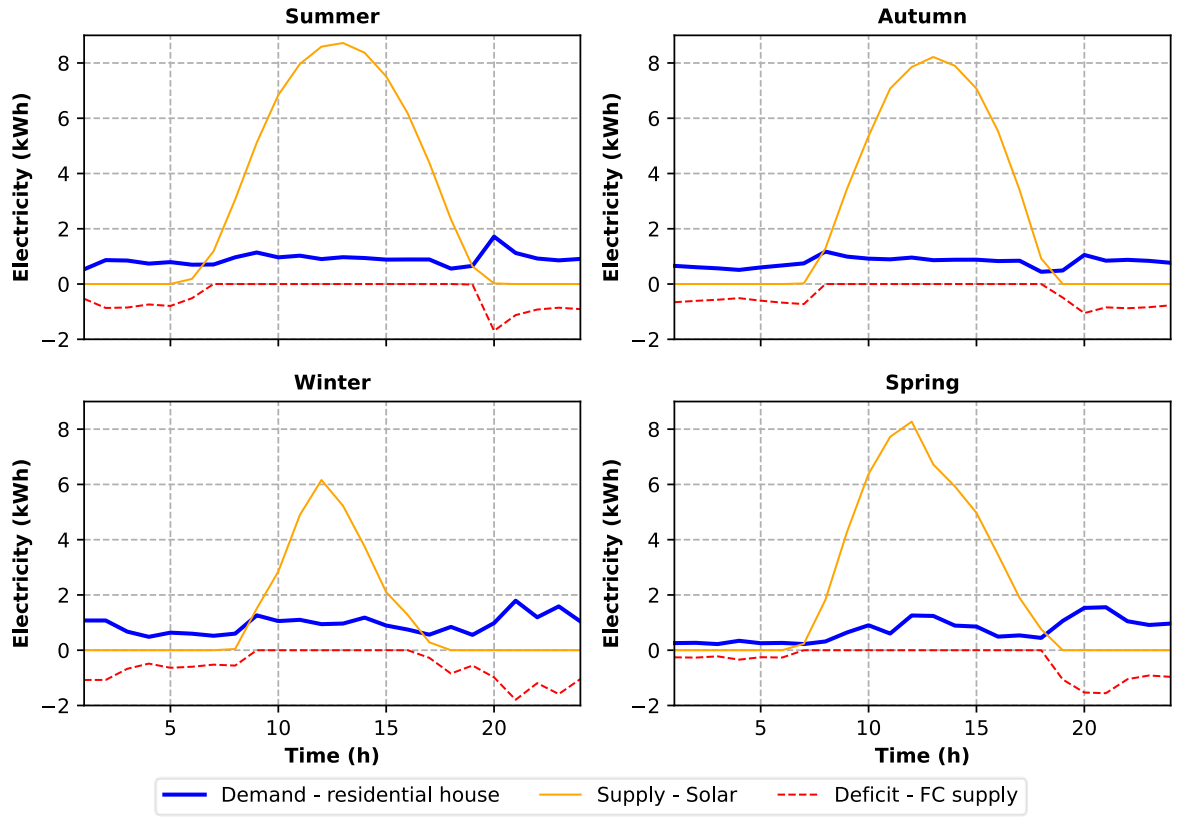

Figure 4-2: Daily power flow analysis of an 11 kW rooftop solar integrated system across different seasons on an hourly basis (Scenario 4).

In spring and autumn, solar levels have increased compared to winter and more electricity has been supplied by solar PV, with excess producing hydrogen for nighttime electricity is supply by the fuel cell. The exact daily balance varies considerably with weather, but with 68 kg capacity of hydrogen storage electricity production from the fuel cell can fill the cap throughout the entire year (Table 4-2). Smaller levels of hydrogen storage and solar PV capacity result in lower levels of self-sufficiency.

An energy balance for the solar integrated system has also been illustrated in Figure 4-3. Starting with 100 units of electricity from Solar PV only 20.1 units have been utilised from the solar energy to meet residential demand, while 76.9 units has been used for green hydrogen production to produce 23.5 units of electricity for the house at times when solar is not available. A large amount of waste heat (56.4 units) has also been produced, of which some could be captured and used for hot water and space heating requirements. This is out of scope and is an area for future work. The process unit efficiency denotes the efficiency of the equipment used in the energy system.

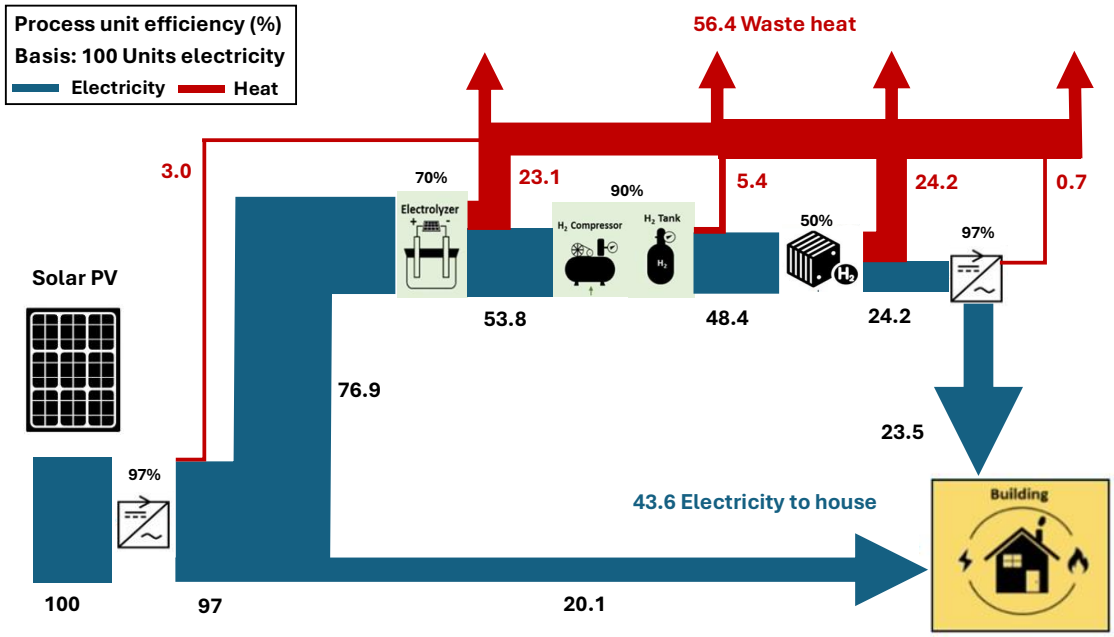

Figure 4-3: Energy flow and efficiency breakdown of a solar PV-hydrogen integrated system to the residential application. (Example)

Monthly, weekly, and daily energy flow modelling was conducted; however, only a summary at the monthly level is presented in Table 4-3 and Figure 4-4. The monthly performance shows that solar energy production (E_{PRO}) exceeded the energy demand needed for self-sufficiency in eight months. This is indicated by the net positive hydrogen production ($E_{H_2\ produced}$) during those months. In contrast, during the winter months (May, June, July, and August), electricity supply required significant support from stored hydrogen via the fuel cell. This is reflected in the net negative hydrogen production during those months. As expected, the demand for electricity generated by the fuel cell (E_{DEF}) peaked in these four winter months when solar energy production was at its lowest.

Table 4-3: Monthly energy balance analysis for an 11 kW solar integrated system over the year.(Scenario 4)

Month	E_{PRO} (kWh)	E_{CON} (kWh)	E_{DEF} (kWh)	$E_{H_2\ produced}$ (kg)
January	2037	375	324	10
February	1712	314	296	7
March	1613	336	309	4
April	1413	325	328	0
May	1075	288	466	-14
June	873	274	498	-19
July	890	267	544	-21
August	1158	266	441	-10
September	1467	209	240	8
October	1601	242	178	14
November	1889	269	187	17
December	1987	397	308	9
Total	17716 (100%)	3561	4120	3 (Excess)

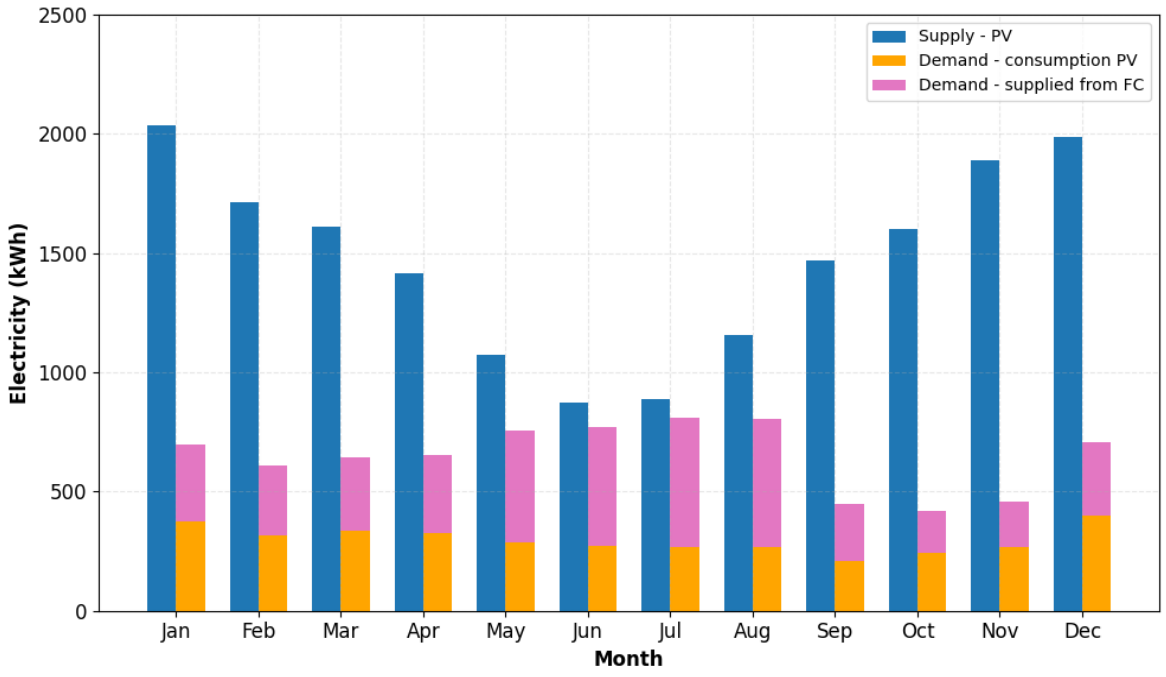

Figure 4-4: Monthly electricity production, consumption, and deficit profile of the 11 kW solar integrated system (Scenario 4).

From Figure 4-4, the maximum solar electricity production has been recorded during the month of January, which is almost 2000 kWh/month. In contrast, the lowest has been recorded during the month of June, which is equivalent to 820 kWh/month. Significant amounts of excess solar PV are needed throughout the year to guarantee supply of electricity via hydrogen and fuel cell However, the annual deficit of 4,120 kWh of electricity needs to be supplied by the fuel cell.

4.3.2 Wind integrated system.

This section evaluates the performance of a wind energy system integrated with green hydrogen and storage for a single residential application. Due to cost and structural concerns, wind turbine installation is less typical for residential applications. However, the Liam F1 wind turbine, developed in the Netherlands, offers a compact and efficient design suitable for rooftop installation [46].

Four different wind turbine capacities: 1.5, 3, 4.5, and 6 kW, were assessed, each coupled with a PEM electrolyser, fuel cell, and hydrogen storage tank. The specifications and results of integrated wind system with different scenarios achieving various levels of self-sufficiency is illustrated in Table 4-4. Among these configurations, Scenario 4, with a 6 kW wind turbine, a 6 kW PEM electrolyser, a 4 kW PEM fuel cell, and 85 kg of hydrogen storage achieved 100% self-sufficiency.

Table 4-4: Specification of the wind-integrated system achieving various levels of self-sufficiency.

Variables	Scenario 1	Scenario 2	Scenario 3	Scenario 4
Wind turbine	1.5 kW	3 kW	4.5 kW	6 kW
PEM E	1 kW	3 kW	4 kW	6 kW
Pem FC	3 kW	3 kW	3 kW	4 kW
Storage	18 kg	29 kg	52 kg	85 kg
self-sufficiency	44%	72%	90%	100%

Figure 4-5 illustrates the hourly power flow throughout the day for each season. The analysis shows that wind generation highly fluctuates throughout the year. In summer, low wind speeds lead to reduced power generation, requiring increased reliance on fuel cells. In contrast, autumn experiences strong wind generation, supplying most of the electricity demand directly. Spring demonstrates moderate performance, with nighttime power supplied from wind and supplemented by a fuel cell during the day. However, in winter, the power has been utilised

from both wind and stored hydrogen. These results indicates that critical trade-off between seasonal supply and demand, in both solar and wind system, highlights the need for further investigation of hybrid approach and how it can fit into the residential settings.

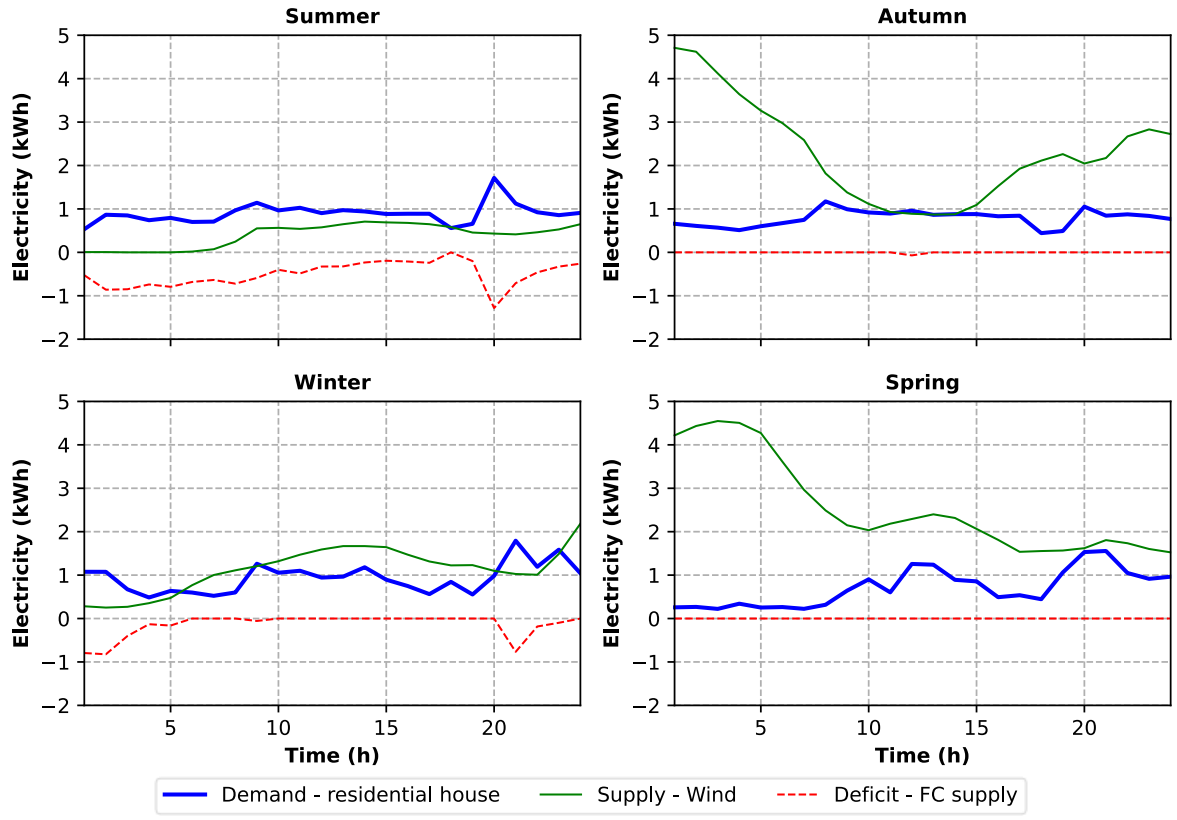

Figure 4-5: Daily power flow analysis of a 6 KW rooftop wind-integrated system across different seasons on an hourly basis (Scenario 4).

The annual energy balance analysis of a 6 kW integrated wind system is presented in Table 4-5. Maximum wind production is observed in August, while the lowest output is recorded in March. The energy balance analysis reveals that, during several months, wind energy production exceeds the residential demand, allowing the excess to be used for H_2 production. However, there is an energy deficit from February to June, which is supplied by the fuel cell due to lower wind availability. On an annual basis, only 35% of the wind-generated electricity is consumed directly by residential households, while the remaining 65% is used for hydrogen production. This seasonal variation directly influences the sizing of the other components of the system. From Figure 4-6, the maximum electricity production from wind has been recorded during the month of August, which is almost 2400 kWh/month. In contrast, the lowest has been recorded during the month of March, which is equivalent to 600 kWh/month. However, the annual deficit of 2,196 kWh of electricity needs to be supplied by the fuel cell.

Table 4-5: Monthly energy balance analysis for a 6 kW wind integrated system over the year (Scenario 4).

Month	E_{PRO} (kWh)	E_{CON} (kWh)	E_{DEF}(kWh)	$E_{H2\ produced}$ (kg)
January	1254	523.73	174	2.53
February	920	428.41	178	-1.93
March	571	327.13	326	-15.20
April	854	422.80	220	-5.54
May	1229	449.51	311	-4.80
June	1232	487.71	282	-3.71
July	1453	613.79	197	3.10
August	2418	641.14	70	27.34
September	1812	382.36	76	20.86
October	2001	368.89	46	26.25
November	1178	343.77	105	8.49
December	1279	513.22	212	0.87
Total	16202	5502	2196	58 (Excess)

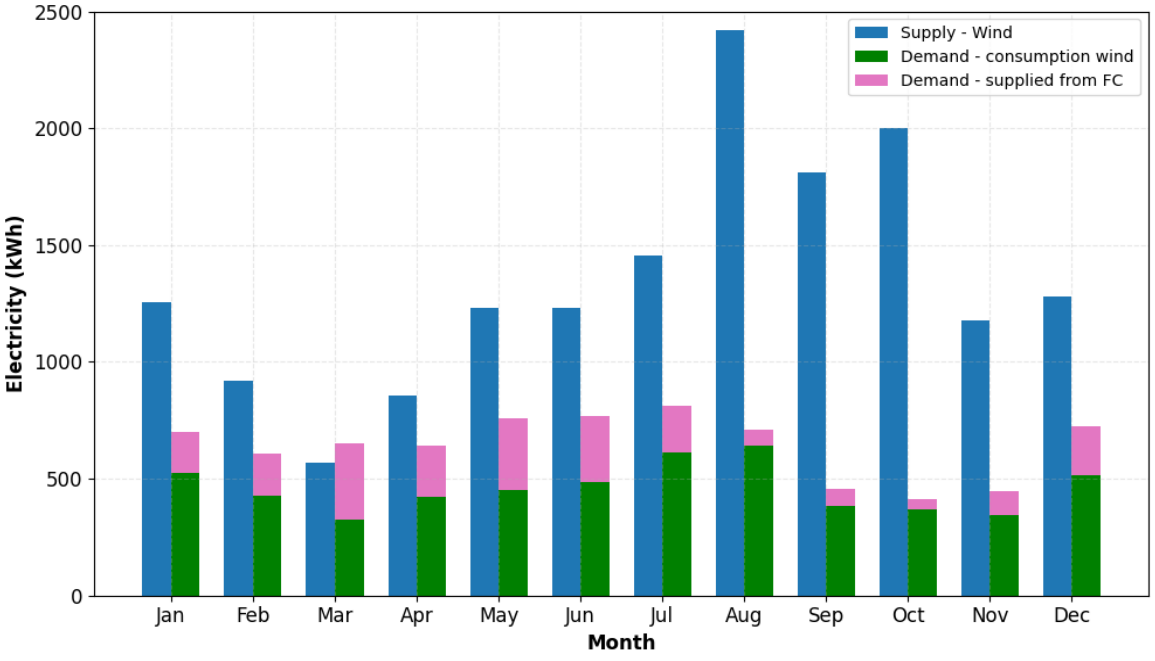

Figure 4-6: Monthly electricity production, consumption, and deficit profile of the 6 kW wind integrated system (Scenario 4).

4.3.3 Integrated hybrid solar PV-wind system energy analysis

This section analyses the hybrid renewable energy system approach comprising rooftop solar PV and wind turbine technology, integrated with green hydrogen production for a single residential house. Although the hybrid approach is less common in residential settings due to complexity and space constraints, recent advancements in technology and a decrease in the cost have made this approach practically viable [9]. The specification of the hybrid integrated system with three scenarios are designed to achieve various levels of self-sufficiency, is illustrated in Table 4-6. Among all, the system with (3 kW solar + 3 kW wind) hybrid capacities is the best possible option to achieve complete self-sufficiency (Scenario 3).

Table 4-6: Specifications of the hybrid integrated system achieving different levels of self-sufficiency.

Variables	Scenario 1	Scenario 2	Scenario 3
Solar PV (kW)	1.5 kW	2 kW	3 kW
Wind (kW)	1.5 kW	2 kW	3 kW
PEM E (kW)	2.5 kW	3 kW	4.5 kW
Pem FC (kW)	4 kW	3.5 kW	3 kW
Storage (kg)	13 kg	28 kg	50 kg
self-sufficiency	61%	80%	100%

Figure 4-7 represents the power flow analysis of the day on an hourly basis across four seasons for the 3 kW + 3 kW optimised hybrid system (Scenario 3). The data highlights the system's ability to balance load and generation more efficiently than standalone solar or wind systems. During the summer, solar PV meets most of the demand, while nighttime consumption is supplied from the fuel cell. In winter, wind generation contributes significantly during both day and night, compensating for the reduced solar generation.

Overall, the hybrid system maintained a consistent power supply for most of the time throughout the year, which may result in reduced hydrogen production and fuel supply, resulting in the reduction of size in the auxiliary equipment's.

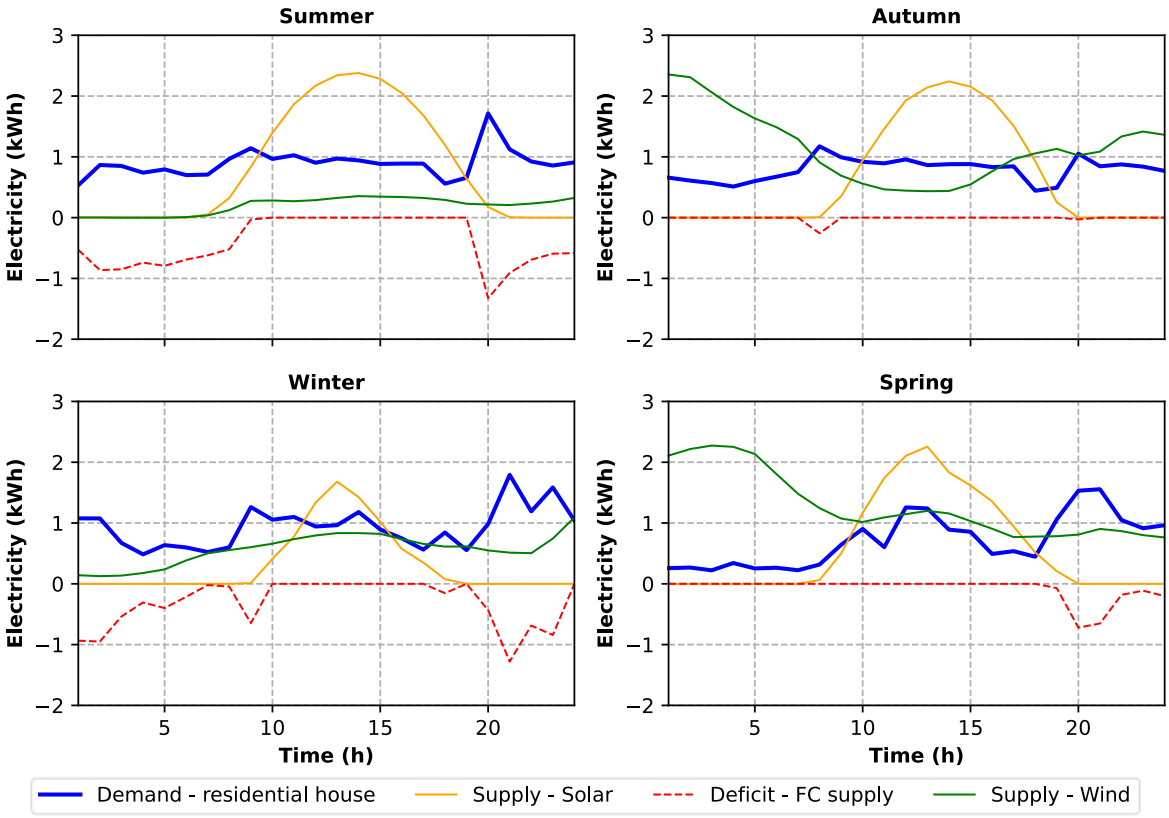

Figure 4-7: Daily power flow analysis of (3 kW & 3 kW) rooftop hybrid solar-PV & wind integrated system across different seasons on an hourly basis (Scenario 3).

The energy balance of the hybrid system monthly is illustrated in Table 4-7. The results indicate that 52% of the annual energy demand was supplied by wind, 18% by solar, and the rest 30% by fuel cell.

Figure 4-8 presents the monthly power flow analysis over the year and highlights the significant seasonal contribution from both solar and wind energy. The hybrid system reduces the H_2 storage capacity, due to a more balanced generation pattern throughout the year. The system is capable of operating for approximately 32% in a year without a fuel cell supply, demonstrating its ability to achieve self-sufficiency.

The hybrid option can provide flexibility and balance to the generation over time, as solar PV supplies daytime energy, especially in summer, while wind turbines can generate power during nighttime or partially in the winter period.

Table 4-7: Monthly energy balance analysis for a (3 kW + 3 kW) hybrid solar PV and wind integrated system over the year (Scenario 3).

Month	E_{PRO} (kWh)	E_{CON} (kWh)	E_{DEF} (kWh)	$E_{H2\ produced}$ (kg)
January	1183	560	138	3
February	927	456	151	-1
March	725	414	239	-9
April	812	462	181	-5
May	908	486	274	-9
June	854	479	291	-11
July	969	553	258	-8
August	1525	606	105	10
September	1306	387	71	12
October	1437	374	41	16
November	1104	376	73	9
December	1182	566	160	1
Total	12933	5718	1981	58 (Excess)

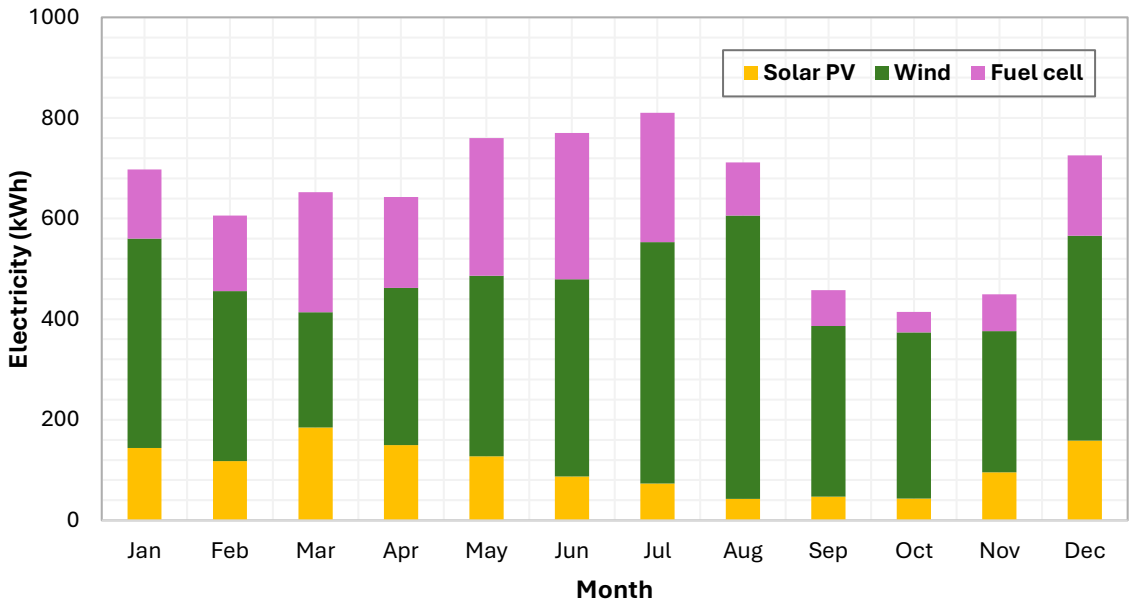

Figure 4-8: Monthly electricity consumption profile from solar, wind and fuel cell of (solar 3 kW + wind 3 kW) hybrid integrated system (Scenario 3).

4.3.4 H_2 storage analysis for three options with the integrated system

Hydrogen storage capacity is crucial for maintaining a reliable energy supply in a renewable-based system where hydrogen is the energy storage medium, especially when generation and demand do not match. In this study, green hydrogen is produced from excess solar and wind energy via a PEM electrolyser, stored at 350 bars, and later used in a PEM fuel cell during periods of energy deficit.

Table 4-8 compares the hydrogen production, consumption, and storage needs for three systems: solar PV (11 kW), wind (6 kW), and a hybrid solar-wind system (3 kW + 3 kW), each designed to achieve 100% self-sufficiency. (Table 4-2, 4-4, 4-6).

Table 4-8: Annual H_2 production and storage requirements of the different systems.

Systems	H_2 produced (kg)	H_2 consumed (kg)	H_2 excess (kg)	H_2 storage tank size (kg)
Solar PV	250	247	3	68
Wind	191	131	58.2	85
Hybrid solar PV & wind	128	119	9	50

As shown in Table 4-8, all three systems generate slightly more hydrogen than they consume over a year, resulting in a small surplus. However, the amount of hydrogen storage required varies significantly based on the system. The solar PV system requires 68 kg of storage, primarily because it generates a large proportion of electricity during the summer period, and the storage capacity needs to be sufficient to carrier over into winter. The wind-integrated system produced less hydrogen compared to solar PV but requires storage of 85 kg to deal with the irregularity and highly variable nature of wind generation throughout the year.

In contrast, the hybrid integrated system had the most balanced generation pattern across the seasons, reducing the storage requirement to 50 kg and still achieving self-sufficiency. Figure 4-9 presents the cumulative hydrogen storage requirements over time for three different system that achieves complete (100%) self-sufficiency. The findings indicate that the hybrid system, which combines both solar and wind energy, achieves more efficient use of hydrogen storage. This combination helps to balance fluctuations in energy generation, resulting in a more stable

power supply and a reduced need for large storage capacity. As a result, energy management is improved, and both storage size and overall costs are lowered.

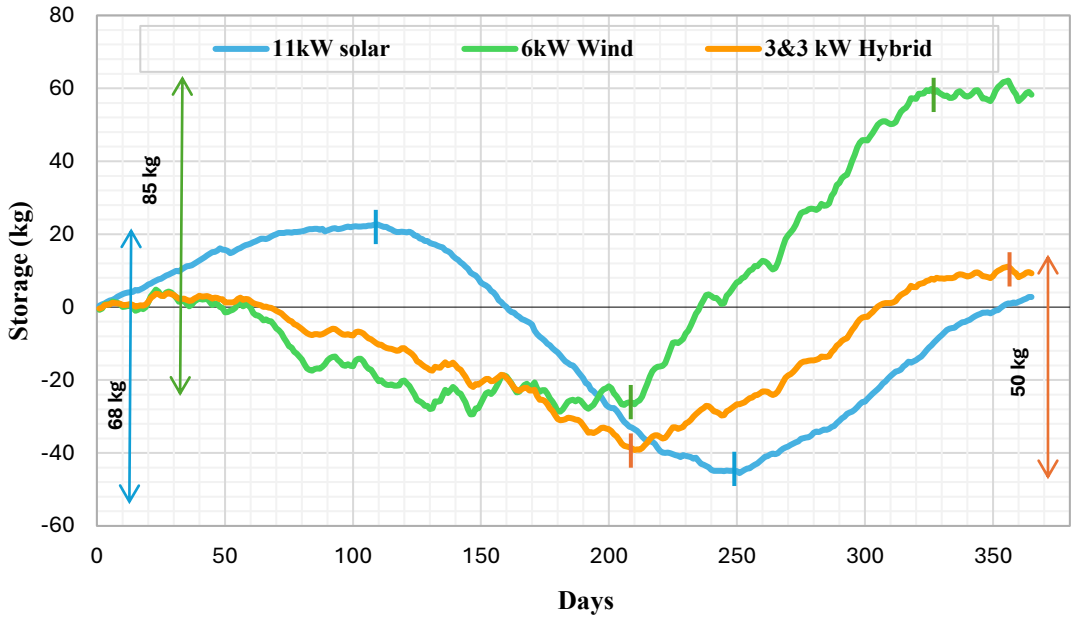

Figure 4-9: The cumulative production of green H_2 throughout the year for the three different systems achieving complete (100%) self-sufficiency.

4.3.5 Levelized cost of energy (LCOE)

Levelized Cost of Energy (LCOE) is a crucial metric for assessing and comparing the economic viability of different energy production technologies. It represents the average cost per unit of electricity (NZD/kWh) generated over the system's lifetime by calculating its total capital, operational, and maintenance expenses over its lifetime.

In this study, LCOE is calculated for each of the energy integrated options – solar PV, wind, and hybrid solar–wind under various self–sufficiency levels (50%, 70%, 90%, and 100%). The LCOE is calculated using the standard formula [47].

$$LCOE = \frac{\sum_{t=0}^{n} \frac{C_t}{(1+r)^t}}{\sum_{t=0}^{n} \frac{E_t}{(1+r)^t}}$$

Where t is the total lifetime, usually taken in years, C_t is the total cost of the system, including capital expenditure (CAPEX), operational expenditure (OPEX), and maintenance over its lifetime. E_t is the total electricity produced over the system's lifecycle, and r is the discount factor. The analysis is conducted for 25 years, with a discount rate of 6%. The OPEX and

maintenance are assumed as 0.5% of the CAPEX. The costing parameters for the system auxiliary components cost have been listed in Table 4-9.

Table 4-9: Cost specifications of the auxiliary equipment of the system [48, 49].

Specifications	Cost	
PEM electrolyser CAPEX (with BOP)	1,600.00	NZD/kW
PEM Fuel cell CAPEX (with BOP)	800.00	NZD/kW
Solar PV CAPEX (with inverter)	2,400.00	NZD/kW
Wind turbine CAPEX (with inverter)	2,665.60	NZD/kW
H_2 storage CAPEX (including compressor)	960.00	NZD/kg

All three integrated options with complete self-sufficiency (100%) are assumed to be off grid. For the rest of the self-sufficiency level, the electricity deficit has been supplied from the local grid. No revenue generation from the H_2 production has been considered in this work.

Figure 4-10 presents the LCOE values for three options across varying levels of self-sufficiency. The x-axis represents the proportion of self-sufficiency, while the y-axis shows the LCOE in NZD/kWh. The capacity (kW) in the figure represents the renewable energy source capacity such as solar, wind and combined values of the hybrid system. The Grid electricity price (Whitianga) is kept as the benchmark reference value to compare the LCOE of the other three options.

Among the three options, the rooftop solar PV system has the highest LCOE, at approximately 0.78 NZD/kWh with 100% self-sufficiency. The increase in cost is due to oversized capacities of the equipment that bridge seasonal generation deficits, especially during the winter period. The rooftop wind option is slightly more cost-effective, with LCOE of 0.73 NZD/kWh, although it requires the largest H_2 storage capacity due to higher variability in power output and unpredictability.

In contrast, rooftop hybrid options consistently achieve the lowest LCOE across all self-sufficiency levels, with the 0.52 NZD/kWh to achieve 100% self-sufficiency. The cost-effectiveness indicates that the hybrid approach smooths the supply profile and reduces the requirement for hydrogen storage capacity. Across all configurations, the LCOE increases with

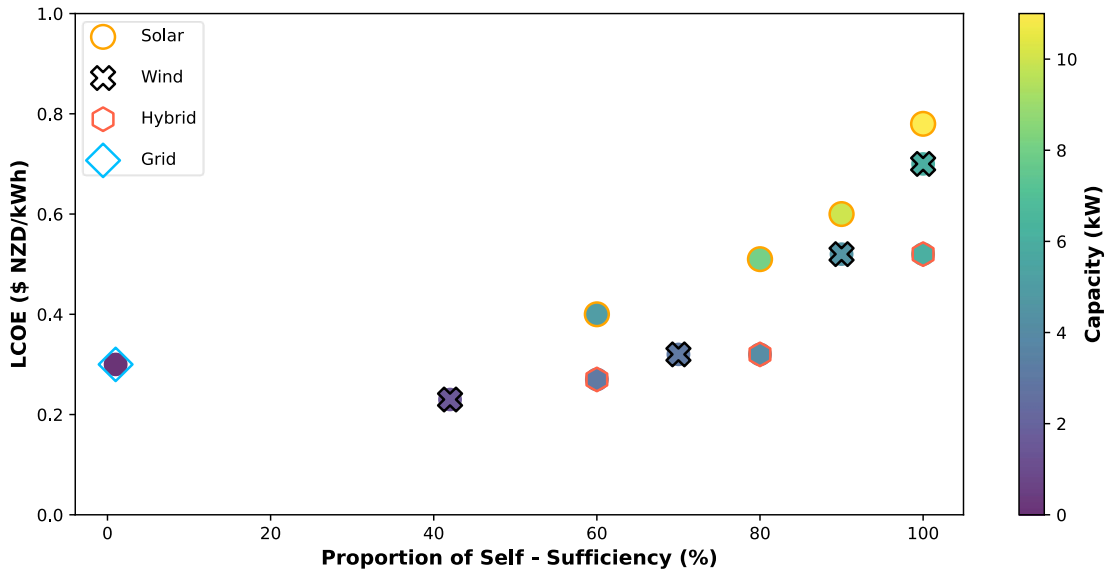

Figure 4-10: LCOE of the three different integrated systems with various levels of self-sufficiency.

Higher self-sufficiency levels decrease with the introduction of wind and solar PV as a hybrid. The high LCOE of each system is due to the expensive installation of hydrogen storage, which accounts for approximately 40% of the CAPEX for the hybrid approach, 80% for wind only, and 74% for solar. With a 50% reduction in hydrogen storage cost, LCOE for the hybrid approach may drop 0.34 NZD/kWh.

4.4 Conclusion

This chapter has systematically evaluated the techno-economic feasibility of integrated green hydrogen systems incorporating rooftop solar PV, wind turbines, and hybrid solar PV and wind turbine systems for a single residential application.

Among the three options, the hybrid solar PV and wind integrated system is the most balanced and cost-effective, achieving 100% self-sufficiency at a levelized cost of energy (LCOE) of 0.52 NZD/kWh. The other systems achieve 100% self-sufficiency at relatively higher LCOEs.

The hybrid results are especially relevant for the rural and remote areas of NZ, such as Northland and the northeastern part of the North Island, where the electricity prices are high, 0.35-0.45 NZD/kWh, due to transmission constraints and geographic isolation. In this context, hybrid renewable energy systems could reduce reliance on the national grid, enhance energy security, and promote a decentralized approach to energy production.

Additionally, from an environmental perspective, scaling the hybrid approach to all rural residential houses nationwide could potentially reduce annual emissions by up to 47.64 kilo tonnes of CO_2-equivalent (kt CO2-e), supporting the nation's sustainable goals.

5 Case study: Integration of Renewables and Green Hydrogen into the Community.

5.1 Introduction

Most of NZ's national electricity is produced from renewables, but still, 17% of the electricity demand was supplied from fossil fuels in 2023 [50]. Having closer to 100% renewable electricity generation needs to be addressed to achieve the net-zero emissions target by 2050 [51]. Small urban centres (remote towns) play a significant role in the nation's economic growth and consume a substantial proportion of electricity from the local grid.

A case study has been conducted in the Coromandel region, renowned for its summer beaches and holiday destinations, focusing on integrating the region with renewables and green hydrogen (H_2) to support transportation and energy needs of the community. During the peak tourist seasons, the Coromandel region experiences a noticeable increase in energy demand compared to regular days, due to a huge influx of temporary residents and visitors from across NZ and the world.

The objective of this work is to compare and contrast the merits of supplying 32 MW_p of new solar PV electricity to the Whitianga region (Lodestone Energy), covered by the Whitianga substation network, through either a single 32 MW_p solar farm scenario or a dispersed, equal-generation 4.3 kW_p PV system per house of rooftop solar scenario.

A holistic approach to renewable energy modelling for the community has been considered, encompassing demand for transportation, commercial, and residential applications. For the rooftop solar scenario, back-up electricity storage from EV batteries is evaluated using the already established Vehicle-to-Grid (V2G) approach [52]. The techno-economic feasibility of the two scenarios has been assessed using the Net Present Value (NPV) method, covering 25 years.

5.2 Case study

The case study has been implemented in the NZ context to explore the integration of renewable energy and green hydrogen into the local communities. The Whitianga region – located in the Coromandel Peninsula, known as a popular holiday destination, has been chosen for conducting the case study. According to the 2023 census, the population of the region is 7774 residents and spans an area of 17.2 km^2 [53].

Due to its long sunny hours and geography, it is a suitable location for installing solar energy, with an average irradiance and temperature of 5 kWh/m² and 16 °C annually. By the end of 2025, Lodestone Energy, a pioneer in solar photovoltaic power generation, plans to install the 32MW_p solar farm in Whitianga, a town in the Coromandel district. The electricity generated from the solar farm is expected to be fed into the local grid and sold on the retail market.

During the peak seasons, such as Easter weekends, New Year, and Christmas holidays, the population of the town is increased by 5 times the normal population. The population increase puts pressure on the local grid, resulting in voltage drops and power outages throughout the region (community). Typically, 50-60 hours per year, mainly during the holidays, the local grid network can't sustain the supply during contingencies [54]. In this study, the local grid network (local grid) refers to the distribution of electricity from substations to nearby areas, including surrounding towns and villages. In contrast, the grid network (or national grid) refers to the transmission of electricity from power plants to substations via high-voltage transmission lines.

This study investigates the feasibility of using solar energy to directly meet the local community's energy demand, rather than exporting to the local grid network at a cheaper price. To evaluate this, two renewable integration scenarios are used in this work. Scenario one is a centralised approach, and power is generated from the solar farm to supplement the community's residential, commercial, and transportation demand. Scenario two uses a decentralised approach, and power is generated from the rooftop solar panel to supplement the residential demand of the community with Vehicle to Grid (V2G) technology.

These two methods are assessed from both a technical and economic perspective, with a focus on long-term sustainability and community energy resilience.

5.3 Methodology

5.3.1 General overview of the modelling approach

The integration of renewables and green hydrogen technology into the community has been divided into two scenarios to assess its techno-economic feasibility and viability of local renewable electricity production. Scenario one comprises a centralised approach to supply the electrical demand from a 32 MW_p solar farm to supplement the energy needs of the community. Scenario two consists of residential installation of rooftop solar panels on each house, totalling the same 32 MW_p capacity for the community.

5.3.1.1 Modelling of scenario one

The modelling process block diagram for scenario one is illustrated in Figure 5-1. The model evaluates the renewable integration through a hierarchical allocation framework. The analysis has been conducted using an Excel spreadsheet model.

The system has two primary components: power supply sources and the electricity demand category. The supply side consists of solar farms (S_R) and the local grid network (S_G). The demand side consists of residentially occupied dwellings (D_A), residentially unoccupied dwellings (D_B), commercial demand (D_C), and transport demand (D_D). The transport demand (D_D) comprises green hydrogen and EV charging demand.

The model uses an algorithm that prioritises solar generation to meet electrical demand categories in a hierarchical order. The system uses the following process sequential steps.

1. Initial steps:

   The model calculates the difference between solar farm production (S_R) and residential occupied dwellings demand (D_A), resulting in either an excess or deficit value as X_1.

2. Conditions check:

   If $X_1 < 0$ (deficit), electricity is supplied from the local grid (S_{G1}).

   If $X_1 > 0$ (excess), the surplus has been sent to the next demand category.

3. Repetition:

   The process repeats for the remaining demand category.

   - For residential non–occupied dwellings (D_B):

     $$X_1 – D_B = X_2$$

     If $X_2 < 0$, the local grid supply S_{G2} is used.

   - For commercial demand (Dc):

     $$X_2 – D_C = X_3$$

     If $X_3 <0$, the local grid supply is used.

   - For transport demand (D_D):

     $$X_3 – D_D = X_4$$

     If $X_4 < 0$, the grid supply is used

4. Grid supply approach (S_G):

   At each step, if the solar output is insufficient (i.e., if $X < 0$), the model draws the electricity from the local grid (S_{G1}, S_{G2}, S_{G3}, S_{G4}).

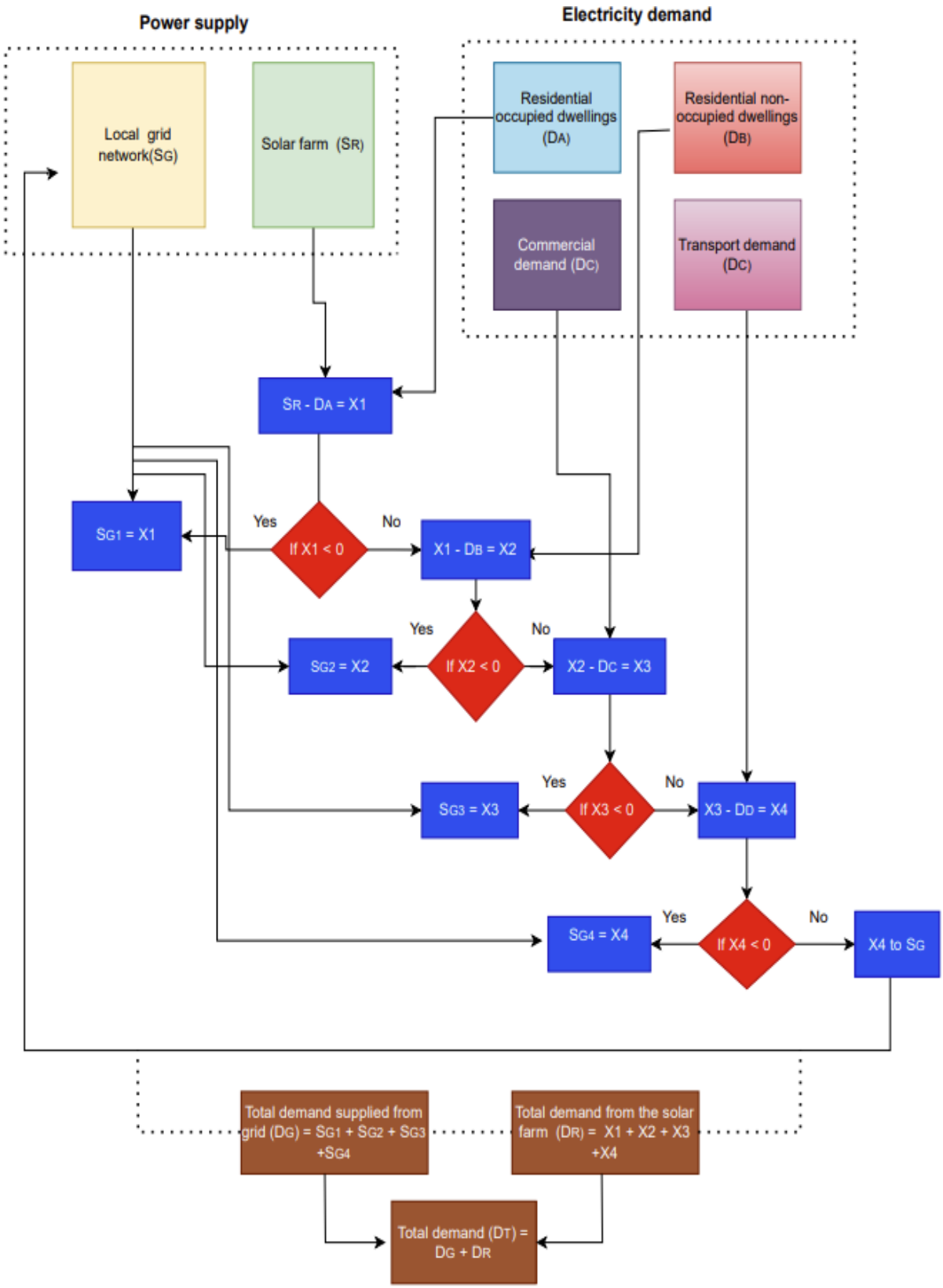

Figure 5-1: The process block diagram for scenario one.

5. Result:
    - Total demand supplied from the local grid (D_G):
      $D_G = S_{G1} + S_{G2} + S_{G3} + S_{G4}$
    - Total solar supplied demand (D_R):
      $(D_R) = X_1 + X_2 + X_3 + X_4$ (positive values)
    - Total demand (D_T):
      $(D_T) = D_G + D_R$

The model uses the above hierarchical approach to supply the electricity from the solar farm (S_R) to various demand categories and prioritize solar generation. If there is any deficit from the solar generation, then the electricity is drawn from the grid.

5.3.1.2 Modelling of scenario two

The modelling process block diagram for scenario two is illustrated in Figure 5-2. The model evaluates the renewable integration through a hierarchical allocated framework. This scenario evaluates renewable energy integration through rooftop solar panels installed on both occupied and non-occupied residential dwellings.

The diagram depicts an energy management framework with (Electric Vehicle) EV car battery as storage of the excess generated from the rooftop solar panel. Only in the residential occupied dwellings, the excess electricity produced from the solar panel has been used to charge the EV battery. Contrarily, in non-dwellings, the EV battery option hasn't been used; instead, they send the excess electricity to the neighbourhood community through the local grid or for H_2 production. The analysis has been conducted in the Excel spreadsheet model.

The system comprises two primary components: Power supply sources and the electricity demand category. The power supply side consists of a solar farm (S_R) and a local grid network (S_G). Meanwhile, the demand side includes residential occupied dwellings (D_A), residential non-occupied dwellings (D_B), non-occupied dwellings (D_B), and EV car charging (D_C). Finally, the excess electricity has been sent through the grid. The model employs an algorithm that prioritises solar generation to meet demand in a specific hierarchical order. The process follows the following steps:

1. The model first calculates the difference between solar panel generation (S_R) and residential occupied dwelling demand (D_A): $S_R - D_A = X_1$. This determines if there's excess generation or deficit after meeting primary residential needs

2. First decision:

   If $X_1 < 0$, the local grid (S_{G1}) provides the deficit electricity

   If $X_1 > 0$, the excess electricity has been sent to charge the EV car.

3. EV car battery charging:

   Any leftover energy from residential occupied dwellings has been used for EV batter charging.

   $X_1 - D_C = X_2$

   Assume that the EV car battery charging has been done only in the peak sunny hours of the day.

4. Second decision:

   If $X_2 < 0$, Deficit of electricity, and no electricity has been drawn from the local grid.

   If $X_2 > 0$, the Excess has been sent through the local grid for H_2 production(H1).

5. Non–occupied dwellings:

   Separately, the model checks the solar electricity available for supplying the demand of residential non–occupied dwellings.

   $X_3 = S_R – D_B$

6. Third decision:

   If $X_3 < 0$, the local grid provides the deficit electricity

   If $X_3 > 0$, the surplus electricity has been sent through the grid for H_2 production (H2).

7. Final calculations:

   The model calculates the aggregated supply and demand.

   Total energy used from solar: $S_R = X_1 + X_2 + X_3$ (positive values)

   Total energy used from the grid: $S_G = S_{G1} + S_{G2}$

   Total energy used for H_2 production

   H_2 production = H1 + H2

The model uses the above hierarchical approach to supply electricity from the solar farm (S_R) to various demand categories and prioritise solar generation. If there is any deficit from solar generation, then electricity is drawn from the local grid

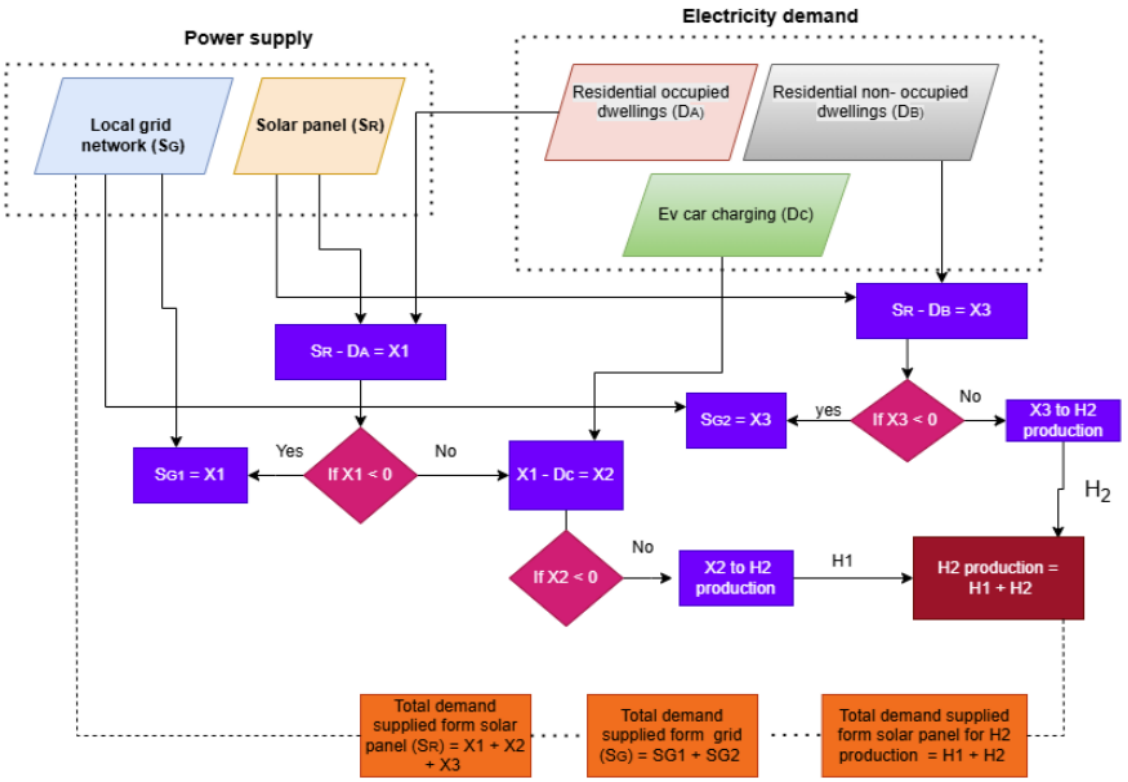

Figure 5-2: The process block diagram of scenario two.

5.3.2 Energy consumption data

The Whitianga region (community) studied is a well-known holiday and retirement destination for people from Auckland and the central north island of New Zealand. The community comprises five different regions: Whitianga, Cooks Beach, Matarangi, Hahei, and Whangapoua.

In this study, a detailed investigation of actual demand has not been undertaken, but instead, the estimation of residential demand for occupied dwellings and non-occupied dwellings has been done by applying the typical NZ residential demand data [43] and scaled to increasing population as predicted by the NZ statistics [5] as shown in Figure 5-3.

Figure 5-3 shows the anticipated population growth of the Whitianga region. Whitianga township has the highest population, accounting for 80% of the total population, while Whangapoua has the lowest population. The population of the region is expected to increase by 1.8 p.a between 2018 to 2050.

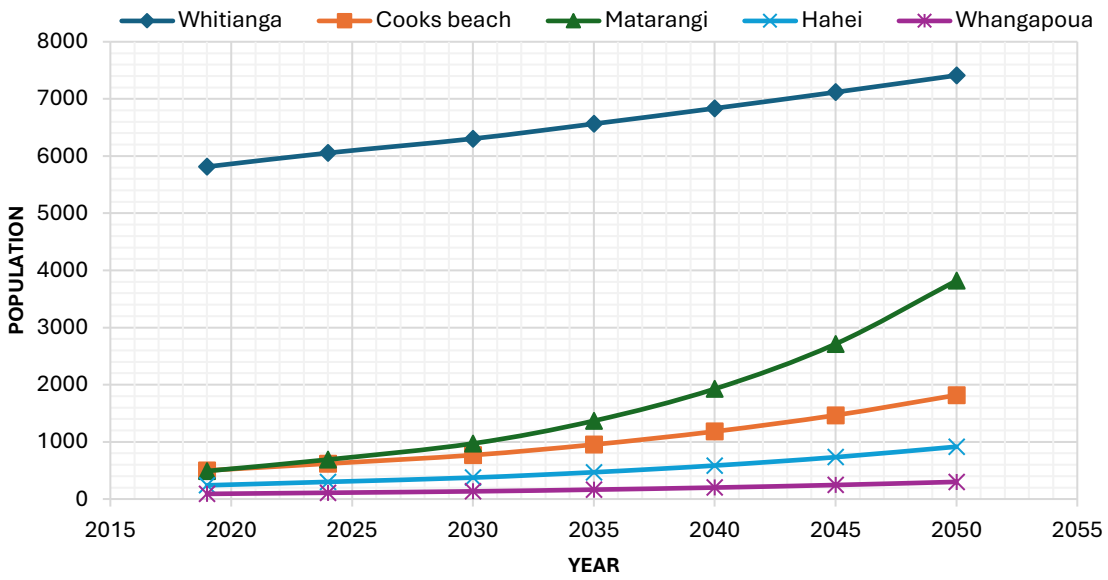

Figure 5-3: Anticipated population growth of the Whitianga region by town or settlement from 2018 to 2050.

The statistics for corresponding residential dwellings (permanent residents) and non-dwellings (temporary residents) have also been projected. Figure 5-4 shows the estimation of both categories from 2024 to 2050. The data up to 2024 is obtained from the official NZ stats [5] and scaled up till 2050 based on the projected population.

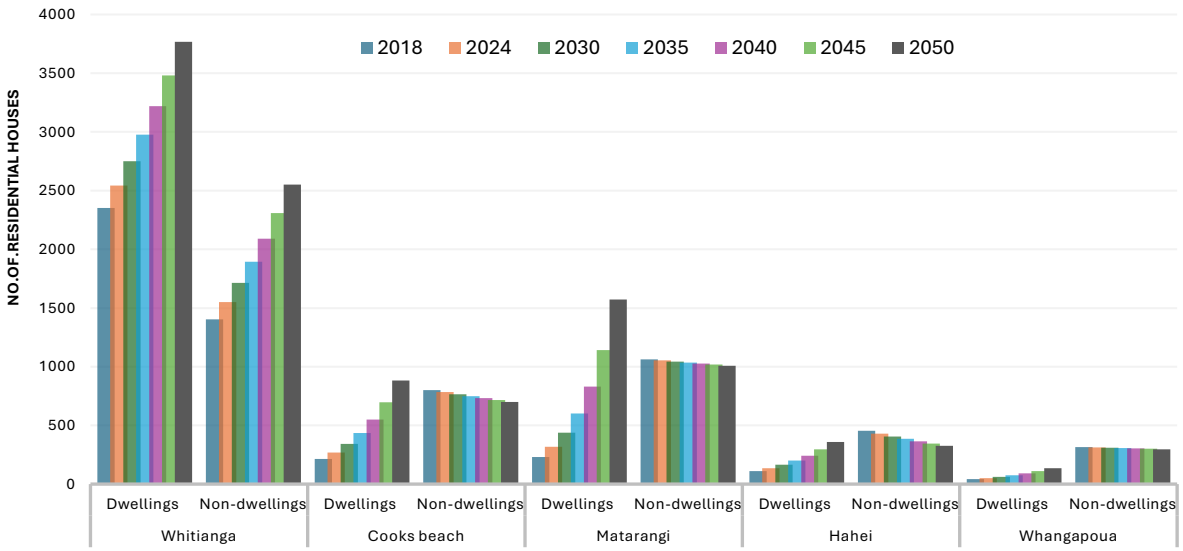

Figure 5-4: Projection of dwellings and non-dwellings statistics over the years for the Whitianga region from 2024 to 2050.

In NZ, commercial and public services also contribute a significant electricity demand. According to Transpower [51] , the commercial sector accounts for approximately 24% of the total NZ electricity demand. The commercial sector includes a wide variety of buildings, including offices, restaurants, supermarkets, and public services (e.g., schools, fire stations, and community buildings). Due to minimal information being available for commercial electricity demand on an hourly basis in the NZ context, the hourly commercial demand profile for the Whitianga region has been estimated using open source and literature data that has been adjusted according to the NZ climatic seasons [55]. The numbers and type of commercial buildings in the Whitianga region have been taken from the NZ census report [6]. Based on the above statistics, the commercial electricity demand of the community on an hourly basis has been estimated.

Regarding the calculation of transport energy demand for the Whitianga region, overall NZ statistics have been considered and then scaled to the smaller population level of the community. Currently, in New Zealand, transport accounts for less than 1% of the total electricity demand, while on an energy basis, it consumes 46% of the total energy demand, mainly supplied from fossil fuels. As NZ transitions towards EV and FCEV, this will increase the transport electrical demand. The demand for transportation has been sourced from the Ministry of Transportation (MOT) [56] and calculated for the community. This is discussed more elaborately in the section 5.4.

5.3.3 About the network.

The electricity demand for the Whitianga substation has been supplied from the Kopu GXP (Grid Exit Point). The Kopu GXP serves as a vital transmission hub supplying electricity to the Eastern Coromandel Peninsula. It is operated by Transpower and interconnected with Power Co's sub-transmission and distribution network. The AC capacity of the two Kopu GXP transformers is 60 MVA (Mega Volt-Ampere), giving a maximum capacity of 60 MVA for N reliability or 120 MVA for N-1 reliability. The power is then transferred to six substations around the Coromandel using 66 kV (kilovolts) high-voltage transmission lines. N reliability means the substation operates with only one transformer, with no backup available. In contrast, N−1 reliability includes an additional standby transformer, ensuring that if one fails, the other can continue to supply power without interruption.

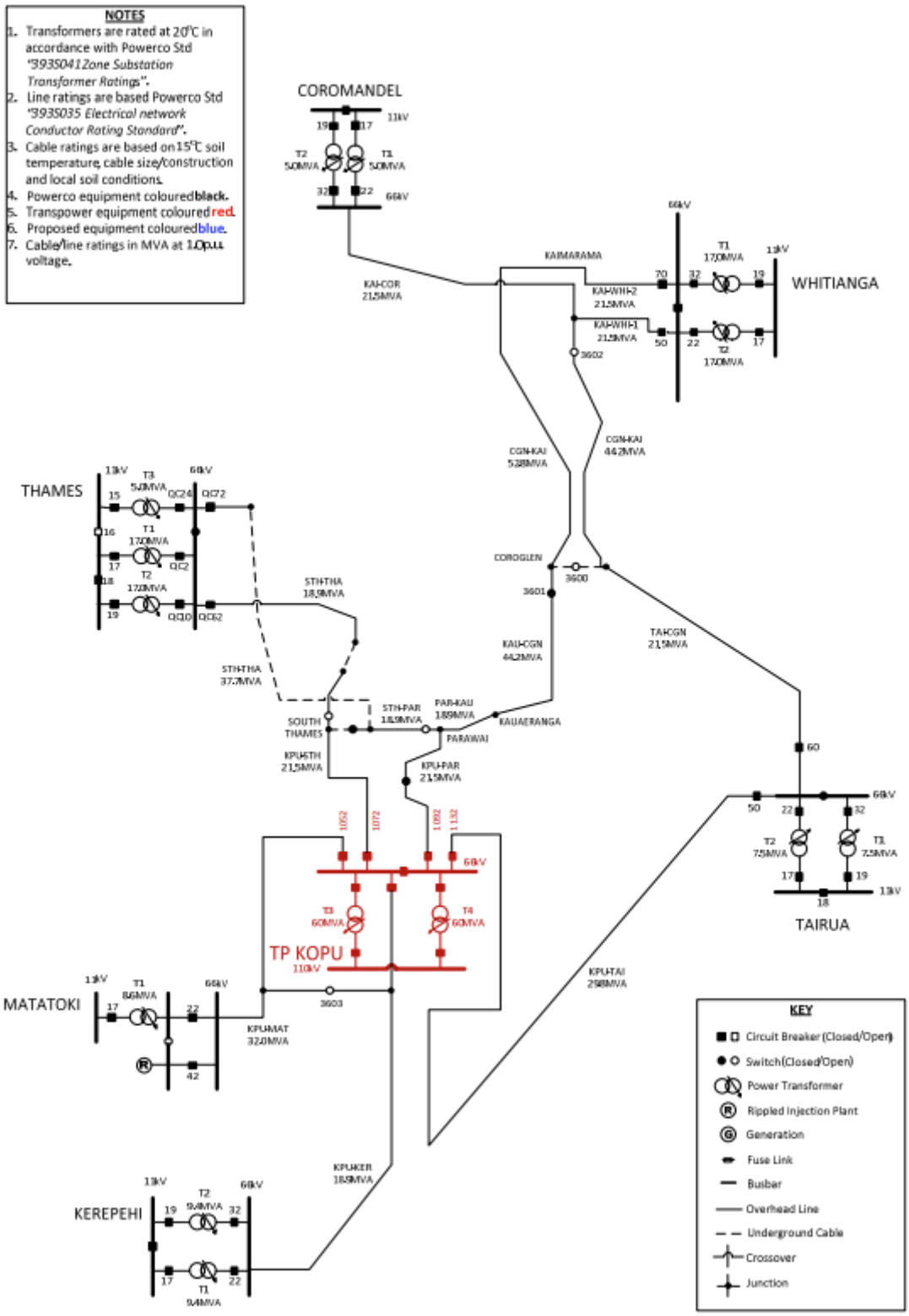

Figure 5-5: Existing KOPU sub-transmission network: one line diagram

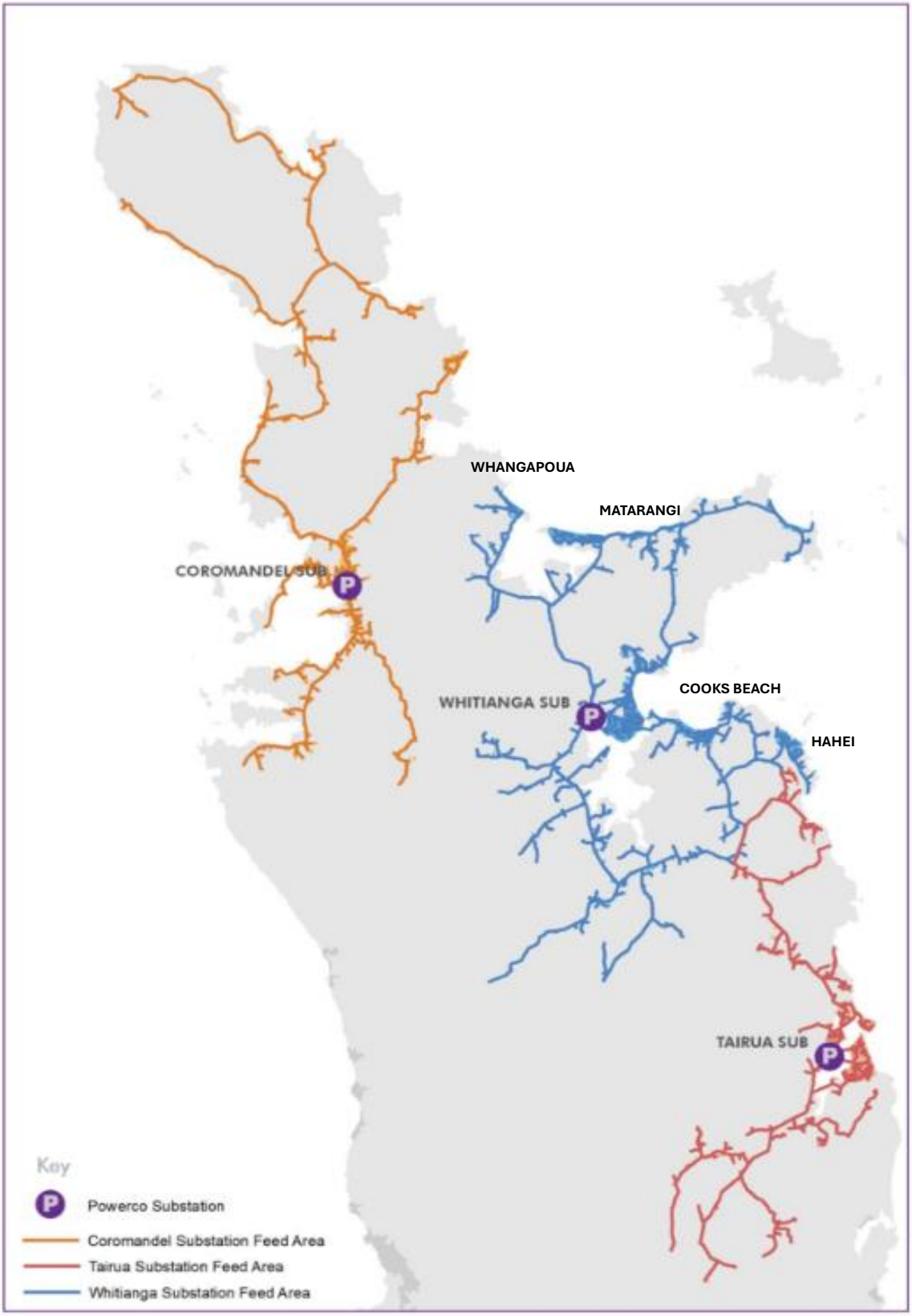

Figure 5-6: The substations network map of Tairua, Coromandel, and Whitianga.

The six substations are Coromandel, Tairua, Thames, Matotaki, Kerepehi, and Whitianga. The capacity of the various substation transformers ranges from 5.0 MVA to 17.0 MVA, with N-1 reliability supported by equal capacity transformers at each substation, except for Thames, which includes an extra 5.0 MVA in addition to two 17.0 MVA substations. The existing Kopu GXP sub-transmission network is illustrated in Figure 5-5, and the map of the Coromandel area is shown in Figure 1-1. From the Whitianga substation, electricity is supplied to nearby regions through the local grid network, as illustrated in Figure 5-6.

The electricity supply and demand profile for the Whitianga substation is not precisely available. From the Kopu–Tairua project report [2], it is stated that the Whitianga substation uses approximately one-third of the total electricity supplied from the Kopu GXP. These values are used to compare the community demand in 2024.

5.3.4 Renewable scenario one: Integration of the community with the solar farm

This scenario examines the potential of integrating a large-scale solar farm with the Whitianga community to generate sustainable electricity. This method is referred to as a centralised approach. The system has been evaluated on an hourly basis over a year in the model.

The centralised system consists of a new 32 MW_p solar farm and an existing local grid electricity as the power supply units. The electricity generated is used to meet the demand of commercial buildings, residential dwellings & non-dwellings, EV chargers, and PEM electrolyser. The specification of the PEM electrolyser and the EV's charger has been determined based on the required demand in the model.

During the daytime hours, particularly between 9:00 AM and 5:00 PM, the solar farm typically generates more electricity than required by the residential and commercial sectors. This surplus electricity has been directed to charging EV and producing green hydrogen via PEM electrolyser. The H_2 produced is stored for later use, specifically for refuelling FCEV. The process flow diagram for scenario one is illustrated in Figure 5-7. Any remaining excess electricity after meeting all the demand has been exported to the grid, where it can be utilised for the neighbourhood communities.

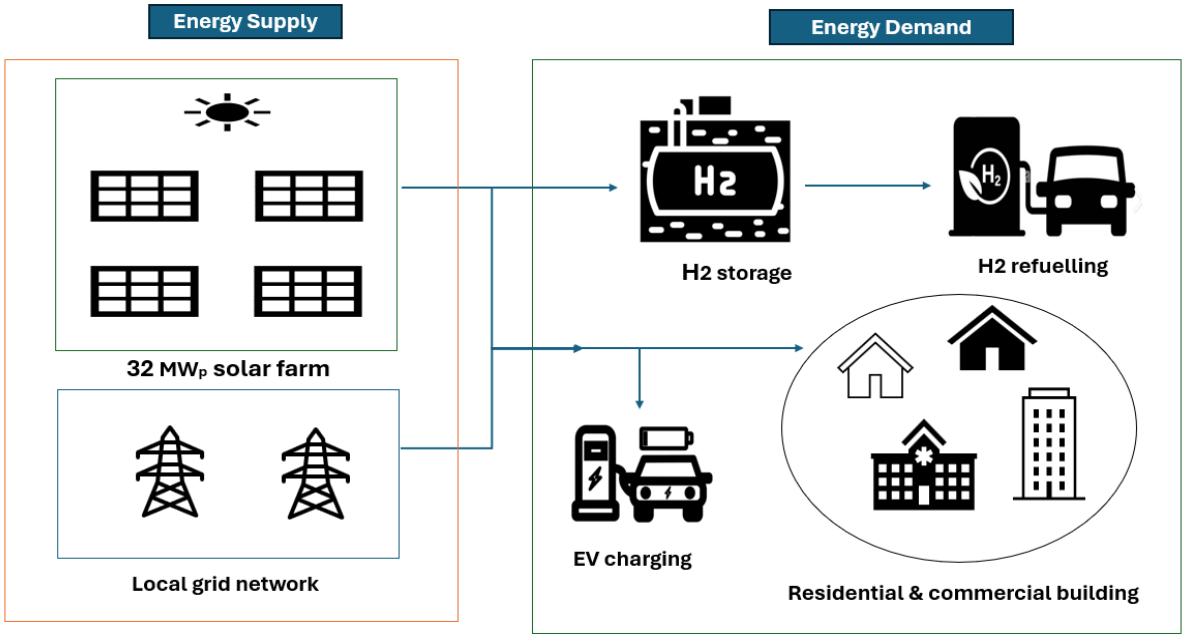

Figure 5-7: Schematic diagram for the scenario one centralised approach

5.3.5 Renewable scenario two: Installation of rooftop solar panels in the community buildings.

This scenario evaluates the potential of rooftop solar panels installed on individual residential buildings to enhance the energy self-sufficiency only for the year 2024. This approach is referred to as a decentralised approach. The decentralised approach consists of rooftop solar panels, an EV car battery, and a grid connection. The analysis was conducted on two categories of residential buildings: occupied dwellings with rooftop solar panels and Vehicle-to-Grid (V2G) capability, and non-occupied dwellings with rooftop solar panels, but without storage systems. For occupied dwellings, each building is assumed to have a 4.3 kW_p rooftop solar system. The generated electricity is first used to meet the residential demand. Any surplus electricity is then used to charge the EV batteries, and if additional excess remains, it is exported to the grid for the other community usage or H_2 production. If there is any shortage from the solar generation, the electricity is drawn from the EV battery (discharge mode) or the local grid, as part of the V2G system. (Note that the car battery has been used only for charging and discharging in this work, and no assumption has been made regarding car usage and driving period.)

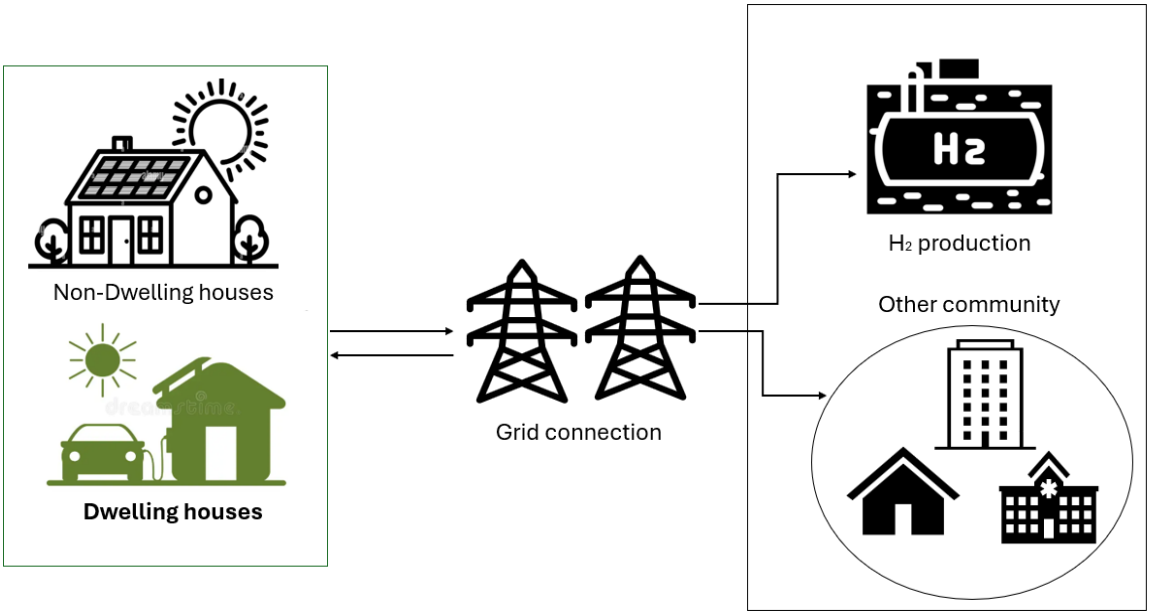

Figure 5-8: Schematic diagram of individual rooftop solar panels for residential applications (decentralised approach).

Similar panel capacity has been used for non-occupied dwellings. As no storage system (EV battery) has been used, the excess electricity produced has been exported to the grid or used for H_2 production. During periods of insufficient solar generation, electricity has been drawn from the local grid.

It is important to note that, analysis in the two scenarios focuses on the energy balance between supply and demand. Electrical losses, such as inverter efficiency, transmission losses, and grid export or import limitations, have not been considered in this work. The aim is to provide a general overview of the energy flows within the community for both centralized and decentralized approaches.

5.4 Demand analysis

This section presents an analysis of electricity demand in the community, focusing on three major sectors: residential, commercial, and transportation. The analysis is initially carried out for the year 2024 and then projected for future years based on population growth estimates, using data from relevant sources [5, 43, 55].

5.4.1 Residential demand

In NZ, the residential sector accounts for approximately 32% of the total electricity demand [51]. The residential demand within the community has been divided into two categories: occupied dwellings, which are inhabited year-round, and non-occupied dwellings, which are used during holidays and weekends by their owners (from another region) or by tourists and beachgoers who rent the houses during these periods [2].

An hourly demand profile for a typical NZ residential house was obtained from [43] and the total residential demand of the community is calculated based on the number of dwellings discussed in the (see section 5.3.2). Each residential unit was assumed to be a fully insulated three-bedroom home equipped with a kitchen, bathroom, and living area. The following subsection provides a more detailed analysis of each dwelling category.

5.4.1.1 Residential occupied dwellings

All the residential occupied dwellings are assumed to maintain a constant electricity demand throughout the year. However, seasonal changes cause variation in the hourly demand profile. As shown in Figure 5-9, dwelling demand (2024) fluctuates throughout the year, with the electricity demand ranging between 1 and 15 MWh on an hourly basis. During the winter season, demand increases due to a rise in space heating consumption. In contrast, the lowest electricity demand typically occurs in spring, particularly in November. Overall, residential occupied dwellings account for 17 GWh of electricity demand annually.

5.4.1.2 Residential non-occupied dwellings

The major occupancy patterns and trends for residential non-occupied dwellings are described in Table 5-1. Table 5-1 outlines the peak-peak usage periods, such as Christmas, New Year, Easter, and King's birthday weekend, during which occupancy can range from 80–100% [2]. However, during the normal period, occupancy ranges below 20%, while in the peak period, occupancy ranges from 50% to 80%.

Table 5-1: Peak-Peak, Peak, and normal occupancy period for non-occupied residential dwellings [2].

Peak-Peak	Vacation	Dec 16- Jan 19
	Easter holiday	Apr 17- Apr 27
	King's birthday	May 30 - June 2
Peak	School term holidays (Two weeks for each term)	Apr 11- Apr 27
		Jun 27 - Jul 13
		Sep 19 - Oct 5
		Jan 20 - Feb 5
Normal	Rest of the year	Remaining days

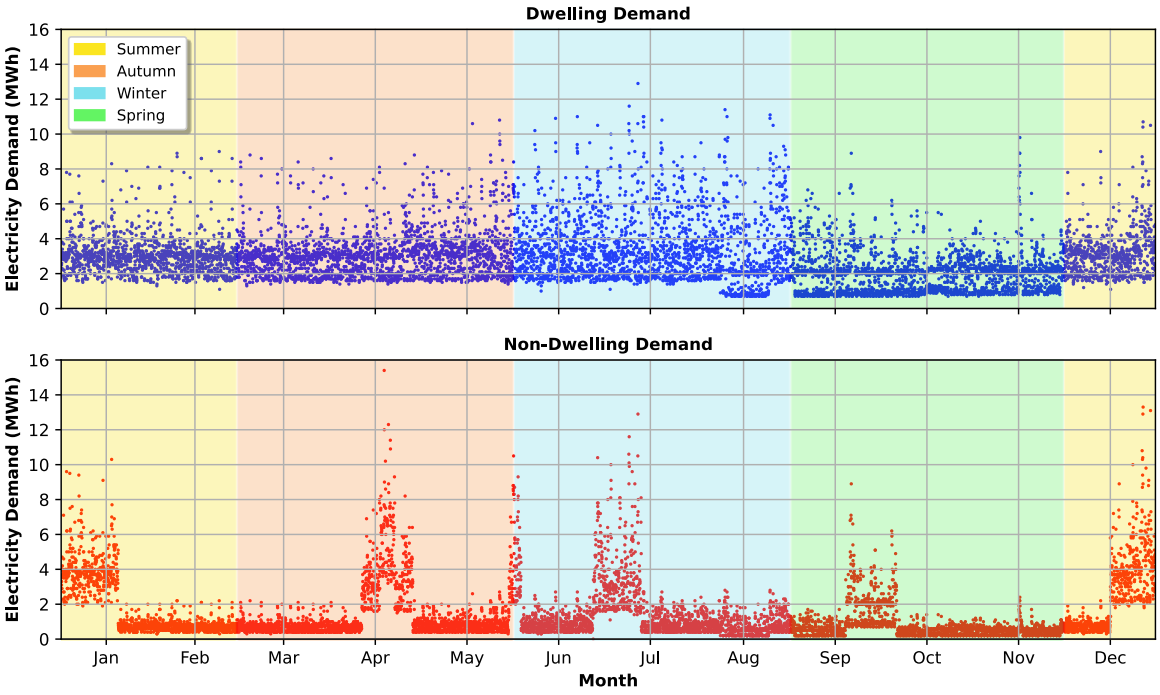

Figure 5-9: Hourly electricity demand profile for the occupied and non-occupied residential dwellings in the community (2024).

Figure 5-9 also illustrates the annual electricity demand profile for non-occupied dwellings (2024), showing that electricity demand during the peak period is five times higher compared to the rest of the year. Annual electricity consumption for non-occupied dwellings ranges from 1 to 13 MWh, with the highest recorded during the Christmas and New Year holiday period. Unlike occupied dwellings, this category does not follow seasonal fluctuations; however, it experiences a higher demand for a shorter period, especially during the holiday season.

5.4.2 Comparative trends of the residential dwellings demand

Figure 5-10 presents the accumulated demand for both categories, sorted from the lowest to the highest hourly consumption in 2024. Both the demand follows a similar trend, it remains low and flat for most of the time (from 0 to 7,500 hours), then suddenly increases at the end. For 80% of the time, non-occupied dwellings use 0-2 MWh of electricity, while dwellings use 0-4 MWh of electricity slightly more than 80% of the time.

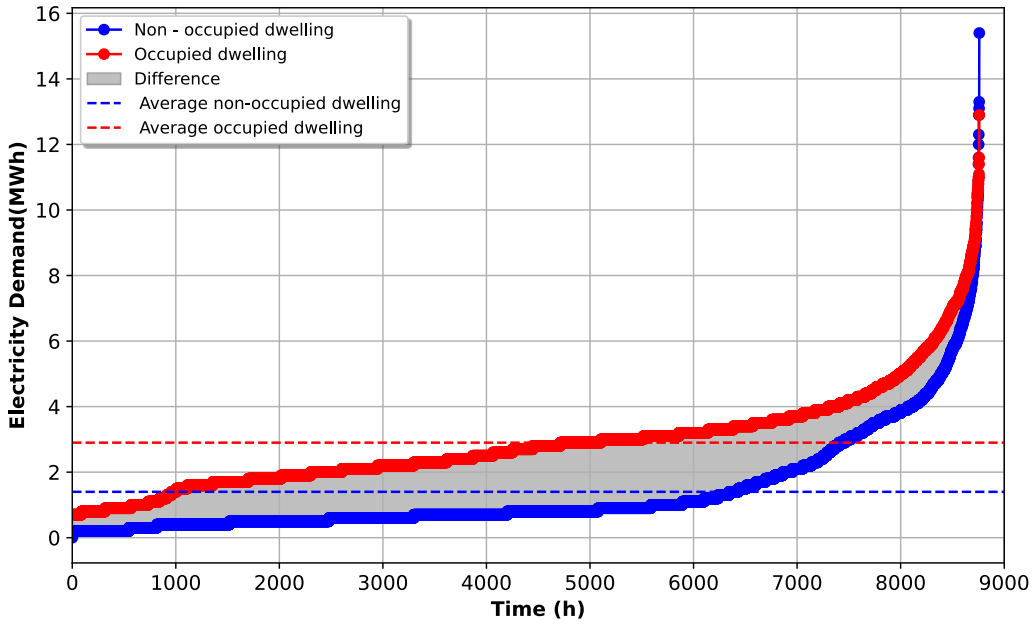

Figure 5-10: Accumulated and sorted hourly demand for residential occupied and non-occupied dwellings (2024).

Overall, there is a large difference in total electricity demand between the two categories, which represents a grey region. The average hourly demand for occupied dwellings is 2.5 MWh, while for non-occupied dwellings, it is 1.6 MWh.

5.4.3 Commercial and public service demand

The commercial building demand profile for various buildings was obtained from the source [55] and used as a benchmark to estimate the total demand of the community. The Whitianga commercial building census is cited from [6] and based on that information a projection has been made until 2050, listed in Table 5-2. The commercial buildings of the community comprise a diverse mix of energy-consuming buildings, including restaurants, offices, supermarkets, a fire station, a police station, and schools. No precise information is available

on the hospitals, so it has not been taken into consideration. As shown in Table 5-2, there has been moderate growth in the commercial building over the years, primarily due to a lack of population and isolation, which has made it challenging for local businesses.

Table 5-2: Whitianga zone commercial building census

Class	2024	2030	2035	2040	2045	2050
School	6	6	6	6	6	6
Fire station	5	5	5	5	5	5
Police station	1	1	1	1	1	1
Supermarket	4	4	4	5	5	5
Office	20	20	20	25	25	25
Restaurants	35	35	35	40	40	40

The demand for each type of commercial building has been analysed in the model. Based on the available data, the total commercial electricity demand in 2024 is estimated as 28 GWh/year. Figure 5-11 represents the total commercial electricity demand analysis on an hourly basis over the year (2024).

From the Figure 5-11 it can be clearly seen that the highest electricity consumption has been recorded in the during the winter period, which is 8.2 MWh, while the lowest electricity consumption has been recorded during nighttime, which is less than 1 MWh.

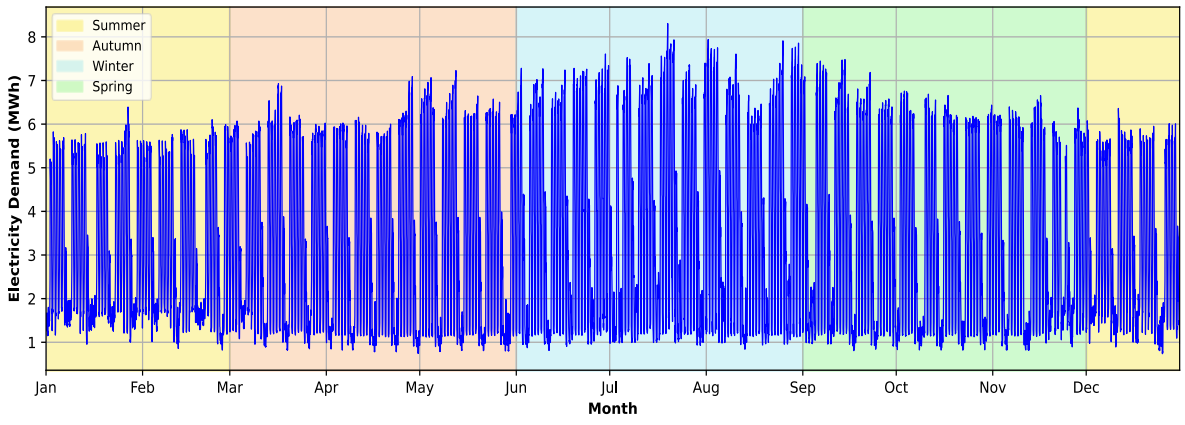

Figure 5-11: Annual hourly commercial demand analysis for the community(2024).

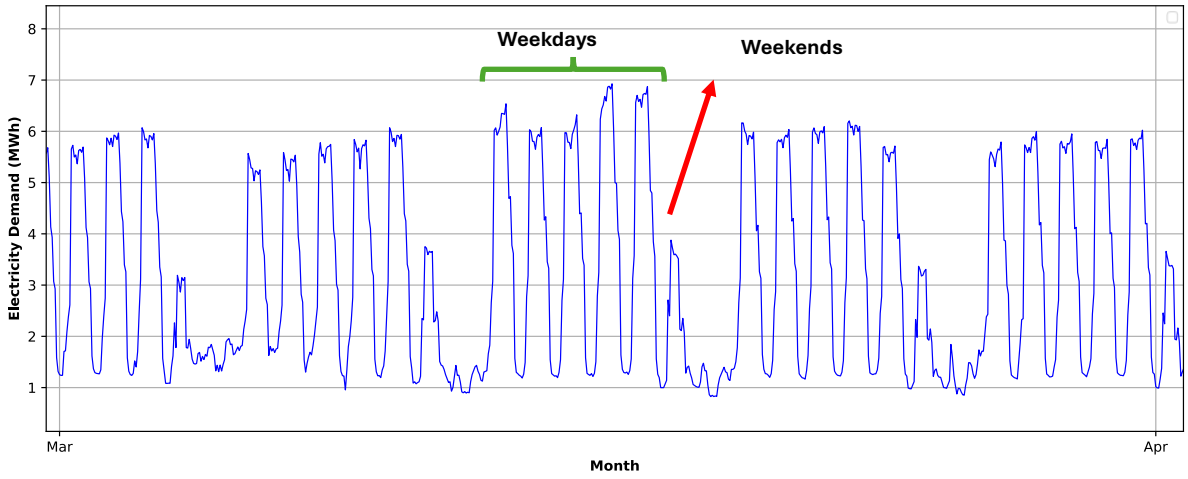

Figure 5-12: Commercial demand analysis weekly for the community (2024).

The commercial demand exhibits a diurnal energy demand pattern, with peak consumption typically recorded during the daytime (8 am – 6 pm), which aligns with most business hours. While the lowest has been recorded during nighttime, the cycle repeats throughout the year for 24 hours. From Figure 5-12, demand is only high on weekdays, while on weekends, demand remains relatively lower. This daytime high demand is due to an increase in space heating demand, as well as lighting and refrigeration demand in schools, offices, and supermarkets, which typically operate during the daytime. This may align with direct solar power utilisation produced in the daytime and reduces the requirement for intermediate storage options.

5.4.4 Transport demand

Transportation plays a significant role in the Whitianga community due to the lack of public infrastructure and the car-dependent population. The community's primary transportation system is dominated by private vehicles, service vehicles, and seasonal tourist traffic. Currently, most transportation demand is met by high-emitting CO_2 fuels, such as petrol and diesel.

As NZ moves towards implementing sustainable transport options like EV and FCEV, electricity consumption may increase substantially. Table 5-3 mentions the estimation of sustainable transport options electricity and fossil fuel demand, which is based on the current maturity of these technologies and the government's roadmap to mitigate emissions by 2050.

Table 5-3: Transport electricity demand for the community

Year	EV (GWh/year)	FCEV (GWh/year)	Fossil fuel (GWh/year)
2024	1	1	60
2030	2	2	54
2035	3	4	45
2040	4	6	39
2045	6	9	35
2050	9	13	25

To estimate the transport demand for the community, vehicle fleet statistics were sourced from Ministry of Transport [56]. First, the national per-capita average distance travelled per vehicle, by each vehicle class and fuel type, was determined. Based on these averages, the vehicle fleet composition for the community was estimated by multiplying the per-capita figures with the local population. The vehicle classes considered include trucks, buses, light commercial vehicles (LCVs), and light passenger vehicles (LPVs).

The energy consumption for each vehicle class is calculated using fuel efficiency values, as shown in Table 5-4.

Table 5-4: Fuel efficiency for EV, FCEV and fossil fuel.

Mode	EV	FCEV		Fossil fuel
	Fuel efficiency(km/kWh)	Fuel efficiency(km/kg)	Fuel efficiency(km/kWh)	Fuel efficiency(km/kWh)
LCV & LPV	8	100	2.54	1.32
Buses	5	16	0.41	0.60
trucks	4	9	0.23	0.50

A detailed breakdown of the projected sustainable transport vehicle fleet for the community is provided in Table 5-5. The vehicle fleet projections are based on the community's population growth, excluding any consideration of tourist vehicle demand. In 2024, only 3% of the total vehicle class is estimated to be electric vehicles (EV). This number is expected to increase steadily over the years and reach 80% by 2050, except for Trucks, which is assumed to be 20%. Conversely, by 2024, only 0.5% of each vehicle class had been converted into FCEV, gradually increasing to 15% by 2050 across all vehicle classes.

Table 5-5: Projected EV and FCEV fleet statistics by vehicle class.

Class	EV				FCEV			
Year	LPV	LCV	Trucks	Buses	LPV	LCV	Trucks	Buses
2024	269	1503	3	0	0	86	3	0
2030	888	193	9	2	6	1	9	1
2035	1647	358	32	5	99	21	16	1
2040	3295	716	39	8	132	29	32	2
2045	5098	1109	62	13	296	55	62	4
2050	6912	1503	96	19	395	86	87	6

As a result of this transition to EV and FCEV, the total transportation electrical demand is expected to increase from 2 GWh/year in 2024 to 22 GWh/year in 2050.

5.4.5 Total demand analysis of the community.

The total electricity demand for the community has been estimated by aggregating the consumption from various sectors: residential occupied dwellings, residential non-occupied dwellings, transportation, and commercial buildings. The demand profile for each sector has been discussed in detail in the sections above (see sections 5.4.1 – 5.4.4). The projected community's annual electricity demand from 2024 to 2050 is summarized in Table 5-6.

Table 5-6: Projected total annual electricity demand of the community by sector from 2024 to 2050.

Year	Dwellings (GWh/yr)	Non-dwellings (GWh/yr)	Commercial (GWh/yr)	EV (GWh/yr)	FCEV (GWh/yr)	Total (GWh/yr)
2024	25	12	28	0.5	0.1	67
2030	29	13	28	1.9	0.8	72
2035	33	13	28	3.5	2.2	79
2040	38	14	33	5.5	3.8	94
2045	44	14	33	8.9	6.8	106
2050	52	15	33	11.8	9.1	119

As shown in Figure 5-13, the community's total electricity is expected to increase from 67 GWh/year to 119 GWh/year. This significant growth is primarily due to an increase in population, the electrification of vehicles, and the expansion of commercial and tourism-related activities.

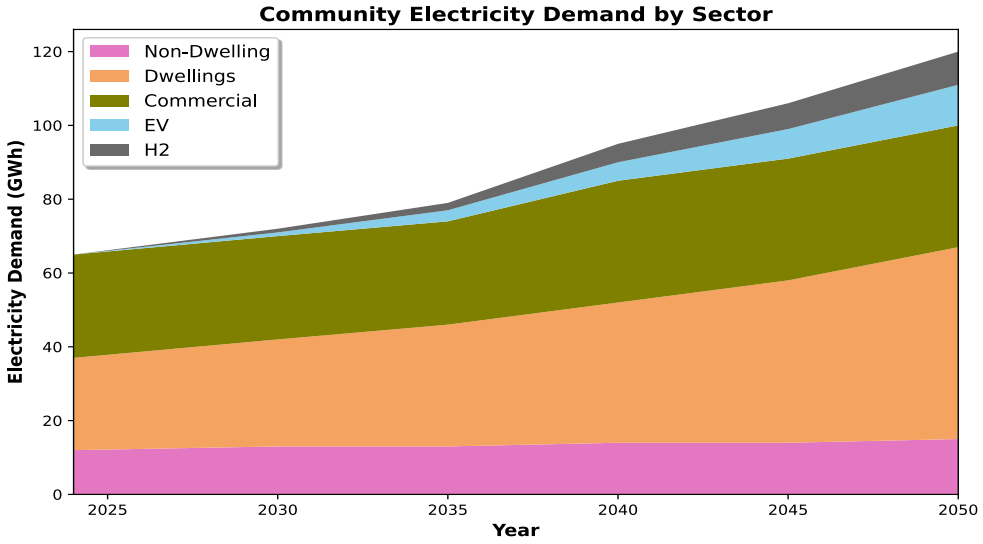

Figure 5-13: Stacked area demand for the community by the sector (2024 – 2025)

In 2024, the bulk of electricity consumption comes from the commercial and residential sectors (dwellings and non-dwellings), which account for 58% and 42% of the total demand, respectively. The increase in demand is primarily due to the demand for space heating, refrigeration, and lighting. This demand may experience a seasonal surge due to the increase in tourists during the holiday season. The report [57] says that all retail, commercial, and service businesses in these regions make up 70% of their revenue during the holiday seasons annually, highlighting the seasonal use of electricity in the Whitianga region.

In 2024, the transportation sector contributes relatively less to total electricity demand, primarily due to the lower market share of electric vehicles (EV) and fuel cell electric vehicles (FCEV). However, by 2050, transport demand is expected to shift drastically due to market policies and incentives promoting sustainable transportation. The projected increase in Vehicle Kilometres Travelled (VKT) and charging needs for electric vehicles (EV) & hydrogen (H_2) production for Fuel Cell Electric Vehicles (FCEV) will significantly increase transport-related demand.

Residential demand is expected to grow by 1.8 times by 2050 compared to 2024 levels. This is due to the increase in population and a broader shift from fossil fuels to electric alternatives for household appliances, space heating, and water heating (e.g., heat pumps). Conversely, commercial demand increased moderately from 2024 to 2050, due to its isolated geography and the seasonal nature of economic activity. Figure 5-14 illustrates the comparison of estimated community's electricity demand patterns by sector for 2024 and 2050.

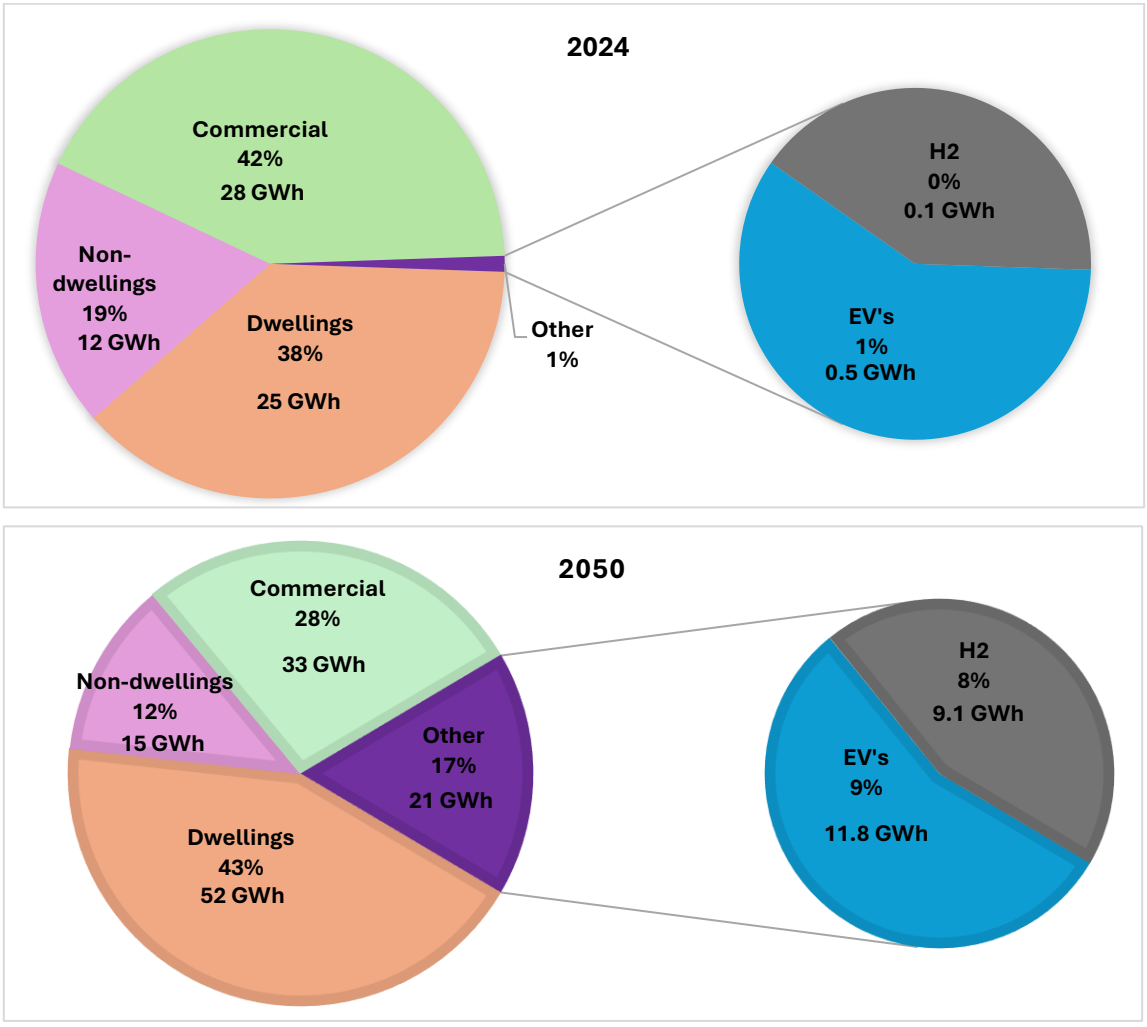

Figure 5-14: Analogy of projected electricity demand for 2024 and 2050 by sectors

The electrical demand data of the Kopu Grid Exit Point (GXP) for 2024 has been sourced from the Electricity Authority NZ [58]. According to Powerco's report [2], the Whitianga substation consumes approximately one-third of the total electrical demand at the Kopu GXP. The hourly demand profile is not available on the website, so the daily demand profile has been used to estimate the demand. Based on that information, an estimate of the Whitianga substation demand is compared in Figure 5-15 to the reported Kopu GXP demand.

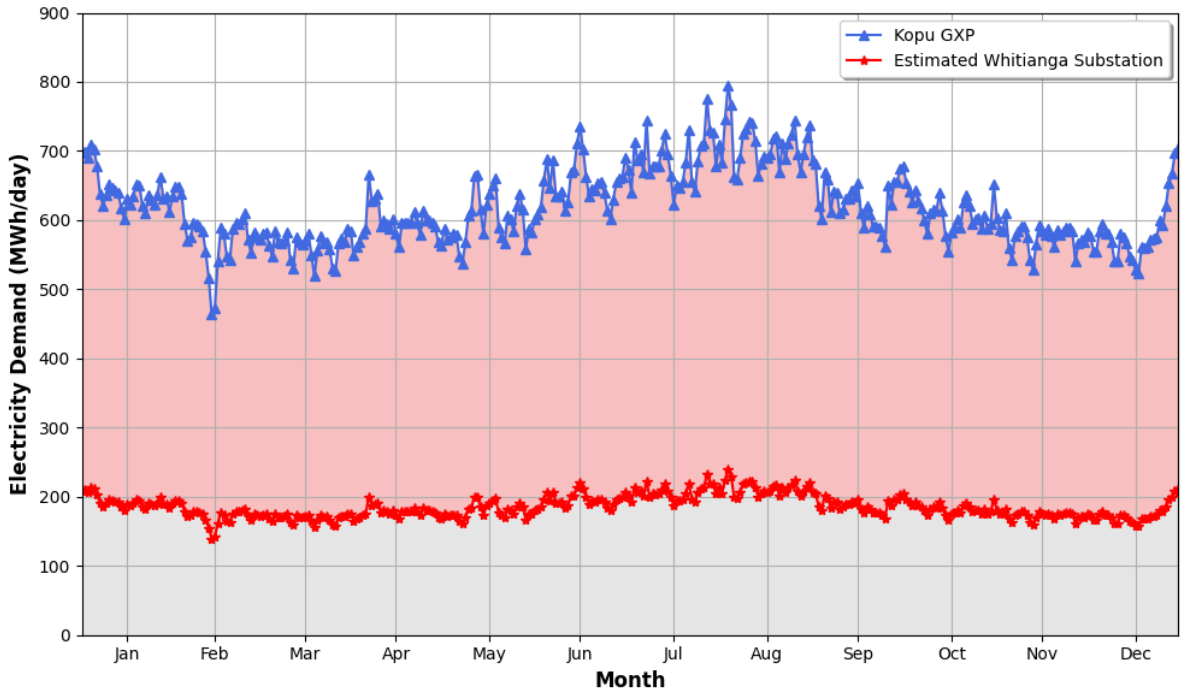

Figure 5-15: Electricity demand of Kopu GXP and Whitianga substation in 2024.

To evaluate the accuracy of the projected community demand (2024) used in this study, a comparison was made between the projected community demand (see Table 5-6) and the estimated Whitianga substation demand reported by Powerco for 2024. As shown in Figure 5-16, the projected community demand for 2024 used in this study aligns well with the estimated substation demand, indicating that the modelling assumptions are reasonable. The exact figure also illustrates the projected community demand for 2050, based on projected population statistics.

This indicates that the current grid infrastructure will not be sufficient to meet future demand. Therefore, upgrading the local grid will be necessary. The next section explores how a solar farm could help reduce the community's dependence on the national or local grid infrastructure.

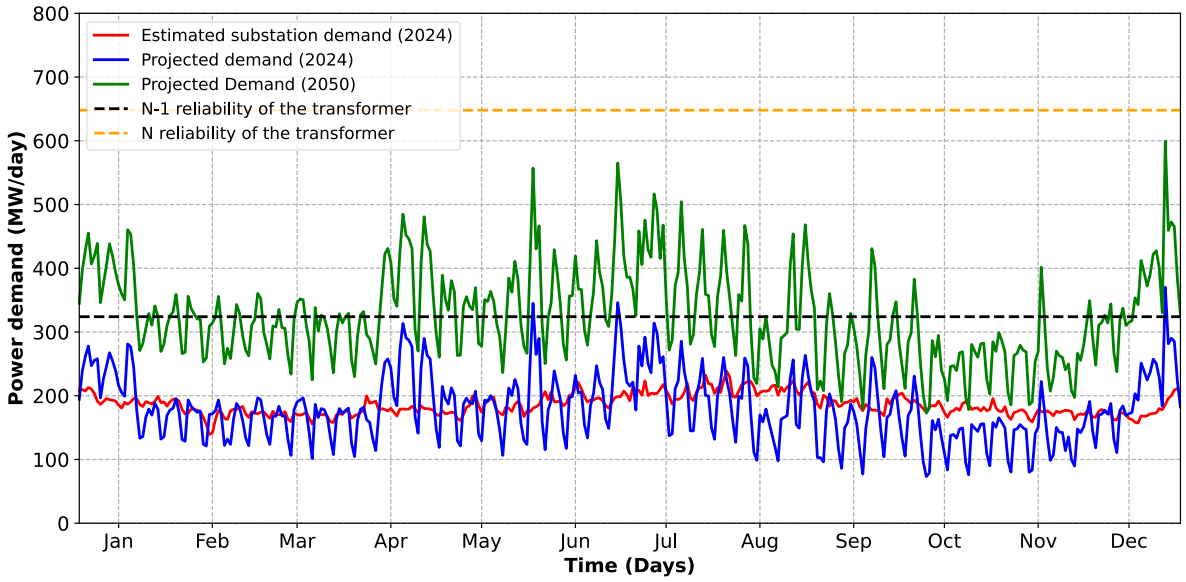

Figure 5-16: Comparison of the projected Whitianga community demand in 2024 and 2050 versus the 1/3rd of the Kopu GXP demand (Estimated Whitianga substation demand).

5.5 Results – centralised approach

This section presents the analysis of electricity supply from the solar farm and its ability to meet the community's annual electricity demand from 2024 to 2050, using the centralised approach.

5.5.1 Solar farm power generation profile

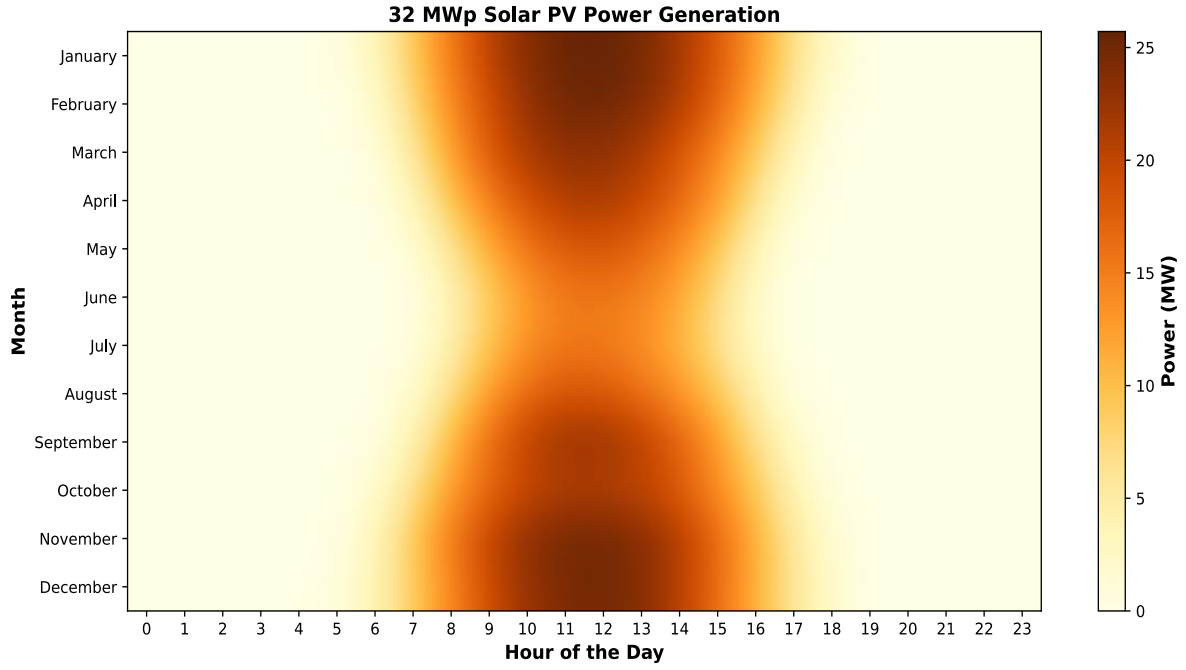

Figure 5-17: Annual hourly power production of a 32 MWp solar farm

A 32 MW_p solar farm, developed by Lodestone Energy, is planned to start operating in Whitianga by the end of 2025. It is expected to generate around 56.15 GWh of electricity each year, with a capacity factor of 18%. Figure 5-17 shows the hourly solar power generation pattern across the year. As expected, electricity is mostly generated during daylight hours, with the highest output occurring in summer, reaching up to 25 MWh in the afternoons. This is due to stronger sunlight and longer days. In contrast, electricity generation is lower in winter, reflecting seasonal changes in sunlight. The red inverted double-cone shape in the figure represents how solar power output varies throughout the day and across the seasons.

5.5.2 Community electricity demand profile

Understanding the demand pattern is crucial for understanding how solar farm power generation can meet the community's demand. Figure 5-18 illustrates the community's residential and commercial demand in 2024, which accounts for most of the daily electricity usage. This demand excludes the transport demand, which contributes less than 1% of the total electricity demand in 2024. However, in 2050, transport demand is considered to have grown to 17% (Table 5-7).

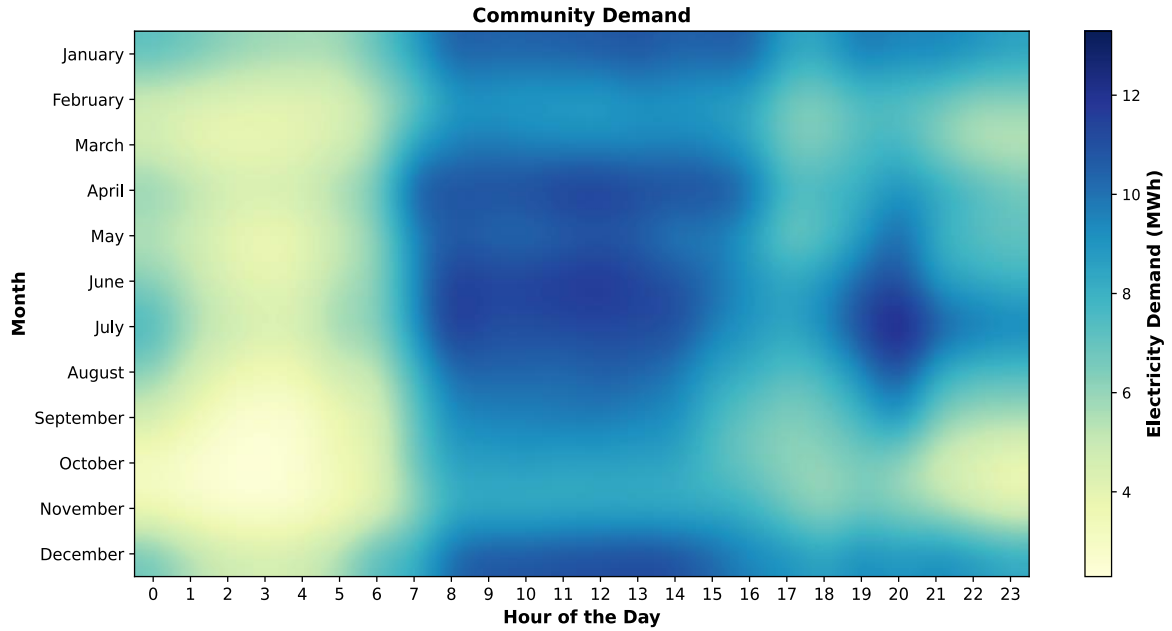

Figure 5-18: Annual hourly community's electricity demand profile in 2024.

From Figure 5-18, electricity demand follows a diurnal pattern, with an increase recorded between 7:00 AM and 6:00 PM. This is due to typical household activities such as cooking, heating, and appliance usage, as well as business operations during these hours.

During summer months, demand is generally lower in the early morning and late evening hours, as the climate favours long daylight hours, reducing lightning and heating demand. In contrast, during the winter months, peak electricity consumption typically occurs in the evening, especially from 6:00 PM to 9:00 PM. This is due to increased space heating requirements, higher indoor occupancy, and shorter daylight hours.

5.5.3 Annual electricity balance

To assess how well the centralized solar farm can meet the community's electricity needs, a yearly electricity balance was carried out for the period from 2024 to 2050. This analysis compares the total annual electricity generated by the 32 MW_p solar farm with the annual demand, including residential, commercial, and transport sectors.

In this analysis, electricity from the solar farm is first used to meet residential and commercial demand. Any excess electricity, especially during midday, when demand is lower, is used to charge Electric Vehicles (EV) and produce hydrogen using a PEM electrolyser. If there is still surplus electricity, it is exported to the local grid to supply nearby areas. When solar generation is not enough to meet demand, electricity is imported from the local grid.

As shown in Table 5-7, annual solar power generation slightly decreases over time due to an assumed 0.3% yearly degradation loss of the solar panels. Meanwhile, the community's electricity demand increases significantly because of population growth, business development, and the wider adoption of electric and hydrogen transport. In 2024, the solar farm supplies 46% of the total electricity demand (31.05 GWh out of 67.0 GWh). By 2050, this share falls to 34% (40.6 GWh out of 119.3 GWh). However, the proportion of solar electricity used within the community increases from 55% in 2024 to 76% in 2050.

Table 5-7: Annual energy demand balance under centralised solar supply scenario (2024-2050).

Year	Solar Farm Electricity generation (GWh)	Residential and commercial demand (GWh)	Electricity supplied from solar (GWh)	Deficit drawn from network (GWh)	Surplus from solar farm (GWh)	Transport demand (GWh)	Projected Community Demand (GWh)
	A	B	C	D	E	F	G
	A = C + E	B = C + D	C = A - E	D = B - C	E = A - C	F = G - B	G = B + F
2024	56.15	66.27	31.05	35.22	25.10	0.73	67
2030	55.59	69.55	32.21	37.34	23.38	2.45	72
2035	55.03	74	33.56	40.44	21.47	5.21	79.21
2040	54.48	84.21	36.9	47.31	17.58	9.85	94.06
2045	53.94	90.83	38.62	52.21	15.32	15.29	106.12
2050	53.40	99	40.6	58.4	12.80	20.3	119.3

The surplus electricity produced from the solar farm after meeting the demand of commercial and residential demand is gradually reducing from 25 GWh in 2024 to 15.55 GWh in 2050. This surplus electricity is insufficient to meet the community's transport demand in 2050, especially during winter. The seasonal reduction of surplus electricity from solar sources during winter affects the ability to meet transport demand. Figure 5-19 presents a comparison of weekly electricity supply and transportation demand in the summers and winters of 2050.

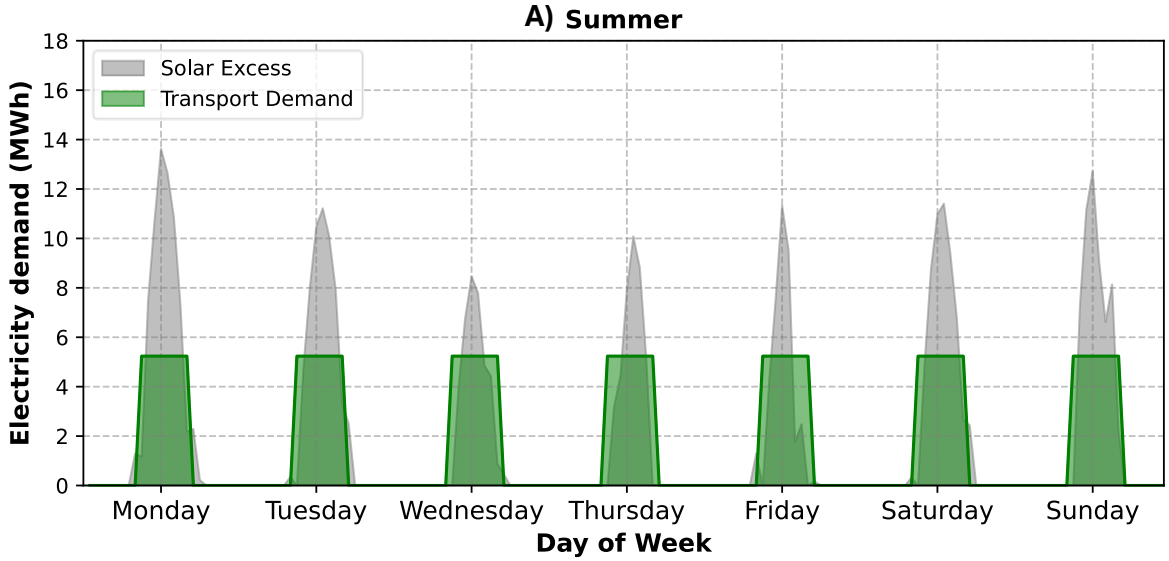

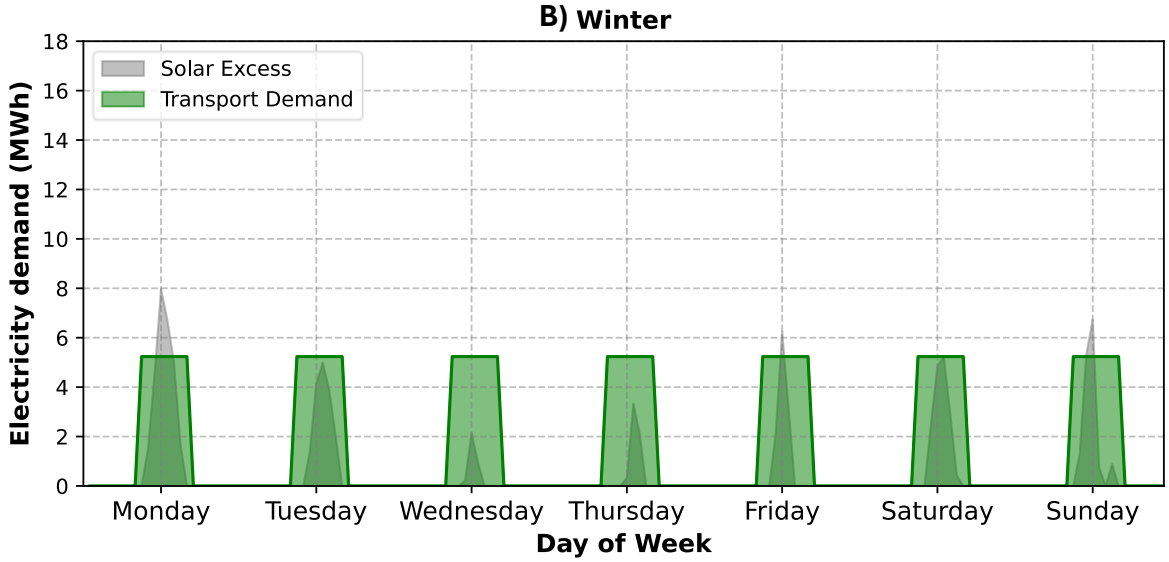

Figure 5-19: Weekly supply and demand analysis of the transport in 2050: A) Summer week , B) Winter week.

During the summer week, solar production exceeds the base residential and commercial demand during daylight hours, allowing surplus generation from the solar farm to be used for EV charging and H_2 production. This highlights the potential of utilising the surplus electricity produced from the solar farm in a demand response approach during the high generation periods. If there is any excess electricity after supplying the transport demand, it is exported to the local grid.

Conversely, in winter, there is a large mismatch between supply and demand. Due to lower sunlight hours and solar irradiance, overall power generation gets lower. As a result, nearly all the available solar power has been utilised by commercial and residential demand, leaving an insufficient surplus for meeting transport demand. The deficit for transportation needs to be supplied from the local grid. This demonstrates a critical seasonal limitation of supplying the demand in the centralised approach.

Additionally, Table 5-7 indicates that grid dependency increases steadily, from 35.22 GWh in 2025 to 58.4 GWh in 2050. This indicates that even a large-scale solar installation is insufficient to meet the total community demand without an external power supply, like the national grid.

5.5.4 Grid dependency and substation comparison.

The annual Whitianga projected demand and the amount that needs to be supplied from the local grid (solar farm deficit) for 2050 is presented in Figure 5-20. The figure is divided into four three-month subplots. Both sets of data have been analysed on an hourly basis over a complete year. The black dotted lines represent the N-1 reliability capacity of the Whitianga transformer, which is 17 MVA, while the red dotted lines represent a N reliability capacity of two transformers combined, which is 34 MVA. To make the comparison of transformer capacity to local grid supply the N-1 and N reliability capacity is presented as 15.3 MWh and 30.6 MWh respectively based on a power factor of 0.9. This assumes 15.3 and 30.6 MW is the transformer capacities maintained for an hour.

In the first quarter of the year (subplot A), the solar farm supplies 51% of the total demand, reducing grid dependency such that the peak demand exceeds the N-1 reliability capacity only 5% of the time, and the N reliability capacity just 0.8% of the time.

During the second quarter (subplot B), the solar farm meets 31% of the total demand. This reduces grid dependency enough that the peak demand exceeds the N-1 reliability 17.3% of the time, and N reliability less than 1.2% of the time.

In the third quarter (subplot C), the solar farm contributes 33.1% of the total demand, with peak demand exceeding N-1 reliability 16.5% of the time and N reliability 2.4% of the time.

In the fourth quarter (subplot D), the solar farm supplies the highest share - 56.15% of the total demand resulting in peak demand exceeding N-1 reliability for only 4% of the time, and N reliability for 0.6%.

Overall, the integration of the solar farm helps reduce the dependence on the local grid network especially during the sunny hours and summer periods and often keeps local grid network demand below the N-1 reliability transformer capacity. However, meeting the demand during holiday time, nighttime and winter period remains challenging. To better understand how often local grid supply exceeds the N-1 and N reliability over the year, the data from Figure 5-20 have been analysed and a yearly summary is presented in Table 5-8.

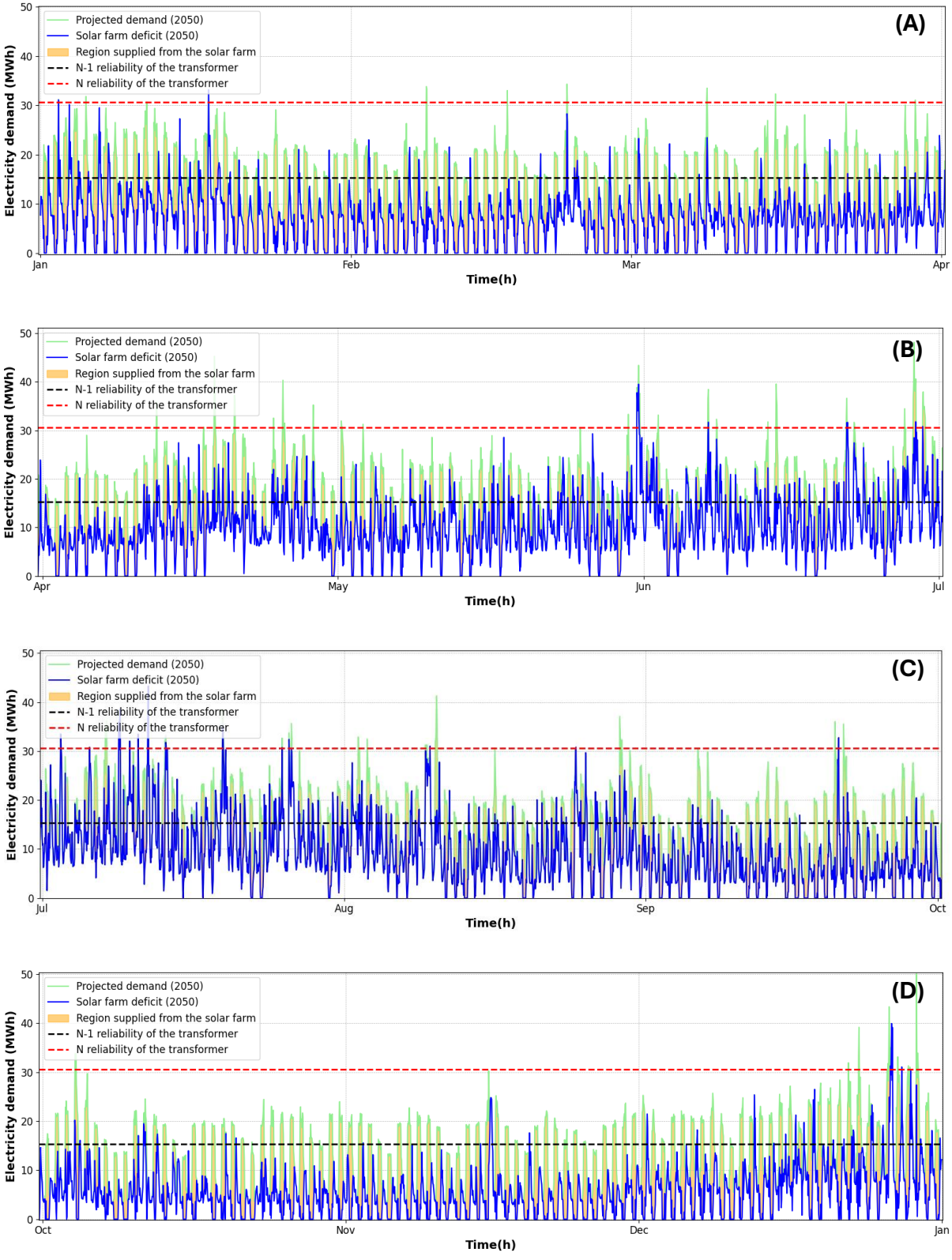

Figure 5-20: Hourly Whitianga projected demand profile and electricity supplied from the local grid (solar farm deficit) for 2050 in 3 month subplots (A) Jan – Mar, (B) Apr – June, (C) Jul – Sept, (D) Oct – Dec, with N-1 and N reliability of transformer capacities.

Table 5-8: Estimated number of hours in 2024 and 2050 when the need for electricity from the local grid exceeds N-1 reliability and N reliability.

	2024		2050	
	N-1 reliability	**N reliability**	**N-1 reliability**	**N reliability**
Solar farm deficit = electricity supplied from local grid (with solar farm)	105 hours	0	929 hours	39 hours
Projected community demand = electricity supplied from local grid (no solar farm)	293 hours	0	3379 hours	141 hours

In 2050, without the solar farm, projected demand exceeds N-1 reliability for approximately 40% of the year (3379 hours) and exceeds N reliability for 3% of the year (141 hours). However, after integrating the solar farm, the number of hours exceeding N-1 reliability drops to 11% (929 hours), and N reliability exceedance is reduced to just 0.04% (39 hours).

In 2050 projected demand exceeds the N-1 reliability for 40% of the time (3379 hours) and exceeds the N reliability for the 3% of the time (141 hours). In contrast, after the integration of the solar farm, exceeding N-1 reliability decreases to 11% of the time (929 hours), while it exceeds the N reliability for 0.04% of the time (39 hours).

The above analysis demonstrates that the centralised solar farm approach helps reduce the community's dependence on local grid electricity significantly during summer months and sunny hours, but much less during winter periods and not at all during nighttime. Reliance on the national grid (via the Kopu GXP), is therefore unavoidable every night of the year, unless grid scale batteries are implemented.

5.6 Results – decentralised roof-top solar approach scenario

This section presents the analysis of a decentralised solar PV system across residential dwellings in the Whitianga region community. The decentralised approach involves the installation of rooftop solar panels on individual houses and operates under two different scenarios.

Occupied dwellings, equipped with rooftop solar panels and (Vehicle to Grid) V2G-enabled battery storage is one scenario. Non-occupied dwellings use only solar electricity without any energy storage, relying on the local grid network, when there is insufficient generation from solar panels is the second scenario.

For both scenarios, a 4.3 kW rooftop solar panel is assumed, derived by scaling the total 32 MWp centralized capacity dispersed equally across all residential units in 2024 (Figure 5-4).

5.6.1 Occupied dwellings with V2G approach.

In this scenario, 4.3 kW_p rooftop solar PV is used with a 20 kWh electric vehicle (EV) battery. It is assumed the EV battery is used exclusively for electricity storage up to a value of 20 kWh, and the EV battery capacity above that, up to 70 kWh, is available for transport.

In this study, the EV transport demand has not been included, and this area is for future work. The EV battery up to 20 kWh stores any surplus electricity generated during the day. It supplies the electricity deficit when there is no production from the solar panel, typically during nighttime and morning, or hours of low sunlight. Local grid electricity has been used only if the EV battery is completely drained. To illustrate the seasonal variability of performance, Figure 5-21 presents the hourly electricity flow for a single-occupied dwelling over a day in summer, winter, spring, and autumn.

From Figure 5-21, it is evident that summer and spring seasons benefit from high solar availability, enabling most of the residential dwellings' demand to be met by direct solar generation and solar stored EV battery supply. In winter, solar availability is much lower, and electricity demand often exceeds solar supply. In such cases, the EV battery can

meet most of the electricity demand during the evening period, while for the morning period, electricity from the local grid is used.

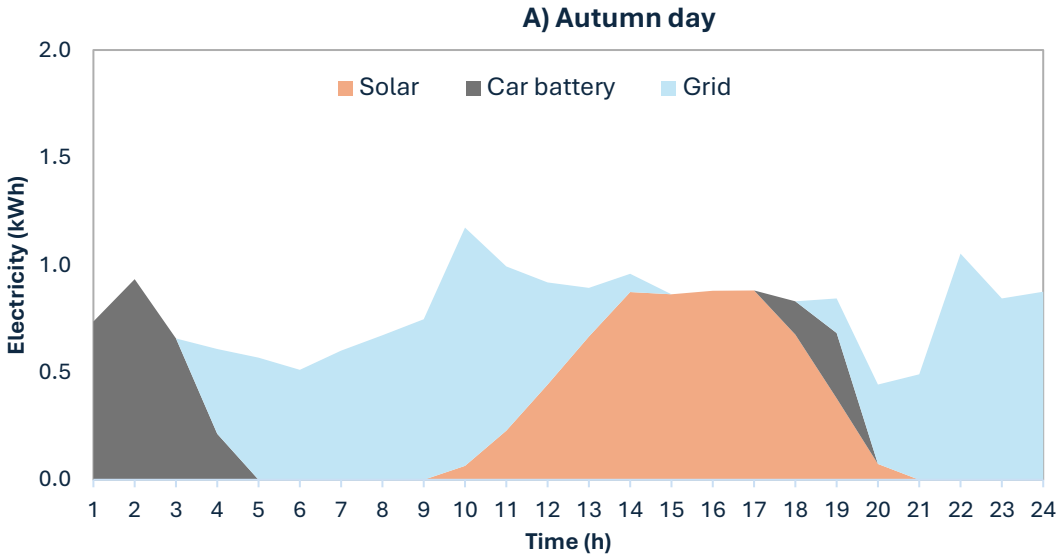

Figure 5-21 (A): Daily electricity balance for a single occupied dwelling using V2G, across Autumn day (2024) on an hourly basis.

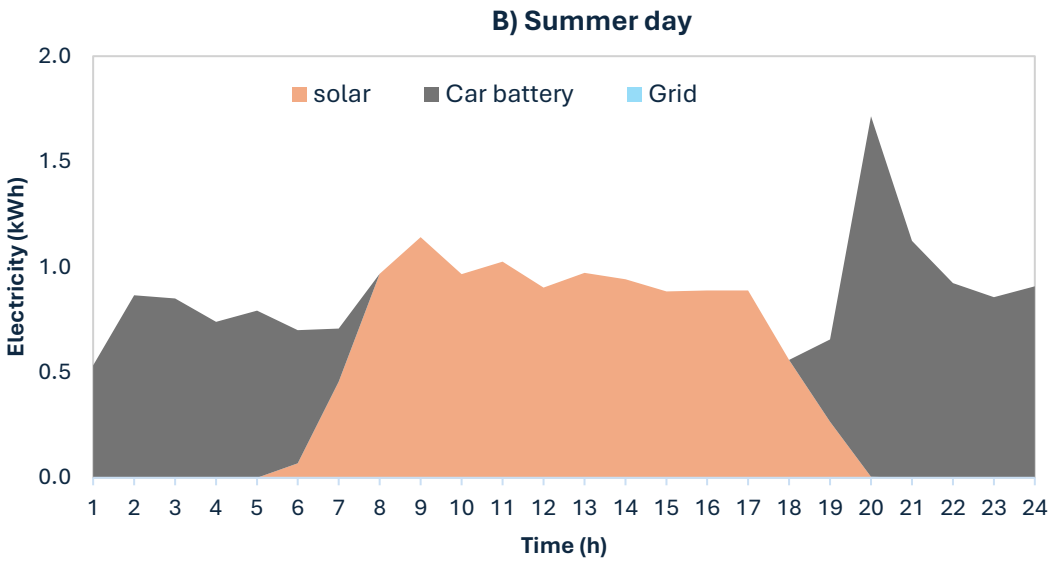

Figure 5-22 (B): Daily electricity balance for a single occupied dwelling using V2G, across Summer day (2024) on an hourly basis.

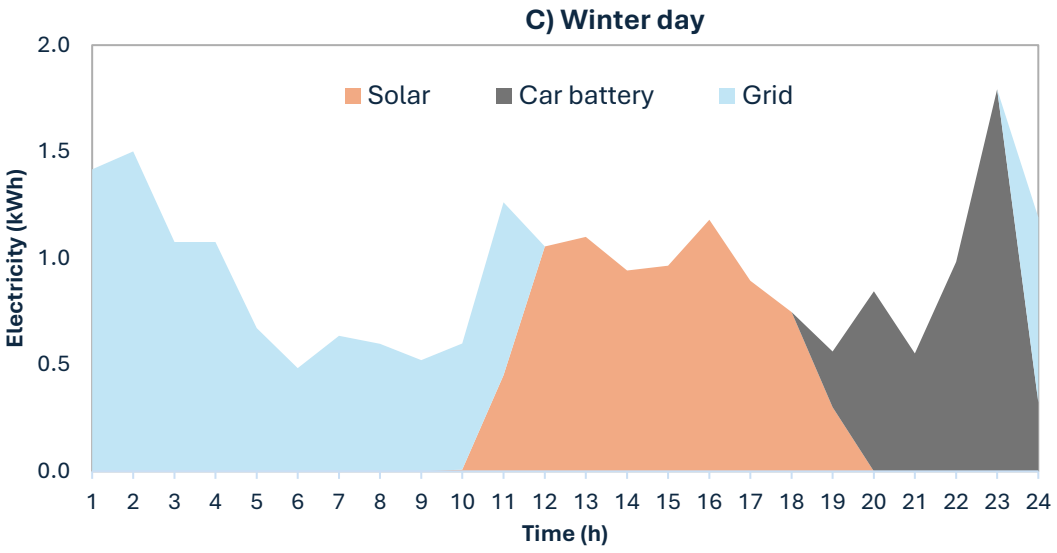

Figure 5-23 (C): Daily electricity balance for a single occupied dwelling using V2G, across Winter day (2024) on an hourly basis.

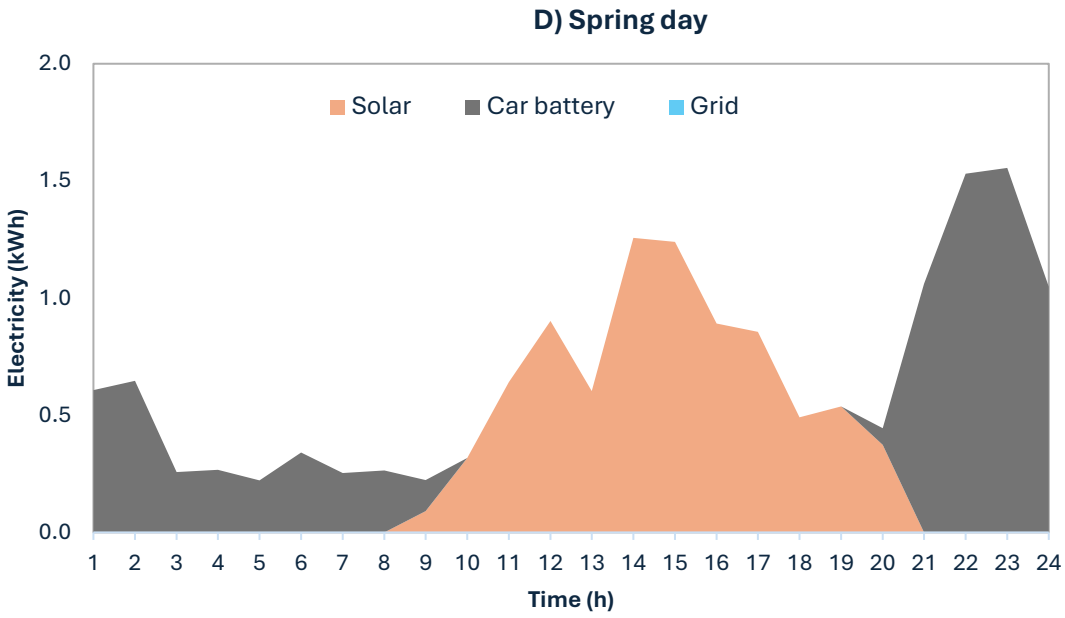

Figure 5-24 (D): Daily electricity balance for a single occupied dwelling using V2G, across spring day (2024) on an hourly basis.

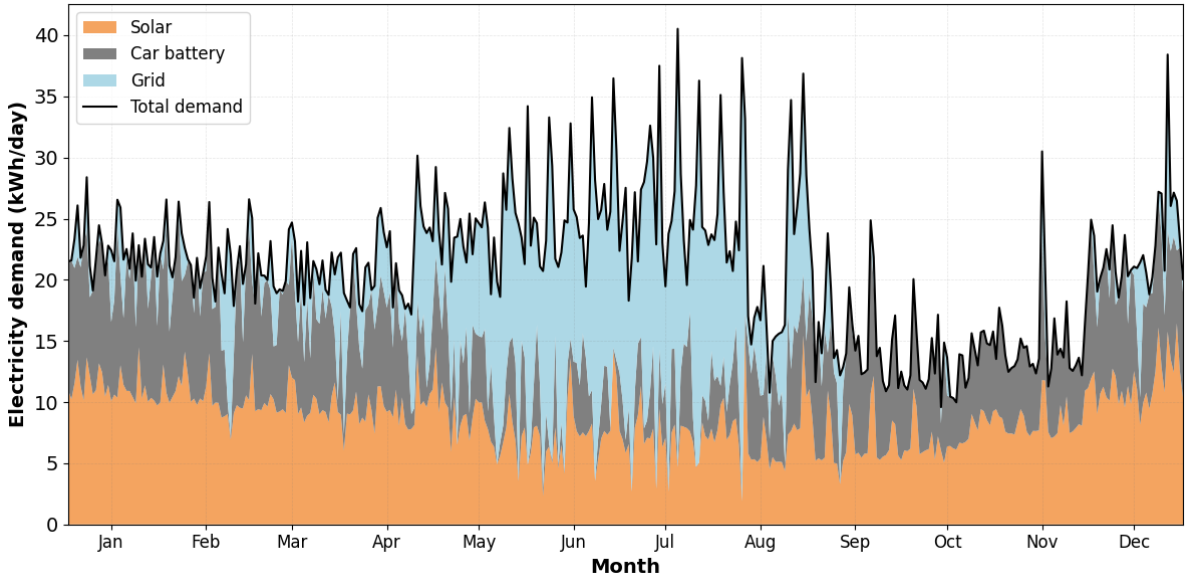

Figure 5-25: Annual electricity demand and supply breakdown (Solar, Grid, Car Battery) for a single occupied dwelling with V2G in 2024.

For autumn, approximately 24% of the electricity is supplied from solar sources, 21% from the EV battery, and 55% from the local grid, reflecting the seasonal variation. However, in the early morning, the electricity is supplied from the EV car from the previous day's stored electricity. To assess the overall performance, an annual electricity supply distribution from various sources has been calculated for a single occupied dwelling. As shown in Figure 5-22, the results

indicate that 41.5% of the electricity is met directly from solar generation, followed by 25.3% from the local grid, and 33.12% is imported from the EV battery.

Scaling this analysis to all the occupied dwellings in the community in 2024, the total electricity balance analysis is summarised in Table 5-9.

Table 5-9: Annual electricity balance for all occupied dwellings with V2G integration (20 kWh EV battery) approach (2024).

Specifications	**Residential 2024 (GWh)**
Solar electricity production	22.89
Residential dwellings demand	25.48
Electricity is supplied from solar	10.58
Electricity supply from a car battery	8.44
Electricity supply from the grid	6.46
Excess electricity is exported to the grid	3.87

The results demonstrate that the V2G significantly enhances energy self-sufficiency by allowing households to use a large portion of their solar-generated electricity directly or indirectly through EV car battery storage. Annually, only 25.36% of the demand has been supplied from the local grid, indicating the potential of localized consumption and reducing stress on the grid network during peak periods.

5.6.2 Non-occupied dwellings

In contrast, non-occupied dwellings are assumed to operate with the same 4.3 kW_p rooftop PV system without any battery storage. During the day, the non-occupied dwelling draws electricity directly from the rooftop solar and relies on grid imports during periods of insufficient generation. The excess electricity produced is exported to the grid network.

The annual electricity balance for a single non-occupied dwelling was conducted and scaled to represent all the non-dwellings in the community. Figure 5-23 illustrates the seasonal variation in electricity demand and supply throughout the year for the total non-occupied dwellings.

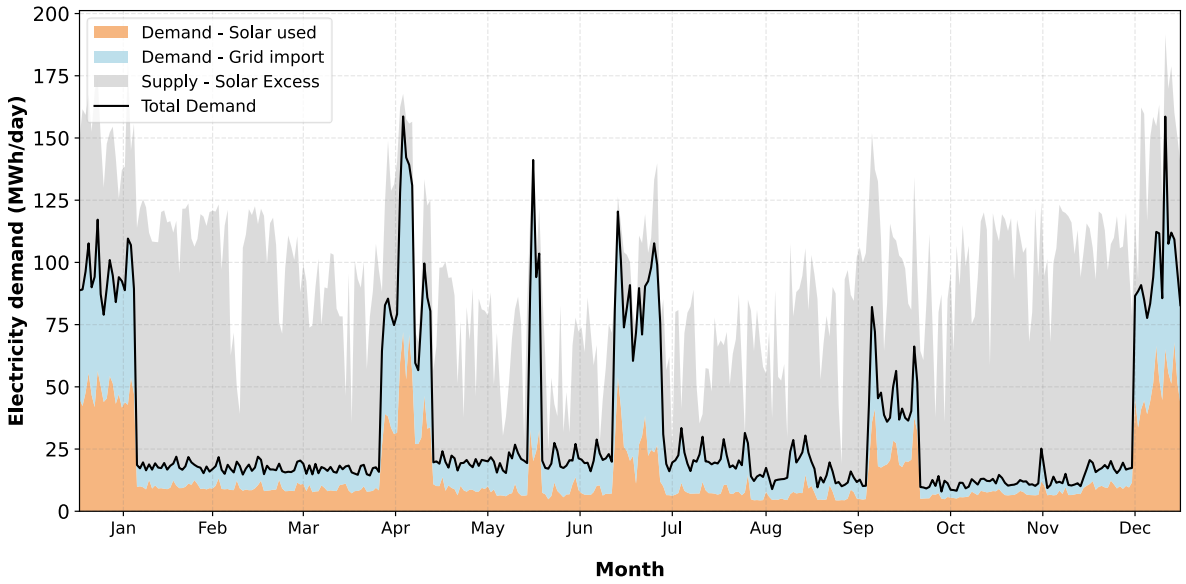

Figure 5-26: Annual daily electricity supply and demand breakdown for total non-occupied dwellings in 2024.

As observed, electricity consumption in non-occupied dwellings is generally low throughout the year, with occasional peak consumption recorded during the holiday seasons, when houses are temporarily rented or used. Due to the lack of storage, a significant proportion of the electricity produced has been exported to the grid. In most cases, solar and grid supply contribute almost equally to daily demand, except on specific days during the season. The annual electricity balance for total non-occupied dwellings has been illustrated in Table 5-10.

Table 5-10: Annual supply and demand balance for total residential non–dwelling applications in 2024.

Specifications	2024 (GWh)	Proportion of supply	Proportion of demand
Solar electricity production	28.48	100%	
Non-dwelling demand	12.37		100%
Electricity is supplied from solar	6.00	20%	49%
Electricity supply from the grid	6.77		51%
Solar-produced electricity is exported to the grid	22.89	80%	

Only 20% of the total solar electricity produced is consumed by the non-occupied dwellings themselves, while 80% has been exported to the grid. The large proportion of exports to the local grid provides a good opportunity to utilise it effectively for EV charging and H_2

production in the community or for meeting neighbouring demands. This sharing of locally produced solar electricity may help reducing stress on the grid network during peak hours of generation and improves overall electricity utilization across the Coromandel region.

5.7 Economic analysis

Economic analysis is a critical component of evaluating the feasibility and long-term viability of energy systems. In this study, a comparative life cycle assessment is conducted for two solar energy supply strategies namely, centralised (solar farm) and decentralised (rooftop solar) using the Levelized Cost of Energy (LCOE) method.

5.7.1 Levelized Cost of Energy (LCOE)

The LCOE represents the average cost per unit of electricity generated over the system's lifetime, incorporating capital expenditure (CAPEX), operational expenditure (OPEX), and maintenance costs. It is calculated using the Net Present Value (NPV) approach over a 25-year period, as shown below [47],

$$LCOE = \frac{\sum_{t=0}^{n} \frac{C_t}{(1+r)^t}}{\sum_{t=0}^{n} \frac{E_t}{(1+r)^t}}$$

Where t is the total lifetime, usually expressed in years, C_t is the total cost of the system, including capital expenditure (CAPEX), operational expenditure (OPEX), and maintenance over its lifetime, E_t is the total electricity produced over the lifetime, n represents the number of years and r is the discount factor. The discount factor is taken as 7% for the NPV method. The maintenance is assumed to be 1% of the CAPEX. The OPEX is assumed to will be varying for both the methods, depends of land cost leased or owned.

The capital expenditure (CAPEX) includes material costs, labour costs, and land costs (if purchased). The OPEX consists of the monitoring software, control system, land cost (if leased), and performance inspections. Any cost associated with component replacement or diagnosis is categorised under maintenance. The cost of the solar farm has been sourced from the Lodestone reports [59]. The cost of the rooftop solar panel has been referenced from the NREL website, converted to NZD at 1.60 NZD to USD [48]. Table 5-11 presents the cost inputs used in the LCOE calculation.

Table 5-11: The costing parameters used for LCOE calculation of solar farm and rooftop solar panel over a 25-year period.

Parameters	Solar farm	Roof-top panel
Total CAPEX ($)	$ 55,000,000	$ 69,656,600
Total OPEX ($)*	$ 7,030,846	$ 8,904,451
Total Maintenance ($)*	$ 3,515,423	$ 8,904,451
Total Electricity (kWh)*	$ 612,208,872	$ 612,208,872
LCOE ($NZD/kWh)	$ 0.107	$ 0.147

(* Discount rate of 7% used)

Figure 5-24 illustrates the LCOE comparison between the centralized (solar farm) and decentralized approaches (rooftop solar) for the community. The centralised system shows an economic advantage from an installation perspective due to its economies of scale with common support structures, electrical systems and control systems.

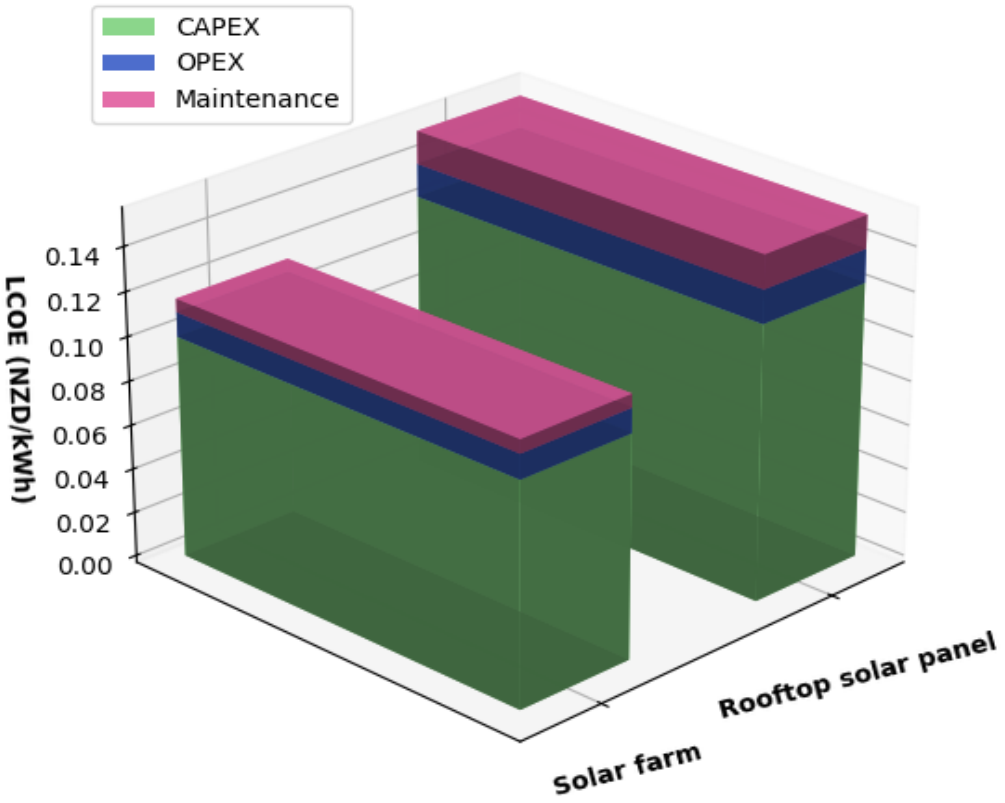

Figure 5-27: LCOE for rooftop solar and solar farm approach over a 25-year period.

On the negative side land is required for the solar farm approach and generated electricity needs to be distributed around the local grid which also incurs a cost. The land is assumed to be leased for 25 years, with a total cost of approximately NZD 4 million over its lifetime, categorized under OPEX. The electricity distribution cost is not included in the LCOE for the solar farm.

5.7.2 Average cost of electricity to households

While the LCOE provides an estimate of the cost to generate electricity per kWh from solar-integrated systems, it does not reflect the actual cost of electricity per kWh paid by households. To get a more realistic view, additional costs such as grid electricity, battery use (for V2G systems), distribution charges, and any revenue generated from exporting electricity to the grid are included. In the solar farm case, the electricity distribution costs are included, but not for rooftops. These factors determine the average cost of electricity to the end user. The average cost of electricity is calculated by the formula

$$Average\ cost = \frac{Total\ cost\ of\ electricity\ used\ (NZD) - Export\ revenue\ (NZD)}{Total\ energy\ consumed\ (kWh)}$$

$$Average\ cost = \frac{(E_{solar} \cdot C_{solar}) + (E_{grid} \cdot C_{grid}) + (E_{battery} \cdot C_{solar}) - (E_{export} \cdot C_{export})}{E_{total}\ (kWh)}$$

Table 5-12 below summarises the key cost components used in this calculation for both the solar farm and rooftop solar approach.

Table 5-12: Costing parameters used in the average cost calculation.

	Parameters	Solar Farm	Roof top solar
A	LCOE (NZD/kWh)	0.107	0.143
B	Local distribution cost (NZD/kWh)	0.10	-
C_{solar} = A+B	Solar electricity cost (NZD/kWh)	0.25	0.143
C_{grid}	Grid electricity cost (NZD/kWh)	0.32	0.32
C_{export}	Grid export electricity price (NZD/kWh)	0.08	0.08

For the centralised solar farm approach, Table 5-13 presents the solar electricity produced, grid electricity use, export electricity, total electricity demand, and cost breakdowns for the years 2024 and 2050. Over time, electricity demand increases, leading to a slight rise in the average cost. Additionally, the revenue from selling excess electricity to the grid decreases, which contributes to this increase.

Table 5-13: Centralised solar farm – Average electricity cost calculations parameters.

Year	Electricity (GWh)				Cost million(NZD)				NZD/kWh
Solar Farm	**Solar PV produced**	**Grid used**	**Grid export**	**Total demand**	**Solar PV produced**	**Grid used**	**Revenue (Grid export)**	**Total**	**Average cost of electricity**
	E_{solar}	E_{grid}	E_{export}	E_{total}	$E_{solar} \cdot C_{solar}$	$E_{grid} \cdot C_{grid}$	$E_{export} \cdot C_{export}$		
2024	56.15	35.22	25.10	66.27	6.52	11.270	2.008	15.782	0.24
2050	56.15	68.31	5.17	119.3	10.70	21.860	0.414	32.152	0.27

For the decentralised scenario, only occupied dwelling household equipped with a 4.3 kW rooftop solar system is evaluated using different battery sizes (0-20 kWh). As shown in Table 5-14, increasing battery capacity allows more solar electricity to be stored and used, reducing grid reliance and lowering the average electricity cost. The lowest cost (0.19 NZD/kWh) is achieved with a 20 kWh battery system. The cost of the car battery has not been included in the analysis (vehicle owned by household).

Table 5-14: Average electricity cost summary of the decentralised V2G approach with 4.3 kW_p rooftop panel and varying battery capacities of the community.

kWh	Electricity (GWh)					Cost (million NZD)				NZD/kWh
Battery capacity	**Solar PV produced**	**Battery used**	**Grid used**	**Grid Export**	**Total demand**	**Solar PV Produced**	**Grid used**	**Revenue (Grid export)**	**Total**	**Average cost of electricity**
	E_{solar}	$E_{battery}$	E_{grid}	E_{export}	E_{total}	$E_{solar} \cdot C_{solar}$	$E_{grid} \cdot C_{grid}$	$E_{export} \cdot C_{export}$		
0	22.91	0	14.89	12.33	25.47	3.28	4.76	0.98	7.06	0.27
5	22.91	5.15	9.75	7.18	25.48	3.28	3.12	0.57	5.82	0.23
10	22.91	7.80	7.10	4.51	25.48	3.27	2.27	0.36	5.18	0.20
15	22.91	8.31	6.59	4.00	25.48	3.27	2.11	0.32	5.06	0.20
20	22.91	8.44	6.46	3.87	25.48	3.27	2.07	0.30	5.03	0.19

5.7.3 Payback period analysis

To evaluate the long-term economic performance of each system, the payback period is calculated. This represents the time required to recover the initial investment through electricity cost savings. The payback period is calculated by using the standard formula represented as

$$Payback\ Period = \frac{Initial\ investment\ cost}{Annual\ profit}$$

Table 5-15 compares the payback periods for the solar farm and rooftop V2G approaches. Although the rooftop system has a higher investment cost, it provides a much shorter payback period of 12.01 years, due to higher savings per unit of electricity. The solar farm has a lower upfront cost but a longer payback period of nearly 14.63 years because of smaller profit margins.

In summary, although the decentralised rooftop system is more expensive to install, it results in greater long-term savings, making it economically attractive over time. The centralised solar farm, while cost-effective in installation, takes longer to recover its cost due to lower electricity savings.

Table 5-15: The specifications for calculating the payback period for both approaches.

	Specifications	**Solar farm (32 MW_p)**	**Roof-top Solar 4.3 kW_p V2G (20 kWh)**
A	Average cost of electricity (NZD/kWh)	$ 0.24	$ 0.19
B	Grid cost (NZD/kWh)	$ 0.32	$ 0.32
C = B - C	Profit per kWh (NZD/kWh)	$ 0.08	$ 0.13
D	Initial investment cost (NZD)	$ 65,546,269	$ 87,465,503
E	Solar generation capacity (GWh/year)	56.15	56.15
F = E * C	Annual profit (NZD/year)	$ 4,480,000.00	$ 7,280,000.00
G = D / F	Payback period (years)	14.63	12.01

5.7.4 Optimisation of the V2G approach for residential system

In addition to centralised and decentralised approaches to economic evaluation, the optimisation of a V2G-enabled single NZ residential house system is performed. The system configuration for V2G approach includes solar panels, a household car battery (via EV), and grid electricity as a backup. The cost of the car battery has been excluded from this analysis (Vehicle owned by the households).

Figure 5-25 illustrates the total household electricity cost paid and savings over the 25 years for various solar and battery capacity configurations. The black dotted line represents the grid electricity cost paid by the household for 25-year period, with retail price of 0.32 NZD/kWh. In figure, the region above the curve represents the savings and below the curve represents the actual cost of the electricity paid by the household for the 25-year period after installing this setup to the residential house.

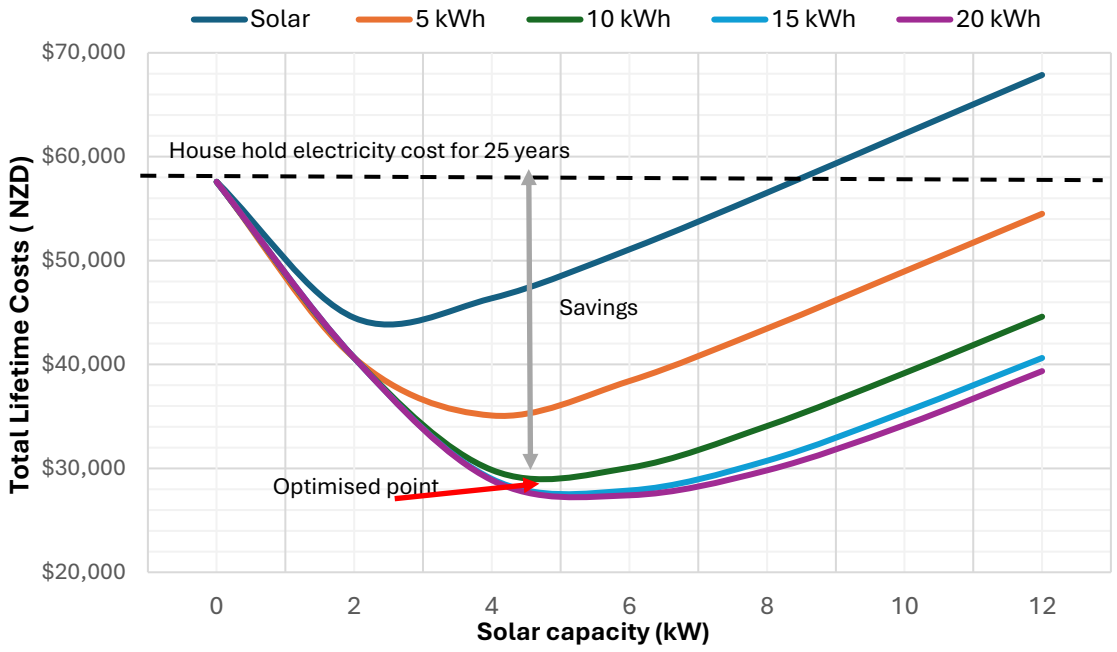

Figure 5-28: Total household electricity cost for 25 years using a car battery vs solar capacity

Each curve represents the combined total cost of the solar PV-battery integrated system and cost of the deficit amount of electricity drawn from the grid for 25-year period. Multiple scenarios are then analysed by adding rooftop solar panels and battery with varying capacities. The results suggests that system capacity with 4.9 kW solar PV, 20 kWh battery, capacity shows best and optimised capacity for the typical NZ residential settings. The optimised configuration for the residential settings can save up to 31500 NZD over the 25-year period.

Findings from an Australian study reveal that maintaining the EV car battery's state of charge between 40% and 60% optimizes the battery's life cycle and increases its longevity through load shifting. [52]. The results demonstrate that optimal solar-battery integration can significantly reduce the long-term overall cost of the household.

5.8 Conclusion

A comprehensive techno-economic assessment of both centralized and decentralized energy systems has been presented in this study. The Levelized Cost of Electricity (LCOE) for the centralized solar farm approach was found to be more economical at 0.107 NZD/kWh, compared to 0.143 NZD/kWh for the decentralized rooftop solar system. However, the decentralized approach particularly when incorporating Vehicle to Grid (V2G) technology demonstrates significant advantages in terms of average electricity cost and payback period, with a shorter payback of 12.01 years due to higher profit margins per kilowatt-hour produced.

Installing large solar farms in remote communities (centralised approach) helps address growing electricity demand and can significantly reduce reliance on the local grid during sunny hours. By 2050, the overall system (solar farm plus grid) is expected to have an N-1 reliability limit of 89% of the time. However, for the remaining 11% of the time, particularly during winter and nighttime, demand exceeds the N-1 limit but remains within the N-reliability threshold, which poses a significant challenge for the local grid network.

To improve energy security, the solar rooftop decentralised approach with some V2G (20 kWh) appears to be a promising solution. In this approach, a significant proportion of the electricity produced in the middle of the day can be stored in the EV car battery for use later in the house or for transport, thus reducing electricity imports and solar grid exports. This local storage strategy enhances the energy resilience and the system's self-sufficiency and can potentially reduce the stress on the local grid network.

Localised solar generation, either as a centralised solar farm or decentralise roof-top can improve electricity reliability for a remote community and prevent costly grid upgrades, especially if V2G energy storage or some other backup energy storage options is widely implemented. This conclusion is supported by the favourable electricity cost reduction arising from both scenarios.

6 Conclusion and Recommendations

6.1 Conclusion

Several conclusions can be drawn from the three major areas of investigation reported in this work. These conclusions are set forth in this chapter.

1. Dynamics of the PEM electrolyser

The result suggests that, when there is a fluctuation in the solar input, the dynamic simulation gives a more robust and real-time hydrogen production rate, which helps in sizing the auxiliary equipment. However, in terms of the cumulative difference between static and dynamic models for hydrogen production is minimal, with an absolute error of less than 0.5%.

2. Single residential application

There is a potential of achieving 100% self-sufficiency for all the three integrated system in the residential settings is relatively at the higher cost, which is 0.52 – 0.78 NZD/kWh. The higher cost is driven due to expensive hydrogen storage. Among all three system, the hybrid option achieves the lowest LCOE with the 100% self-sufficiency levels, which is 100 of the electric. If the cost of the hydrogen storage is reduced by 50%, then LCOE of the hybrid integrated system may achieve the levelized cost of 0.34 NZD/kWh. The hybrid approach especially may be relevant remote islands, where it experiences the higher electricity prices.

3. Techno-economic assessment of two scenarios

Roof-top solar combined with V2G will lower electricity cost significantly to households, with a shorter payback of 12.01 years due to higher profit margins per kWh produced. However, in terms of the Levelized Cost of Electricity (LCOE), the centralized solar farm model was found to be more economical at 0.107 NZD/kWh, compared to 0.143 NZD/kWh for the decentralized rooftop solar system.

4. Grid dependency scenario for the centralised approach scenario

Installing large solar farms in remote communities (centralised approach) helps address growing electricity demand and can significantly reduce reliance on the local grid during sunny hours. By 2050, the overall system (solar farm plus grid) is expected to have N-1 reliability limit 89% of the time. However, for the remaining 11% of the time, particularly during winter and nighttime, demand exceeds the N-1 limit but remains within the N-reliability threshold. This indicates the potential need for upgrading the grid infrastructure. To minimise costly grid

upgrades, a hybrid system or large-scale battery storage should be implemented to manage the energy deficit during the winter period.

6.2 Recommendations.

Several areas for future work have been identified that may yield valuable insights. These recommendations are outlined in this chapter.

Chapter 3 – Complete simulation of the PEM electrolyser.

In Chapter 3, only the dynamic behaviour of H_2 production has been examined. Future work can be carried out for simulating the complete dynamics of the PEM electrolyser for variable changes such as temperature, pressure, and water flow rate.

Chapter 4 - Heat recovery and optimisation

Heat recovery from the PEM electrolyser and PEM fuel cell in household applications can be considered for future work. Given that the efficiencies of the PEM electrolyser and PEM fuel cell are approximately 70% and 50%, respectively, a significant portion of the input electricity is converted into heat. This waste heat could potentially be recovered and used for domestic heating purposes in houses.

Additionally, the sizing of both the PEM electrolyser and fuel cell in this study was based on peak demand values, which contributed to higher system costs. If an optimisation process is carried out, the required system size could be reduced, leading to lower overall costs.

Chapter 5 – Wind integrated approach for the centralised scenarios

The centralized approach considers only a solar farm integrated with the local grid to meet the community's future energy demand. However, even with high solar penetration, reliance on the local grid remains significant, particularly during the winter months when solar output is limited. Future research could explore the integration of wind energy or energy storage systems into the current setup to assess their potential in supporting winter demand and further reducing the need for grid upgrades in the future.

References

1. Campus, M.U.W. Urban–rural profile , Environmental Health Intelligence New Zealand. 2024; Available from: https://www.ehinz.ac.nz/indicators/population-vulnerability/urbanrural-profile/?utm_source.
2. PowerCo, Kopu-Tairua project overview document. 2024.
3. government, N., Towards a productive, sustainable, and an inclusive economy, Hiringa Energy. 2025.
4. MOT. Vehicle fleet statistics of Aotearoa. 2024; Available from: https://www.transport.govt.nz/statistics-and-insights/fleet-statistics.
5. stats, N. Population and dwelling statistics. 2024; Available from: https://www.stats.govt.nz/tools/2018-census-place-summaries/whitianga-south.
6. herald, N., Whitianga public service census. 2025.
7. council, W., Waikato Regional Economic Profile, Technical Report. 2020.
8. Rezaei, M., A. Akimov, and E.M.A. Gray, Levelised cost of dynamic green hydrogen production: A case study for Australia's hydrogen hubs. Applied Energy, 2024. **370**: p. 123645.
9. Sorgulu, F. and I. Dincer, A renewable source based hydrogen energy system for residential applications. International Journal of Hydrogen Energy, 2018. **43**(11): p. 5842-5851.
10. Khezri, R., A. Mahmoudi, and M.H. Haque, Optimal capacity of solar PV and battery storage for Australian grid-connected households. IEEE Transactions on Industry Applications, 2020. **56**(5): p. 5319-5329.
11. Ahmed, S., A. Ali, and A. D'angola, A review of renewable energy communities: concepts, scope, progress, challenges, and recommendations. Sustainability, 2024. **16**(5): p. 1749.
12. Krishnan, S., et al., Present and future cost of alkaline and PEM electrolyser stacks. International journal of hydrogen energy, 2023. **48**(83): p. 32313-32330.
13. Arsad, A., et al., Hydrogen electrolyser technologies and their modelling for sustainable energy production: A comprehensive review and suggestions. International Journal of Hydrogen Energy, 2023. **48**(72): p. 27841-27871.
14. Ogumerem, G.S. and E.N. Pistikopoulos, Dynamic Modeling and Explicit Control of a PEM Water Electrolysis Process. Smart and Sustainable Manufacturing Systems, 2018. **2**(2): p. 25-43.

15. Hernández-Gómez, Á., et al., Cell voltage static-dynamic modeling of a PEM electrolyzer based on adaptive parameters: Development and experimental validation. Renewable Energy, 2021. **163**: p. 1508-1522.
16. Awasthi, A., K. Scott, and S. Basu, Dynamic modeling and simulation of a proton exchange membrane electrolyzer for hydrogen production. International journal of hydrogen energy, 2011. **36**(22): p. 14779-14786.
17. Yigit, T. and O.F. Selamet, Mathematical modeling and dynamic Simulink simulation of high-pressure PEM electrolyzer system. International Journal of Hydrogen Energy, 2016. **41**(32): p. 13901-13914.
18. Liso, V., et al., Modelling and experimental analysis of a polymer electrolyte membrane water electrolysis cell at different operating temperatures. Energies, 2018. **11**(12): p. 3273.
19. Molho, S., Dynamic modelling of a PEM electrolysis system: optimal operation for coupling with renewable energy sources. 2020.
20. Garibaldi, L., et al., Holistic and dynamic mathematical model for the assessment of offshore green hydrogen generation and electrolyser design optimisation. Energy Conversion and Management, 2023. **294**: p. 117488.
21. Abdin, Z. and W. Mérida, Hybrid energy systems for off-grid power supply and hydrogen production based on renewable energy: A techno-economic analysis. Energy Conversion and management, 2019. **196**: p. 1068-1079.
22. Kumar, Y.P. and B. Ravikumar, Integrating renewable energy sources to an urban building in India: challenges, opportunities, and techno-economic feasibility simulation. Technology and Economics of Smart Grids and Sustainable Energy, 2016. **1**: p. 1-16.
23. Ramírez-Sagner, G., et al., Economic feasibility of residential and commercial PV technology: The Chilean case. Renewable Energy, 2017. **111**: p. 332-343.
24. William, F., Sustainable Energy Solutions for Urban Residences in Australia through Hybrid Systems. Journal of Energy and Environmental Policy Options, 2023. **6**(3): p. 1-7.
25. Hossain, J. and A. Mahmud, Renewable energy integration: challenges and solutions. 2014: Springer Science & Business Media.
26. Lee, J., et al., Renewable energy potential by the application of a building integrated photovoltaic and wind turbine system in global urban areas. Energies, 2017. **10**(12): p. 2158.

27. Saxena, N., et al., Implementation of a grid-integrated PV-battery system for residential and electrical vehicle applications. IEEE transactions on industrial electronics, 2017. **65**(8): p. 6592-6601.
28. Obuseh, E., et al., A Systematic Review of Barriers to Renewable Energy Integration and Adoption. Journal of Asian Energy Studies, 2025. **9**: p. 26-45.
29. Scott, M. and G. Powells, Towards a new social science research agenda for hydrogen transitions: Social practices, energy justice, and place attachment. Energy Research & Social Science, 2020. **61**: p. 101346.
30. Khalid, F., I. Dincer, and M.A. Rosen, Analysis and assessment of an integrated hydrogen energy system. International Journal of Hydrogen Energy, 2016. **41**(19): p. 7960-7967.
31. Barzola-Monteses, J. and M. Espinoza-Andaluz, Performance analysis of hybrid solar/H2/battery renewable energy system for residential electrification. Energy Procedia, 2019. **158**: p. 9-14.
32. Belmar, F., P. Baptista, and D. Neves, Modelling renewable energy communities: assessing the impact of different configurations, technologies and types of participants. Energy, Sustainability and Society, 2023. **13**(1): p. 18.
33. Bhattacharyya, S., Rural electrification through decentralised off-grid systems in developing countries. 2013: Springer.
34. Yildiz, Ö., Financing renewable energy infrastructures via financial citizen participation–The case of Germany. Renewable energy, 2014. **68**: p. 677-685.
35. Dorotić, H., et al., Integration of transport and energy sectors in island communities with 100% intermittent renewable energy sources. Renewable and Sustainable Energy Reviews, 2019. **99**: p. 109-124.
36. Emrani, A., et al., Improved techno-economic optimization of an off-grid hybrid solar/wind/gravity energy storage system based on performance indicators. Journal of Energy Storage, 2022. **49**: p. 104163.
37. Nishanthy, J., S.C. Raja, and J.J.D. Nesamalar, Feasibility analysis of solar PV system in presence of EV charging with transactive energy management for a community-based residential system. Energy Conversion and Management, 2023. **288**: p. 117125.
38. Sood, S., et al., Generic dynamical model of PEM electrolyser under intermittent sources. Energies, 2020. **13**(24): p. 6556.

39. Selamet, Ö.F., et al., Development and testing of a highly efficient proton exchange membrane (PEM) electrolyzer stack. International Journal of hydrogen energy, 2011. **36**(17): p. 11480-11487.
40. Government, I. IRELAND'S OPEN DATA PORTAL. 2024; Available from: https://data.gov.ie/.
41. H2, N., Water electrolysers and hydrogen generators C model series. 2025: IRENA.
42. NASA. Renewables ninja data report. 2024; Available from: https://www.renewables.ninja/.
43. Apperley, M., et al., The role of smart community microgrids in Aotearoa's energy future. Journal of the Royal Society of New Zealand, 2025: p. 1-20.
44. Qiu, K. and E. Entchev, Modeling, design and optimization of integrated renewable energy systems for electrification in remote communities. Sustainable Energy Research, 2024. **11**(1): p. 10.
45. Lokar, J. and P. Virtič, The potential for integration of hydrogen for complete energy self-sufficiency in residential buildings with photovoltaic and battery storage systems. International Journal of Hydrogen Energy, 2020. **45**(60): p. 34566-34578.
46. IEA. The Archimedes Liam F1 urban Wind Turbine. 2025; Available from: https://www.ienergy-us.com/products/detail/42.
47. Wolf, N., M.A. Tanneberger, and M. Höck, Levelized cost of hydrogen production in Northern Africa and Europe in 2050: A Monte Carlo simulation for Germany, Norway, Spain, Algeria, Morocco, and Egypt. International Journal of Hydrogen Energy, 2024. **69**: p. 184-194.
48. NREL, Renewable utility scale PV cost reports. 2024: p. Capital Expenditure.
49. Nasser, M. and H. Hassan, Techno-enviro-economic analysis of hydrogen production via low and high temperature electrolyzers powered by PV/Wind turbines/Waste heat. Energy Conversion and Management, 2023. **278**: p. 116693.
50. agency, N.t. Source of electricity generation in NZ. 2024; Available from: https://www.mbie.govt.nz/building-and-energy/energy-and-natural-resources/energy-statistics-and-modelling/energy-publications-and-technical-papers/energy-in-new-zealand.
51. Transpower, Empowering our Energy Future. 2024: MBIE.
52. Lehtola, T.A. and A. Zahedi, Electric vehicle battery cell cycle aging in vehicle to grid operations: A review. IEEE Journal of Emerging and Selected Topics in Power Electronics, 2019. **9**(1): p. 423-437.

53. stats, N. Population statistics of Aotearoa. 2025; Available from: https://www.stats.govt.nz/topics/population/.
54. Brunsdon, N., Peak population study for Thames-Coromandel District. April 2021: Infometrics.
55. Florita, A.R., et al., Classification of Commercial Building Electrical Demand Profiles for Energy Storage Applications. Journal of Solar Energy Engineering, 2013. **135**(3).
56. Trasnsport, M.o. Vehicle fleet statistics 2024. Available from: https://www.transport.govt.nz/statistics-and-insights/fleet-statistics/annual-fleet-statistics/.
57. council, C.d., Summer tourists provide a boost to local businesses. 2023.
58. Authority, E. Demand trends profile by regions. 2024; Available from: https://www.emi.ea.govt.nz/Wholesale/Reports/W_GD_C.
59. Energy, L. Whitianga solar farm reports. 2024; Available from: https://lodestoneenergy.co.nz/whitianga-solar-farm/?utm_source.

Appendix

A-1: Python coding for plotting the voltage and current profile.

```
import matplotlib.pyplot as plt
import numpy as np
import math
import pandas as pd

# --- Load data ---
data = pd.read_csv('solar_current_profile.csv')
I = data['Power']

# --- Constants ---
T = 353.15  # Temperature in Kelvin
F = 96485
R = 8.314   # Universal gas constant [J/(mol·K)]
P_total = 101325  # Pa (1 atm)
V_0 = 1.229  # Nernst potential at std. conditions
t_mem = 0.0254  # Membrane thickness in meters
A_membrane = 100  # Active area [cm²]
i = I / A_membrane  # Current density [A/cm²]

# --- Antoine coefficients for water (valid for 1–100°C) ---
A_H2O, B_H2O, C_H2O = 8.07131, 1730.63, 233.426

# --- Time conversion: 720 min = 12 hours => from 6 AM to 6 PM ---
t = np.linspace(6, 18, len(I))  # in hours

# --- Water vapor pressure ---
T_C = T - 273.15
p_H2O_mmHg = 10**(A_H2O - B_H2O / (C_H2O + T_C))
p_H2O = p_H2O_mmHg * 133.322  # mmHg to Pa
```

```
# --- Partial pressures ---
y_H2 = 1.0
p_H2 = y_H2 * (P_total - p_H2O)
y_O2 = 1.0
p_O2 = y_O2 * (P_total - p_H2O)

# --- PEM Electrolyser Model Equations ---
def calculate_lambda(T):
    return (0.0533 * T) - 6.77632

def calculate_thv(V_0, R, T, F, p_O2, p_H2, p_H2O):
    return V_0 + (R * T / (2 * F)) * np.log((p_H2 * np.sqrt(p_O2)) / p_H2O)

def calculate_activation_an(i):
    return (R * T / (2 * F)) * np.arcsinh(i / (2e-7))

def calculate_activation_ca(i):
    return (R * T / (2 * F)) * np.arcsinh(i / (2e-3))

def calculate_sigma(lambda_val, T):
    return (0.00514 * lambda_val) - 0.00326 * np.exp(1268 * ((1 / 303) - (1 / T)))

def calculate_ohm(i, t_mem, sigma_val):
    return (t_mem / sigma_val) * i

# --- Voltage & Power Calculations ---
lambda_val = calculate_lambda(T)
sigma_val = calculate_sigma(lambda_val, T)
ohm_vol = calculate_ohm(i, t_mem, sigma_val)
act_val = calculate_activation_ca(i) + calculate_activation_an(i)
Theoretical_Volt = calculate_thv(V_0, R, T, F, p_O2, p_H2, p_H2O)
Total_volt = Theoretical_Volt + act_val + ohm_vol
P = (Total_volt * 25) * I / 1000  # Power in kW
```

```
eff = 1.48 / Total_volt

# --- Output ---
print("Theoretical Voltage (Nernst):", round(Theoretical_Volt, 4), "V")
print("Activation Overpotential:", round(np.mean(act_val), 4), "V")
print("Ohmic Loss:", round(np.mean(ohm_vol), 4), "V")
print("Total Cell Voltage:", round(np.mean(Total_volt), 4), "V")

# --- Plotting ---
fig, ax = plt.subplots(figsize=(10, 4))
ax.plot(t, P, color='tab:green', label='Solar Power Output (kW)')
ax.axhline(10, linestyle='--', color='black', label='100% capacity')

ax.set_ylabel('Power (kW)', fontweight='bold')
ax.set_xlabel('Time (min)', fontweight='bold')

# Format x-axis as AM/PM
hour_ticks = np.arange(6, 19, 1)
hour_labels = [f"{h if h <= 12 else h - 12}a:00 {'AM' if h < 12 else 'PM'}" for h in
hour_ticks]
ax.set_xticks(hour_ticks)
ax.set_xticklabels(hour_labels, rotation=360, fontsize=10)

ax.legend()
ax.grid(True, alpha=0.5)
ax.set_xlim(t.min(), t.max())
plt.tight_layout()
plt.show()
```

A – 2 : Python code for plotting the static and dynamic model plot.

```
import pandas as pd
import numpy as np
import matplotlib.pyplot as plt
from scipy.integrate import solve_ivp
from scipy.interpolate import interp1d

# --- Load current data (Power clipped to limits) ---
df = pd.read_csv('solar_current_profile.csv')  # columns: 'Power' (Watts)
I_data = df['Power'].clip(lower=0, upper=191).values   # Power values clipped (W)
time_data = np.arange(0, len(I_data))                  # Time in minutes

# Interpolation function for continuous input
I_interp = interp1d(time_data, I_data, bounds_error=False, kind='quadratic',
fill_value=(I_data[0], I_data[-1]))

# --- Constants ---
F = 96485                    # Faraday constant [C/mol]
M_H2 = 0.002016              # Molar mass of H2 [kg/mol]
tau_H2 = 5                   # Residence time [min]
dt = 1                       # Time step in minutes
n = 25
# --- Time Evaluation Range ---
t_start = time_data[0]
t_end = time_data[-1]
t_eval = np.arange(t_start, t_end + dt, dt)  # Explicit time array

# --- Static Model ---
I_static = I_interp(t_eval)                          # Current in A
H2_rate_static = ((M_H2 *  n * 60)/ (2 * F)) * I_static    # kg/min
H2_total_static = np.sum(H2_rate_static * dt)              # Total H2 (kg)
```

```
# --- Dynamic Model (ODE for accumulation + release) ---
def dH2_mass_dt_min(t, m):
I_t = I_interp(t)
production = ((M_H2 *  n * 60)/ (2 * F)) * I_t
loss = m[0] / tau_H2
return [production - loss]

sol = solve_ivp(dH2_mass_dt_min, (t_start, t_end), [0], t_eval=t_eval)
m_H2_dynamic = sol.y[0]
H2_rate_out = m_H2_dynamic / tau_H2                    # kg/min
H2_total_dynamic = np.sum(H2_rate_out * dt)              # Total H2 (kg)

time_hours = (time_data / 60) + 6  # start from 6 AM
hour_ticks = np.arange(6, 19, 1)
hour_labels = [f"{h if h <= 12 else h - 12}:00 {'AM' if h < 12 else 'PM'}" for h in hour_ticks]
Absolute_error = np.abs(H2_rate_static - H2_rate_out)
Percentage_error = np.where(H2_rate_static != 0, (Absolute_error / H2_rate_static) * 100, 0)
Absolute_error_1 = np.abs(np.cumsum(H2_rate_static) * dt - np.cumsum(H2_rate_out) * dt)
Percentage_error_1 = np.where(np.cumsum(H2_rate_static) != 0, (Absolute_error_1 /
(np.cumsum(H2_rate_static) * dt)) * 100, 0)

plt.figure(figsize=(10, 6))
plt.plot(time_hours, cumulative_static, label='Static Model', linewidth=2)
plt.plot(time_hours, cumulative_dynamic, label='Dynamic Model', linestyle='--',
linewidth=2)
plt.xticks(hour_ticks, hour_labels)
plt.xlim([6, 18])
plt.xlabel('Time (min)', fontweight='bold')
plt.ylabel('Cumulative H₂ Produced (kg)', fontweight='bold')
plt.title('Static vs Dynamic H₂ Production (kg/min)', fontweight='bold')
plt.grid(True, linestyle='--', alpha=0.5)
plt.legend()
plt.tight_layout()
```

```
plt.show()

# --- Plot: Instantaneous H2 Production Rate ---
plt.figure(figsize=(10, 6))
plt.plot(time_hours, H2_rate_static, label='Static Model', linewidth=2)
plt.plot(time_hours, H2_rate_out, label='Dynamic Model', linewidth=2, linestyle='--')
#extract the portion of the plot
X = time_hours[(time_hours >= 6) & (time_hours < 8)]
y = H2_rate_static[(time_hours >= 6) & (time_hours < 8)]



# --- Plot: Absolute Error Over Time ---
plt.figure(figsize=(10, 6))
plt.plot(time_hours, Absolute_error, label='Absolute Error', color='red', linewidth=2)
plt.xticks(hour_ticks, hour_labels)
plt.xlim([6, 18])
plt.xlabel('Time (min)', fontweight='bold')
plt.ylabel('Absolute Error (kg/min)', fontweight='bold')
plt.title('Absolute Error Between Static and Dynamic H₂ Production', fontweight='bold')
plt.grid(True, linestyle='--', alpha=0.5)
plt.legend()
plt.tight_layout()
plt.show()
```